Abstract

NEWSOME, JUSTIN CARLYLE. Development of a Ground-based Test Facility for Studying Reel-in Dynamics of Tethered Satellite Systems. (Under the direction of Dr. Andre Mazzoleni.)

Tethered Satellites offer benefits for the space industry. Several applications are being found which utilize their unique dynamics; from sensing characteristics of the atmosphere to providing a propellantless mode of propulsion. Ground-based experimentation is useful as a cost effective means to develop a thorough understanding of tether dynamics. A number of experiments are required to fully investigate the behavior. After examining a number of experiments previously conducted, a new experiment is devised and tested. The experiment consists of designing a low friction representation of a satellite, the design of a stationary post to be tethered to the satellite representation, choosing an adequate test facility, and developing a means of acquiring data from the experiment. In order to check that the experiment is a useful tool for tether analysis, a mathematical model for the system is developed and then the experimental and mathematical results are compared.

Development of a Ground-based Test Facility for Studying Reel-in Dynamics of Tethered Satellite Systems

by
JUSTIN NEWSOME

A THESIS SUBMITTED TO THE GRADUATE FACULTY OF NORTH CAROLINA STATE UNIVERSITY IN PARTIAL FULFILLMENT OF THE REQUIREMENTS FOR THE DEGREE OF MASTER OF SCIENCE

MECHANICAL ENGINEERING

RALEIGH
DECEMBER, 2006

APPROVED BY:

CHAIR OF ADVISORY COMMITTEE
DR. ANDRE MAZZOLENI

DR. GREGORY BUCKNER

DR. LARRY SILVERBERG

Dedication

A year into my Master's study I got married. As such it is only fitting that I dedicate this to my wonderful wife, Cindy Lee Newsome. Also, since I should hopefully be completed with the two year graduate degree about the right time:

Happy Anniversary!

Biography

Justin Carlyle Newsome was born on March 14, 1981 in King, North Carolina. He was educated in the Stokes County school system and upon graduation entered North Carolina State University. While attending North Carolina State University, Justin participated in Engineers' Council and the American Society of Mechanical Engineers. He then graduated in 2004 with an undergraduate degree in Mechanical Engineering. In 2004, he enrolled in the graduate program for Mechanical Engineering at North Carolina State University.

Acknowledgements

My peers and the faculty at NC State University have been a great help in completing my thesis. Alex Hartl and I initially worked together on my experiments. He also aided with various mathematic queries. Brian Vonk also assisted in the experiments and introduced me to Data Studio to take the inertial measurements. Thank you both for your help and, in general for breaking up what can tend to be a monotonous routine of data gathering. Without my advisor, Dr. Andre Mazzoleni, I would not have even known about tethered satellites, let alone be able to study them. He provided direction for my goals, interests, and thesis for the past two years, and so I especially hope my aim meets his expectations.

The faculty of Charmichael Gymnasium also deserve mention. Without them there would have been no convenient location to conduct the experiments. The custodians provided conversation which at first was awkward but eventual became visits that broke up what would have otherwise been a tedious routine.

I would also like to thank all the freeware contributors out there. Without open-source software scientists and engineers would not be able to conduct studies unless under corporate supervision. Eric Engler's EmbeddedGNU is a great tool for microcontroller programming. And the sample code I built from was originally written by Jonathan W. Valvano and Steven Lamb. Also, I would have had no idea where to go from those programs without the aid of Dr. M. K. Ramasubramanian.

LaTeX, primarily developed by Donald Knuth and Leslie Lamport, has a number of contributors who made it the word processor it is today. A great introduction is given in Kopka & Daly (1993). Thesis templates from both the University of Calgary written by Harish Bhanderi and another by N. Mancell were used to create a patchwork thesis to meet the NC State Mechanical Engineering Departments thesis guidelines.

Finally, there is the ultimate freeware contributor, Google. I was fortunate to learn about the full value of the somewhat hidden features of Google. Google Scholar lead me to several resources on both hovercraft and tethered satellites. Another time saver was the ability to automatically generate the LaTeX code for the bibliography; even for references that were not found on Google. Now if my wife would only let me apply for Google's Copernicus project...

Contents

List of Tables

List of Figures

Nomenclature[1]

Roman Symbols

a	Acceleration
C	A coefficient
CM	Origin of frame located at the center of mass
F	Force
f	Friction
H	Height of the Hovercraft
h	Moment of Momentum
I	Inertia
$\{i, j, k\}$	Unit vectors
M	Moment
m	Mass
P	Origin of reference frame at the geometric center of the body
Q	Origin of reference frame where the tether is attached to the body
O	Origin of the inertial reference frame
r	Displacement
v	Velocity

Greek Symbols

α	Angular acceleration
δ	Denotes angle of thrust force in P frame
ϕ	Angle of frame P about frame Q
μ	Viscocity of air
θ	Angle of frame Q about inertial frame O
$\{\varsigma, \chi, \psi\}$	Euler Angles
τ	Shear stress
ω	Angular velocity
ξ	Angle of frame CM about frame P

Subscripts

[1] Any symbol which is not a vector is assumed to be a magnitude or scalar

A	Specifies the frame A
A/B	Frame A with respect to frame B
$body$	Inertial Body
ext	External forces acting on the body
$fric$	Friction
rot	Rotational
ten	Tension
$thru$	Thrust
tot	Total
$trans$	Translational
$\{x, y, z\}$	Axes
τ	Shear stress

Superscripts

${}^{B}A^{C}$	Frame C with respect to frame B
${}^{O}A$	Derivitives are taken in the O frame

Other Symbols

[cos]	Cosine matrix
$\left[\vec{C}\right]$	Rotation matrix
$\vec{A}$	Specifies that A is a vector
$\left\{A, \dot{A}, \ddot{A}\right\}$	Derivitives of A with respect to time

Chapter 1

Literature Review

Ancient civilizations strived to build the tallest towers as a means to bring them closer to heaven. Today, space tethers take towers to new heights. While some designs allow alternative options for man's entry into space, others find applications leaving earth all together. The focus of this chapter is to follow the highlights of the nascent technology from its technical foundry to its current adolescence as it becomes familiar to the popular culture and into the future when the proposed applications come into fruition.

The idea of space travel has had an infectious appeal. In 1901, H. G. Wells first published *The First Men in the Moon* where the fictitious Cavor, due to an unexpected mishap with carbon, stumbled upon an antigravitational substance which he and a companion used to travel to other worlds. In 1961, Tsiolkovskii published *The Way to Stars*. Rather than a fiction novel, this paper set forth the first technical groundwork for a tether going from earth into space. He discussed the effects of the change of gravity on long bodies; the gravity gradient effect. Also, it was proposed that if the tether were a certain length it would be in a stable geosynchronous orbit. Tsiolkovskii (1961) It's ironic that a peculiar fiber of carbon could be the cable tethering earth to space; a much more plausible antigravitation scheme. Of course, even though the idea strikes most people as very unusual, it was bound to eventually catch on. After all, "[w]hatever it was, it was a thing with mechanical possibilities."Wells (2004)

Other pioneers in the field of tethered satellite research include Clement L. Tai and M. H. Lou. In 1964, they used the Lagrangian method to study the vibra-

tional modes of a tether. As a point of interest, they used an IBM 7094 to solve the fourth order Runge-Kutta. They showed that adding a velocity-proportional damping device to the satellite would effectively damp the vibration of the tether caused by the gravity gradient. Tai & Loh (1965) Other notable researchers during this time were Gerber and Chobotov who, in individual papers, showed that transverse vibrations occur due to parametric excitation because of coupling of the differential equations governing their motions. Gerber assumed point masses such that the tether was essentially the only body. He studied this scenario for the possible application of communication towers. Padgett (2006) Misra & Modi (1982) Also, C. Desmond Pengelley conducted a qualitative experiment[1] which demonstrated the inertial constraints required to have a stable tethered system. Pengelley (1966)

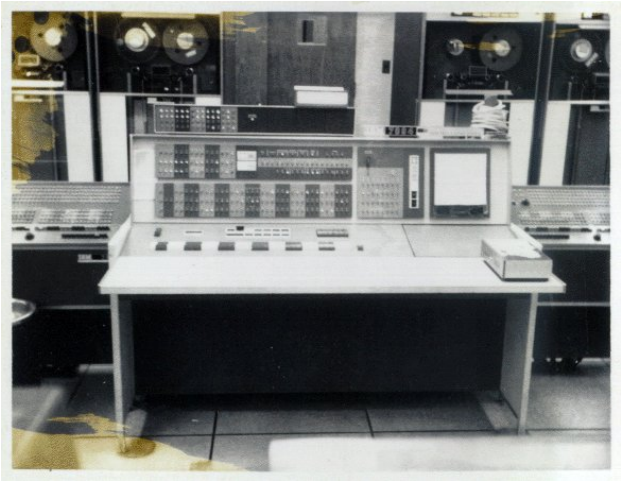

Figure 1.1: The IBM 7094 as used by Tai and Lou in 1964

There were other astronomical accomplishments in the 60's than just landing a man on the moon. Those first technical papers served as the small steps leading to the Gemini missions. Much of the Gemini XI and XII missions, flown in 1966, were concerned with testing the results of the papers by tethering the manned Gemini space capsule to the orbiting Agena spacecraft. The effects due to the gravity gradient were observed and some insight was obtained as to the

[1]It will be discussed further in the next section

capabilities of tethered satellites to produce an artificial gravity. Trivailo *et al.* (2002)

While research into the dynamics of tethered satellites continued to become more established, people began to realize that tethers offered more potential than originally conceived. The ideas range from simple application to complex maneuvers. Carroll (1985) It has been realized that by utilizing free electrons in space a tether can be used to create a sort of circuit. It creates flux forces that, depending on the direction of the current, can either boost or lower a satellites orbit. Chobotov (1963) This useful ability has found uses in deorbiting satellites which have been decommissioned. The Small Expendable Deployer System (SEDS-1) was launched in 1993 to test the theory. A tethered end mass was unreeled to 20km and then the tether was cut. The satellite was deorbited in a few months rather than years. Also, satellites can use the tether circuit to maintain a stable parking orbit; referred to as an electrodynamic reboost. The International Space Station is a potential candidate for the latter ability. Doty *et al.* (1995) Johnson & Herrmann (1998)

The Tethered Satellite System (TSS-1) experimented with the electrical potential of tethers. It experienced difficulties which turned out not to be altogether fruitless. During the first flight in 1992 the tether failed to reel out entirely. However, the experiment was still conducted up to the point of failure yielding results. In the second attempt (TSS-1R), launched in 1996, the electron density in the ionosphere was significantly greater than expected which resulted in a design failure. The tether managed to reach its full length, but eventually the cable broke due to an electrical arc. This event validated and strengthened arguments to exploit the ionosphere in future missions. NASA (2000)

A major concern was how long a tether would last in a space environment. The Tether Physics and Survivability Spacecraft (TiPS) was flown in 1996. The 4km cable is still in space and can actually be seen with just a pair of binoculars. Purdy *et al.* (1997)

Another field of research looks at some of the same principles to utilize tethers as sensors. If a tether creates a circuit in the ionosphere, then it can measure the electric field and make predictions of the content of the ionosphere in the vicinity. Similar statements can be made for the electric wave, magnetic field,

particle measurements, gravity, etc. The Oedipus A (1989) and Oedipus C (1995) missions took advantage of those abilities to measure the characteristics of the earth. Tyc *et al.* (1996)

More complicated missions demand a thorough knowledge of the spacecraft kinematics. Part of the challenge of space travel is to get to the destination as quickly and efficiently as possible. Trivailo *et al.* (2002) A common method is to use a gravity assist from another planet to alter the trajectory to increase velocity. Penzo suggests that if a spacecraft could use a tether to temporarily hold on to a nearby asteroid to alter the trajectory. Penzo & Mayer (1986) That would be an interesting and frightening challenge to overcome.

Fortunately, there is a more controlled alternative which offers the same benefit. It is commonly called the Momentum Exchange/Electrodynamic Reboost (MXER) tether. In this scenario, a tether is put in orbit and is given a certain orbit. The spacecraft still has to temporarily dock with the tether. At which point the tether and spacecraft exchange momentum. The exchange launches the spacecraft into a higher orbit. The trade off is that in order to conserve momentum the tether drops into a lower orbit. It can then use the electrodynamic reboost previously discussed to raise it back to its original orbit. Sorensen (2003)

Much of the current research focuses on various methods of control of the tethered bodies. Rather than using a thruster system reduce the oscillations, another approach is to alter the length of the tether to compensate. Modi *et al.* (1997) Bekey (1997)

1.1 Ground-Based Experimentation

Ground-based experimentation is a useful ability for verifying the initial results of theoretical analysis. It can save time and money in designing future missions to be conducted in space. However, there are a number of shortcomings listed by Schultz that result by conducting tests on earth which must be considered. They include gravity, scale of testing, temperature variations, humidity, the presence of air, and load history and load rate of the tether. Schultz designed an experiment to test the tether material properties over time which provides partial answers to

a few of the concerns. Higuchi developed an experiment which allows the effects of the gravity gradient on the kinematics of a tethered body.

Schultz considers the potential for both vertical and horizontal tethers to resemble the effects of the gravity gradient effect. In space, the force distribution along the tether takes on a parabolic profile, while a vertical configuration on a smaller test scale on the earth is nearly linear. Instead, he recommends using a horizontal test tether which is supported intermittently along its length. Working with the Canadian Space Agency he constructed a lab where a 38m tether sample could be tested. In addition to an approximation of the gravity gradient, the lab setting was designed to make temperature differences and load frequencies similar to actual mission scenarios. Schultz *et al.* (2002)

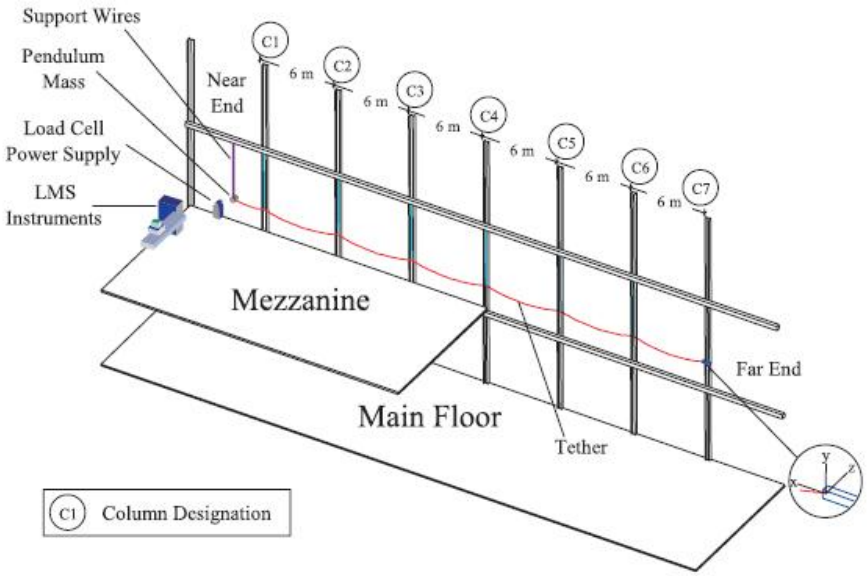

Figure 1.2: The Experiment Designed by Schultz

In order to fully observe the effects of the gravity gradient, Higuchi devised an entire rotating test environment. He utilizes the platform to create an artificial gravity. In order to reduce the effects of air drag, the area around the test environment is surrounded by a wind shield. An interesting feature of the experiment is that a block of dry ice was used to represent the end body. Higuchi *et al.* (1997)

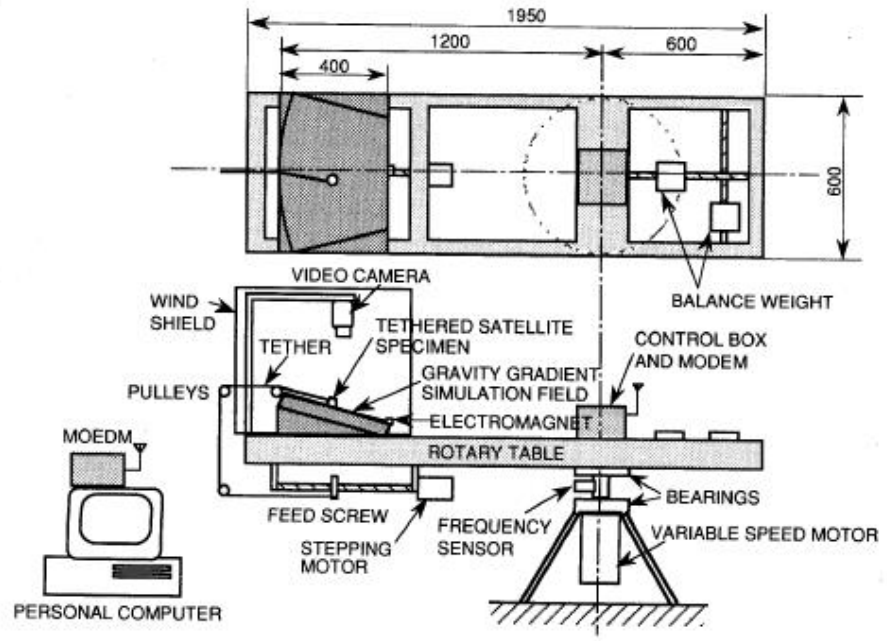

Figure 1.3: The Experiment Designed by Higuchi

One of the first experiments was conducted by Pengelley and tested the stability requirements of a tethered system. The tethered apparatus is shown in the following figure. One body has a hobby model rocket motor attached to it. The other has been fitted with an approximate equivalent mass. The apparatus was catapulted as the rocket ignited, spinning the system into either a stable or unstable orbit depending on inertial requirements. As Pengelley states, "It is well known that a 'rigid' body is unstable when made to spin about its principal axis of intermediate moment of inertia." His experiment qualitatively showed the system would be stable as long as the moment of inertia about his I_3 axis is greater than his I_1 axis.

Modi conducted a couple experimental investigations into the dynamics of tethered satellites. In 1990, he utilized a 2 axis position table to validate his research into an offset control strategy. Once the tether was disturbed the actuators on the table would compensate to keep it vertical. In his experiment the gravity gradient was neglected. Modi *et al.* (1990) Another experiment by Modi rotated

the end body in order to identify the modes of the tether. Several geometries of the end body were tested to see the effects. Modi *et al.* (1996)

Developing a single experiment which is fully representative of an entire tethered satellite system is too great a challenge. However, conducting several experiments which individually represent a fraction of the system is possible. This thesis represents one more piece for the puzzle.

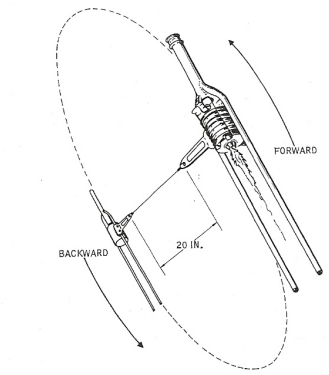

Figure 1.4: The Tethered Apparatus utilized by Pengelley

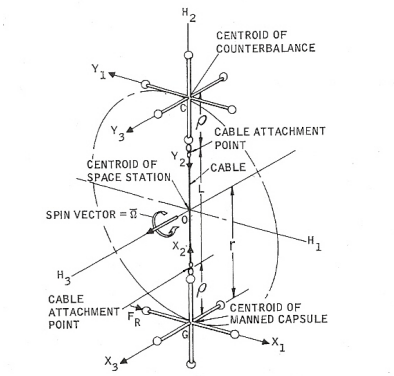

Figure 1.5: The Coordinate System Pengelley Used

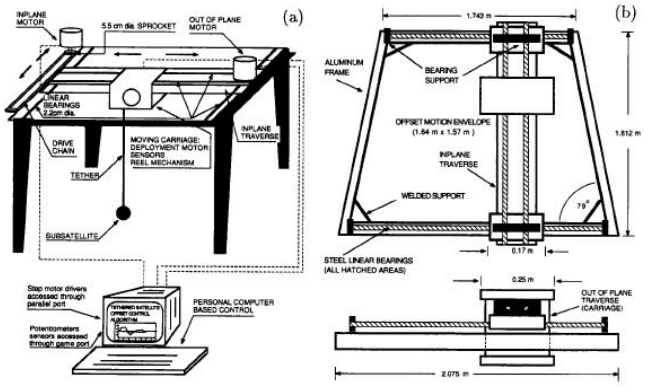

Figure 1.6: Diagram of the Table Setup used by Modi

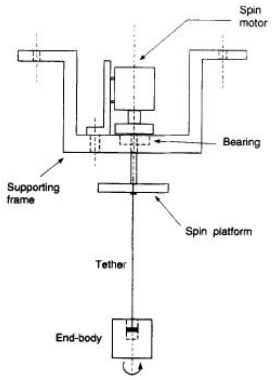

Figure 1.7: Diagram of the Spin Setup used by Modi

Chapter 2

Introduction

Tethers are finding several applications in the space industry. They can provide an alternative to using propellant for propulsion. By using tethered satellites as momentum exchangers they can be used to transfer their momentum to a payload, sending the payload into a higher orbit. Since the tether losses momentum it falls into a lower orbit. Another proposed application is to use the Earth's magnetic field to interact with a conductive tether for orbital correction, or alternatively, to bring decommissioned satellites out of their orbits in a shorter amount of time. Typically, the reboost application is considered along with the momentum exchanger concept to reboost the tethered satellite. This is commonly referred to as MXER (Momentum eXchange Electrodynamic Reboost). TUI (2006)

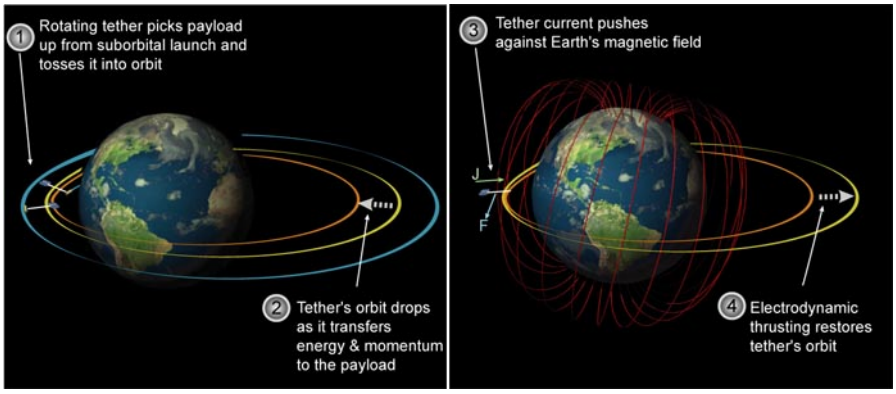

Figure 2.1: Description of a MXER System

Before attempting such complicated missions it is useful to conduct ground-based experiments. As briefly stated in the literature review, ground-based experimentation has several advantages. It is cost effective and provides an opportunity to gain a greater understanding of the feasibility of tethered space applications. Each one offers different insights into the total description of the tethered behavior; from survivability to dynamics. An experiment is presented to provide one more tool in the analysis of tethers. In order to check that the experiment describes the system, it is compared to a mathematical model derived using Newton-Euler methods. The findings are discussed in the conclusion.

Chapter 3

The Experimental Apparatus

3.1 Overview of the Experiment

The primary objective of the experimental design is to emulate a tethered satellite which has stabilized into a planar orbit. Only one end of the tether is necessarily attached to a satellite. It is also possible to attach both ends of the tether to a separate satellite, however that setup is more difficult to control. In general, the other end of the tether is attached to an inertial body which represents the center of mass of the system. A primary concern with the design for a model of a satellite is to minimize friction. A hovercraft was designed to meet that criteria.

In order to gather information from the experiment a camera was mounted in a position where it could observe the full testing area. The video from the camera was transfered to a computer for analysis. MatLab[1] has the ability to find objects in an image as well as information about the objects. To aid the program in finding the object, a cover was place over the hovercraft. The following table lists the parts utilized in the experiment. The ensuing sections describe the various components of the experiment and how the parts were utilized.

[1]Object recognition using MatLab requires the Image Acquisition and Image Processing toolboxes

Bill of Materials

Cost of a Hovercraft

Item #	Component	Supplier	Item #	Quantity	Cost/ Component	Total Cost
1	Microcontroller	Technological Arts	NC12DXSSMI	1	$90.00	$90.00
2	Batteries	Electrifly	GPMP0830	2	$39.00	$78.00
3	Servo	HiTEC	33065	1	$29.89	$29.89
4	3'x4' Sheet of Aluminum	Lowes		1	$25.00	$25.00
5	Electric ducted Fan	GWS	EDF-50	2	$11.73	$23.46
6	15'x2" Velcro	Lowes	90198	1	$15.90	$15.90
7	10ft of .5" Diameter Plastic Tubing	Lowes		1	$5.00	$5.00
8	foam board	Lowes Foods		1	$2.99	$2.99
9	Garbage Bags	Lowes Foods		1	$2.99	$2.99
Cost of Inertial Base						
1	Journal Bearing	Lowes		1	$7.99	$7.99
2	Base of Lamp			1	0	0
Cost of Vision Equipment						
1	Panasonic Mini DV Camcorder	Best Buy	PV-GS39	1	$349.99	$349.99
2	Clamp Set	Lowes	212050	1	$22.96	$22.96
					Total	$643.19

3.2 The Lab Environment and Camera Mount

One ordeal with using a hovercraft for research is finding a large enough flat surface to test it. The optimal location turned out to be a squash court in Charmichael Gymnasium at North Carolina State University. After placing the inertial mass in the center of the court it provided 9' 2" on every side. The court has a 15' high ledge typically used by an instructor to observe students' performance. In this instance it provided the perfect mount for a camera. The camera was secured inside of an altered box. A rope attached the box to another platform designed to clamp to the ledge. By changing the length of the rope and the positioning of the apparatus on the ledge, the camera angle could be easily manipulated. To prevent damaging the surface of the ledge by the clamps a towel was place under the entire apparatus.

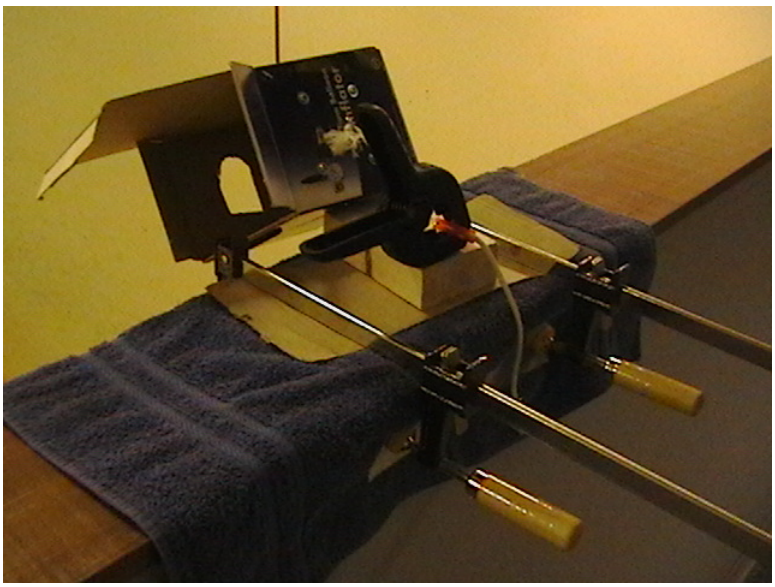

Figure 3.1: The Camera Mount on the Squash Court Observation Ledge

3.3 The Inertial Mass

The inertial mass consists of a heavy base (the base of a standing lamp) which is low to the ground. Rubber grippers were used to further prevent the base from

sliding. A journal bearing was used to prevent the tether from snagging on the base due to friction or lack of tension.

Figure 3.2: The Inertial Mass

3.4 The Hovercraft

A hovercraft was used to minimize friction. However, there were still a number of other factors to design around. In order to maximize stability a base with a large area and close to the ground profile were desired. Ducted fan motors were used both to provide the air cushion for the craft to hover and the thrust for it to maneuver around the inertial mass. A servo was used to reel and unreel the tether. To provide power to the various components, 1500mAh 7.4V lithium ion batteries were used. One battery was used for both of the lift fans. Two batteries in parallel were also tested on the lift fans. While they provided extra lift, a single battery was less weight, less complication, and still provided adequate lift. The lift fans needed to stay on continuously, so the battery could be connected directly to them with only minor circuitry. However, control over the thrust fans and servo were desired. The implementation of a microcontroller made making

changes to the system as simple as altering a few lines of code. Freescale (2002) The microcontroller requires a 5V source. It possesses voltage regulators which allow one of the batteries, even though they are 7.4V, to be utilized to control the various components. The microcontroller allowed the use of one or two thrust fans. The use of a switch statement allows the fans and servo to turn on or off in any sequence. Also, the thrust of the fans is controlled by altering the duty cycle. The duty cycle is controlled by an 8 bit integer which theoretically should give 256 levels of thrust. However, due to friction in motor joints and other real world factors, it was observed that the motor would no longer run when the duty cycle's low time integer variable was 45 or greater. A thrust map for both 1 fan and for 2 fans is shown in the figure below. The forces were measured at various battery voltage levels without significant change. The voltage regulators in the microcontroller reduce any effect that varying voltages would have.

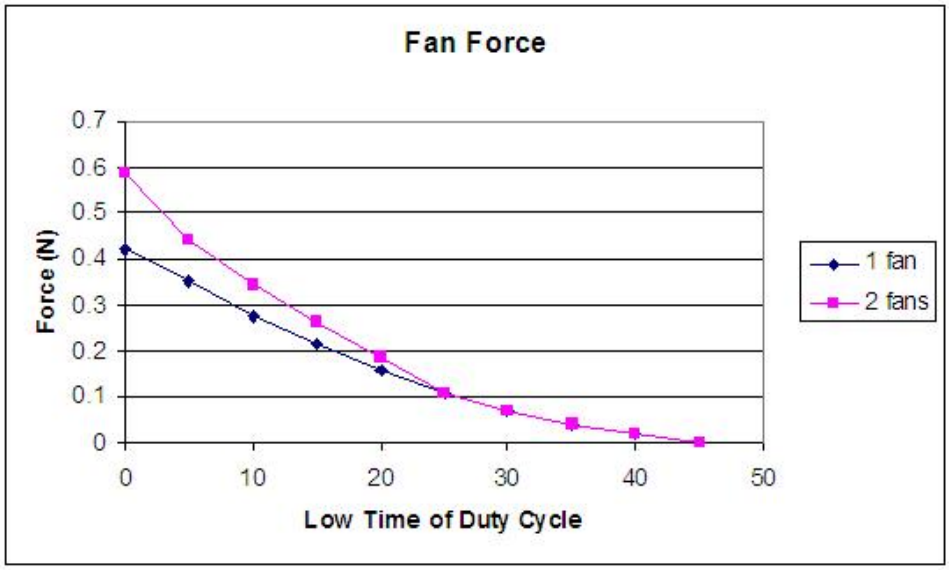

Figure 3.3: Thrust Map

An important design consideration was the fabrication of the skirt. There are several methods for making a skirt; each for different environments. Industrial hovercrafts, which may be used to go over rough terrain or water, typically have "fingers". As a rock or other impediment passes under the cushion the finger

slides over the object while still maintaining an acceptable air pressure under the craft. These designs are rather complicated and necessarily create friction. Lavis (1985) In some toy hovercraft the air pressure is first used to inflate a tube around the perimeter of the hovercraft. The air then escapes though holes in the tube under the main body of the craft and finally passes under the tube to the environment. Using this setup would reduce friction, however the design and fabrication is still rather complicated. The California Institute of Technology utilized a plastic dinner plate in their design for a research hovercraft. While it would be appropriate for their applications (formation control of multiple objects), a dinner plate sized skirt would not have a suitable area to hold all the equipment. Also, durability was a concern. Jin *et al.* (2004)

Since no other methods seemed adequate, a new method of assembly of the skirt was devised. After deciding on the general shape and size of the hovercraft a length of 1/4" plastic tubing was cut to cover the perimeter. The ends of the tubing were taped together. The tubing was laid on a garbage bag, and the bag was then cut around the perimeter leaving about 2" extra all around. The extra was folded over the tubing and duct tape was used to secure it in place. The completed skirt is shown in the following figure.

Figure 3.4: Skirt of the Hovercraft

Both a circular and an elliptical hovercraft were constructed. An elliptic hovercraft is able to lift more weight for a given surface area than a circular craft. The reason for this is that the air maintains its velocity as it is directed along the major axis of the elliptic hovercraft and escapes at the further edges. In a circular hovercraft, the air loses velocity in every direction. This is the reason that industrial hovercraft are designed about twice as long as they are wide. Lavis (1985)

A couple options were considered for the material for the main structure of the hovercraft. Several variables needed to be tested which required the setup to be altered several times. Velcro allows all the components to be firmly held in place during testing and then easily relocated to test other factors. Foam board is especially lightweight and is durable enough for the base of the craft. Another option was aluminum. Even though it is significantly heavier than foam board, it could also be bent to serve as housings for the other components. Also, the extra durability would help ensure that through multiple trials the integrity would remain. It was decided that the components which needed structural stability would be made of aluminum, while the cover used to help the camera see the hovercraft would be made of foam board.

Even though the foam board for the cover was white, a long, black strip of paper was taped in the center. The program does not attempt to locate the object based on the black or white segments of the cover separately. Instead, it looked for a black strip surrounded by an area of white. The background of the image appeared to be a black object. However, since the background is not surrounded by a white border, the background is not recognized. Another advantage of looking for an object inside of another object is that little regard needs to be given to the clothing the experimenter wears during the tests. Dark clothing is not distinguished from the rest of the background. As long as light clothing does not have a dark pattern or emblem on the fabric, the program will also recognize that it is not of importance. Being able to distinguish a person from the hovercraft implied that detection could begin as soon as the hovercraft was released; an important ability to record initial conditions.

Once the hovercraft was finished an additional concern was noted. If the base of the hovercraft is perfectly flat and the mass of the hovercraft is located at

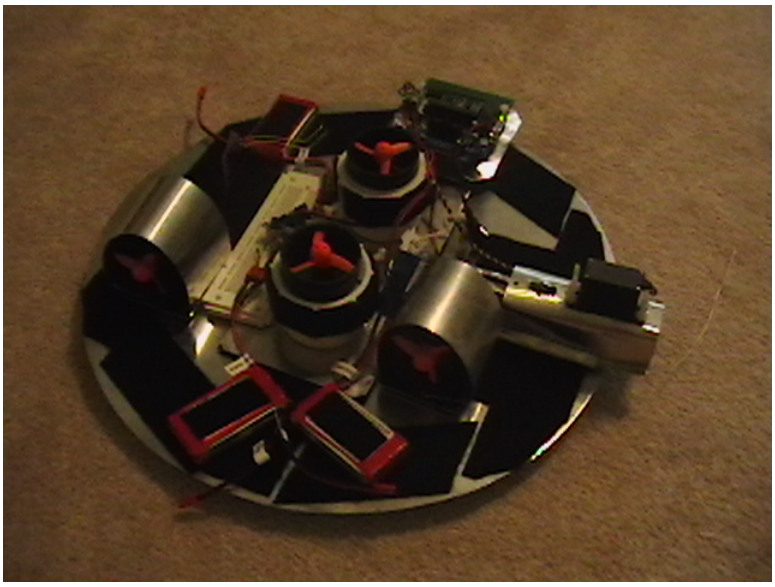

Figure 3.5: The Completely Assembled Circular Hovercraft

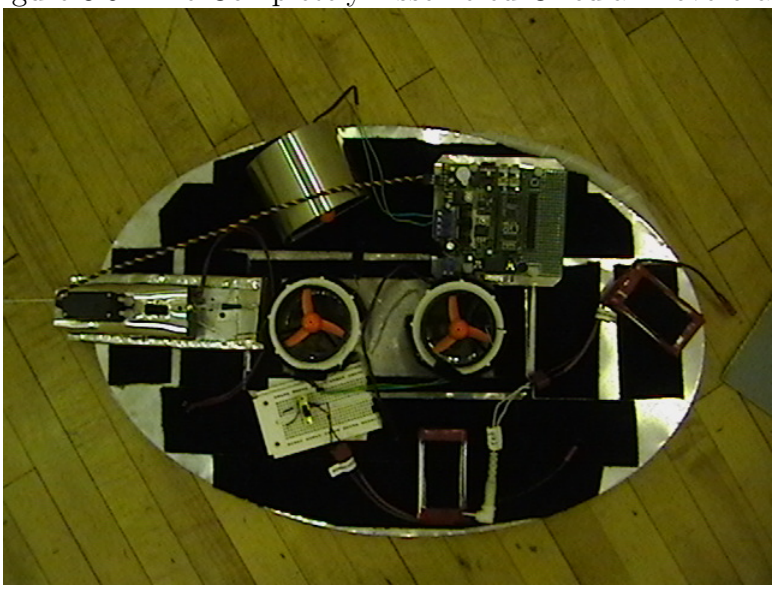

Figure 3.6: The Completely Assembled Elliptical Hovercraft

its center, it will hover in place. However, if the mass is shifted away from the center more air escapes from one side of the skirt that any other causing it to move forward or rotate. However, since aluminum was used the base does not have to be perfectly flat. It can be bent to compensate for a mass which is off center. The figure below illustrates this idea. This allows for the variable of where the center of mass is located to be tested to some degree. However, the entire geometry is sensitive and there will always tend to be some translation or rotation. Also, if there is too much bending the skirt could drag on the surface at points dramatically altering the results. The practice can be used advantageously, but it can also be a burden to correct.

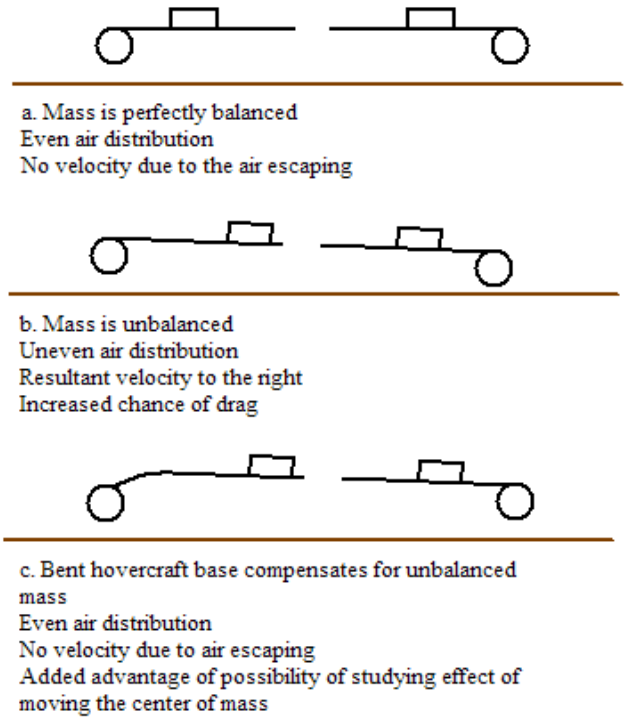

Figure 3.7: The Effects of an Off-Center Mass and a Method to Correct the Unbalance

3.5 Vision Recognition

The program for vision recognition subtracts one image with an object of interest from another image which is identical to the background. After the subtraction all that is left is the object. Once the program finds the object it can determine a variety of information about it. All the information is stored in a structured array. The object's center is given as two numbers; the number of pixels the center is from the left side of the image and the number of pixels the center is from the top of the image. It also tells the angle the object makes relative to a horizontal row in the image. To reduce the error of this piece of information it is best to use as long of a black strip as possible. Testing a black strip 18" long and 3" wide yielded angles that were within $\pm 3°$.

The first step in using the program for vision recognition is to do configuration. The simplest configuration involves telling the program where certain locations on the squash court are located. The figure below shows the background image for a particular test. The various locations which need to be specified are indicated.

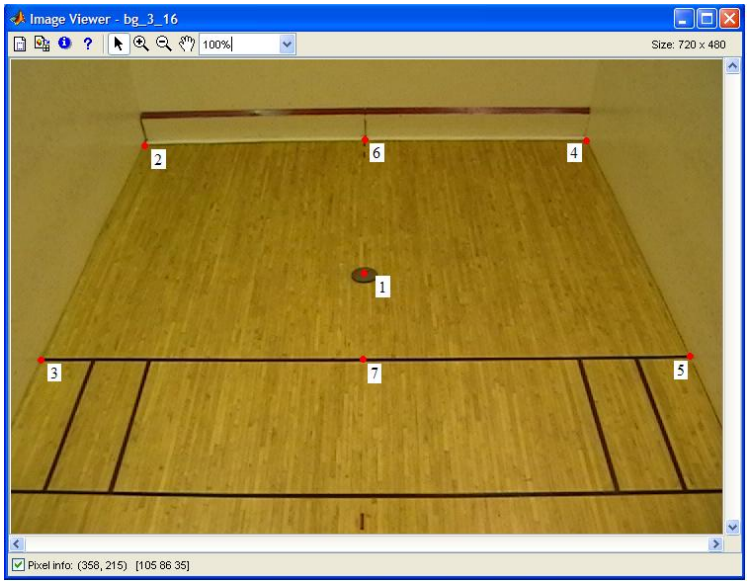

Figure 3.8: Seven Positions on the Image of the Squash Court Needed for Configuration

The first position is where the tether is attached to the inertial mass. In the

bottom left hand corner of the image the window shows (358,215). When the picture was copied, the pixel was over the inertial mass, so those two numbers represent the number of pixels from the upper most and the left most part of the image, respectively. Alternatively, the position of the inertial mass could simply be measured; which ever is more convenient. Positions 2, 3, 4, and 5 represent four corners which which are utilized to determine the position of the hovercraft. First, they are used to specify four individual lines represented below. The actual distance between the points is also measured and specified within the program. Determining the distances from the left and upper wall requires separate analysis.

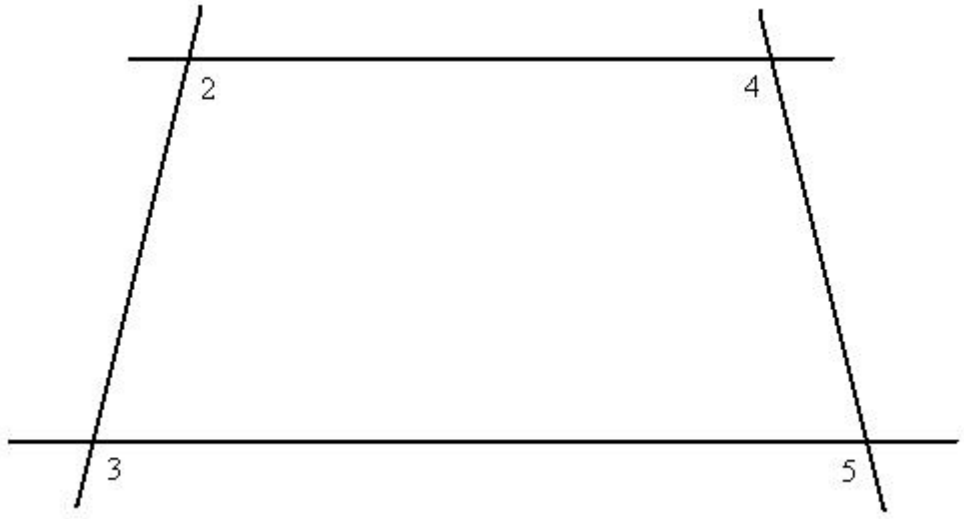

Figure 3.9: Four Positions Are Used to Specify Four Lines

The distance of the hovercraft from the left wall is straight forward. It is determined as a percentage between the two parallel walls. Determining the distance from the upper wall is more problematic. The difficulty arises because the camera is mounted at an angle. The pixels directly under the upper wall represent a greater distance that the pixels further down the image. Using geometry a polynomial expression can be obtained to correct for the discrepancy. Once accomplished, tests were conducted to check the accuracy of the program. The cover was positioned at various locations around the court. The distance

was measured from both the left and upper walls. The program yielded results within $\pm 1in$. Once the position of the hovercraft and the inertial mass are both known, the angle between them can be determined with simple trigonometry. The method of acquiring the experimental data is similar to that of Higuchi *et al.* (1997).

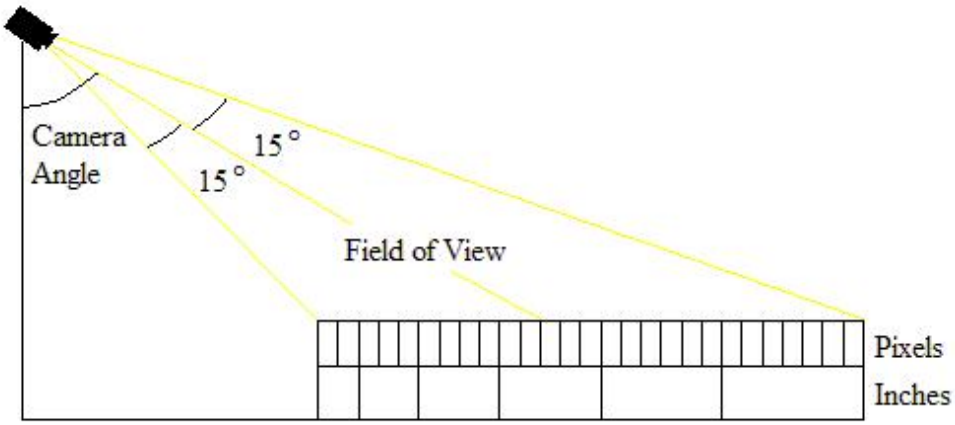

Figure 3.10: The Discrepancy Between Distance and Pixel Intervals

Glare can cause problems. Occasionally, there may be an instance where multiple objects may be found. One common solution is to be more stringent with the sizes of the objects that the program recognizes. Also, the entire image does not necessarily need to be analyzed. It is easy to specify a block of rows to entirely ignore. If sections can be ignored they can be deleted from the array of images, saving both memory on the hard drive and time analyzing them.

Chapter 4

Modeling and Simulation of the Dynamics of the System

4.1 Introduction

Considering each aspect of the tethered system all at once is a rather complex system. Instead, simpler systems are first analyzed working up to the completed model. Ginsberg (1998) may be referenced as a guide to the general procedure of the analysis. A simpler system implies that more assumptions have been made which make the analysis more straight forward. The beginning of each section describes in detail the model being analyzed and the assumptions being made for that model. However, this section may be useful in visualizing the simplifications of the subsequent chapters.

The final model is described here to give a better understanding of the final goal. It is shown in figure 4.1. The inertial reference frame has its origin at point O. Another reference frame, Q, makes an angle θ with the inertial frame. The distance between the Q and O is described by $\vec{r}_{Q/O}$. This distance is the length of the tether. The rate of change of $\vec{r}_{Q/O}$ may not be constant. A body frame has its origin at point P which is embedded in the geometric center of the craft. It makes an angle ϕ with the Q frame. A constant length, $\vec{r}_{P/Q}$, characterizes the distance from the from P to the end of the tether at point Q. Another frame is located at the center of mass of the craft. The distance between the center of mass of the craft and the geometric center is a constant length, $\vec{r}_{CM/P}$.

There are three forces acting on the system. The force of the tension in the tether acts at Q in the direction of the tether. A thrust force acts at point P. It always points in a constant direction relative to the body fixed P frame. The magnitude of the thrust can either be constant or vary with time. And a friction force which is assumed to act at the center of mass and opposes the velocity of the craft. An exact expression for the amount of friction is unclear. However, a reasonable approximation can be developed by considering the kinetic coefficient of friction and the viscous damping terms.

The positive Z axis of each plane comes out of the page. From the right hand

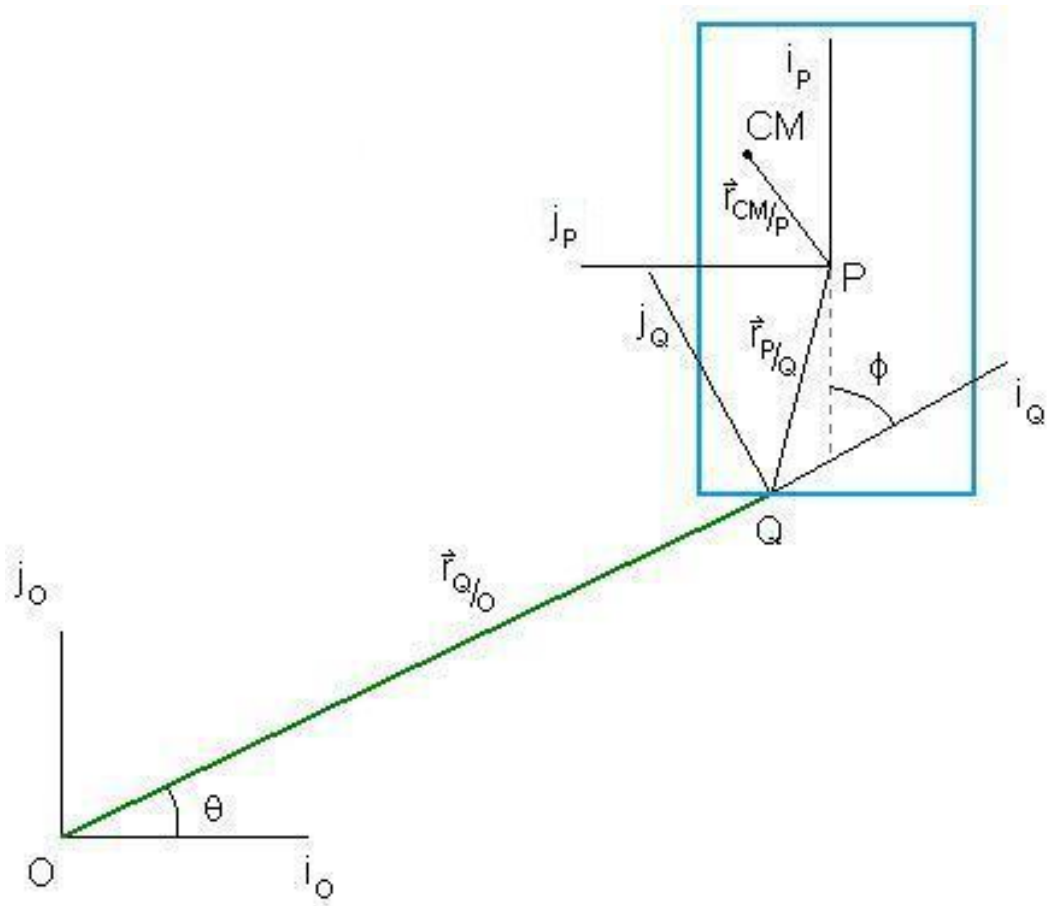

Figure 4.1: Completed Model

rule a positive rotation is given to be in the counter-clockwise direction. Every system is considered planar such that the only rotation is about the Z axis.

4.2 The Simplest Model of the Tethered System

4.2.1 Physical Description

The initial system has considerable simplifications. It is assumed that the tether is a constant length. This implies that derivatives of $\left|\vec{r}_{Q/O}\right|$ are 0.

$$\frac{{}^{O}d}{dt}\left|\vec{r}_{Q/O}\right| = 0 \tag{4.1}$$

$$\frac{{}^{O}d^2}{d^2t}\left|\vec{r}_{Q/O}\right| = 0 \tag{4.2}$$

The origins of frames Q and P coincide.

$$\vec{r}_{P/Q} = 0 \tag{4.3}$$

A final simplification is that there is no friction.

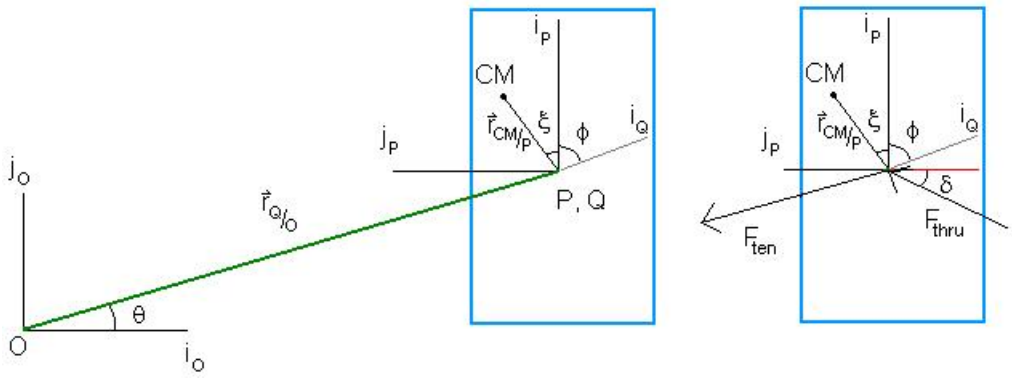

Figure 4.2: Simplified Model and Free Body Diagram

Figure 4.2 shows the system to be discussed. The free body diagram shows the two forces acting on the body; the force from the tension in the tether, $\vec{F}_{ten}$,

and the force from a source of thrust, $\vec{F}_{thru}$. In this scenerio they both act at the geometric center of the body. Examples of devices to provide the thrust are a rocket or fan for a satellite or hovercraft, respectively. The thrust device is assumed to be fixed on the body of the craft. This implies that the angle δ is a constant with respect to the body frame.

4.2.2 Equations of Motion of the System

Before getting into the details specific to the simplified case it is useful to first develop the equations that will be used to solve every system.

The Moment Equation

The moment of momentum equation taken at the center of mass of a rigid body is given in Thomson (1986) and Ginsberg (1998). The angular velocity and moment of momentum take the following form in general.

$$
\begin{aligned}
{}^{O}\vec{\omega}^{CM} &= \omega_x \vec{i}_O + \omega_y \vec{j}_O + \omega_z \vec{k}_O && (4.4)\\
\left\{ {}^{O}\vec{h}_{CM,body} \right\}_O &= [I_{CM}] \left\{ {}^{O}\vec{\omega}^{CM} \right\} && (4.5)\\
&= \begin{bmatrix} I_{xx} & -I_{xy} & -I_{xz} \\ -I_{xy} & I_{yy} & -I_{yz} \\ -I_{xz} & -I_{yz} & I_{zz} \end{bmatrix} \begin{Bmatrix} \omega_x \\ \omega_y \\ \omega_z \end{Bmatrix} && (4.6)\\
&= \begin{Bmatrix} I_{xx}\omega_x - I_{xy}\omega_y - I_{xz}\omega_z \\ -I_{xy}\omega_x + I_{yy}\omega_y - I_{yz}\omega_z \\ -I_{xz}\omega_x - I_{yz}\omega_y + I_{zz}\omega_z \end{Bmatrix} && (4.7)\\
{}^{O}\vec{h}_{CM,body} &= \left(I_{xx}\omega_x - I_{xy}\omega_y - I_{xz}\omega_z\right) \vec{i}_O && (4.8)\\
&+ \left(-I_{xy}\omega_x + I_{yy}\omega_y - I_{yz}\omega_z\right) \vec{j}_O && (4.9)\\
&+ \left(-I_{xz}\omega_x - I_{yz}\omega_y + I_{zz}\omega_z\right) \vec{k}_O && (4.10)
\end{aligned}
$$

However, since the motion is planar, ω_x and ω_y are negligible. Also, if principle axes are assumed, I_{xz} and I_{yz} also drop out.[1] Also, the angular velocity term can

[1] In the experiment discussed in later chapters, the flat profile of the hovercraft helps to identify the principle axes for this assumption.

be broken down into its components. Note that since all rotations occur along the k axis each of the frames can be translated to the inertial reference. Also, the frame at the center of mass rotates with frame P which implies ${}^{P}\vec{\omega}^{CM}$ is 0. So, expressions which are more appropriate for the system at hand can be written for the angular velocity and the moment of momentum.

$$\begin{aligned} {}^{O}\vec{\omega}^{CM} &= {}^{O}\vec{\omega}^{Q} + {}^{Q}\vec{\omega}^{P} + {}^{P}\vec{\omega}^{CM} = {}^{O}\vec{\omega}^{Q} + {}^{Q}\vec{\omega}^{P} \\ &= \left({}^{O}\omega_z^{Q} + {}^{Q}\omega_z^{P}\right)\vec{k}_O \qquad (4.11) \\ {}^{O}\vec{h}_{CM,body} &= I_{zz}\omega_z\vec{k}_O = I_{zz}\left({}^{O}\omega_z^{Q} + {}^{Q}\omega_z^{P}\right)\vec{k}_O \qquad (4.12) \end{aligned}$$

For a rigid body the moment equation taken at principal axes at the center of mass is the derivative of the moment of momentum. The planar assumption is again used to simplify the expression for the derivative of ${}^{O}\vec{\omega}^{CM}$. However, since angular accelerations are not actually addititive it cannot be broken down as in quite the same fashion as 4.11.

$$\begin{aligned} {}^{O}\vec{\alpha}^{CM} = {}^{O}\vec{\alpha}^{Q} + {}^{Q}\vec{\alpha}^{P} + {}^{P}\vec{\alpha}^{CM} &= {}^{O}\alpha_z^{CM}\vec{k}_O \\ &= \frac{{}^{O}d}{dt}\left({}^{O}\omega_z^{CM}\vec{k}_O\right) \\ &= \frac{{}^{O}d}{dt}\left({}^{O}\omega_z^{Q}\vec{k}_O + {}^{Q}\omega_z^{P}\vec{k}_Q + {}^{P}\omega_z^{CM}\vec{k}_P\right) \\ &= {}^{O}\alpha_z^{Q}\vec{k}_O + {}^{Q}\alpha_z^{P}\vec{k}_O + {}^{O}\omega_z^{Q}\vec{k}_O \times {}^{Q}\omega_z^{P}\vec{k}_O \\ &= {}^{O}\alpha_z^{Q}\vec{k}_O + {}^{Q}\alpha_z^{P}\vec{k}_O \\ &= \left(\ddot{\theta} + \ddot{\phi}\right)\vec{k}_O \qquad (4.13) \end{aligned}$$

The frames oriented at point P and point CM rotate together which implies that ${}^{P}\omega_z^{CM}\vec{k}_P$ is 0. Since the Z axes of every frame are oriented in the same direction the cross product term cancels out. This leads the moment equation to be

$${}^{O}\vec{\tau}_{CM,body} = I_{zz}\left(\ddot{\theta} + \ddot{\phi}\right)\vec{k}_O \qquad (4.14)$$

Sum of the Forces

Newton's Second Law of motion provides the other required equations.

$$(\Sigma\vec{F})_{sys,ext} = m_{tot}\frac{{}^{O}d^2}{dt^2}(\vec{r}_{CM/O}) \tag{4.15}$$

Once expressions for all the terms have been developed they must all be in terms of the inertial reference frame. The terms can be altered through a rotation matrix. For a planar case it is a straight forward calculation. However, since it is used frequently, it is worthwhile to develop the transformation here.

Let there be two reference frames, A and B, with axes (x_A, y_A, z_A) and (x_B, y_B, z_B), respectively. If a vector $\vec{C}$ is fixed in the B frame and the frame B undergoes a NASA rotation sequence with respect to frame A, $\{\varsigma, \chi, \psi\}$, the components of $\vec{C}$ in terms of A can be determined.

Now, for a planar case ς and χ are 0. So, the following expressions represent the individual rotations.

$$[cos]_z = \begin{bmatrix} \cos(\psi) & -\sin(\psi) & 0 \\ \sin(\psi) & \cos(\psi) & 0 \\ 0 & 0 & 1 \end{bmatrix} \tag{4.16}$$

$$\begin{aligned} [cos]_y &= \begin{bmatrix} \cos(\chi) & 0 & \sin(\chi) \\ 0 & 1 & 0 \\ -\sin(\chi) & 0 & \cos(\chi) \end{bmatrix} \\ &= \begin{bmatrix} 1 & 0 & 0 \\ 0 & 1 & 0 \\ 0 & 0 & 1 \end{bmatrix} \end{aligned} \tag{4.17}$$

$$\begin{aligned} [cos]_x &= \begin{bmatrix} 1 & 0 & 0 \\ 0 & \cos(\varsigma) & -\sin(\varsigma) \\ 0 & \sin(\varsigma) & \cos(\varsigma) \end{bmatrix} \\ &= \begin{bmatrix} 1 & 0 & 0 \\ 0 & 1 & 0 \\ 0 & 0 & 1 \end{bmatrix} \end{aligned} \tag{4.18}$$

The rotation matrix is the product of the cosine matrices, but for a planar case

two of the direction cosine matrices reduce to identity, such that the expression for the rotation matrix in an A frame, $\left\{\vec{C}\right\}_A$, with respect to a B frame is

$$\left\{\vec{C}\right\}_A = \begin{bmatrix} \cos(\psi) & -\sin(\psi) & 0 \\ \sin(\psi) & \cos(\psi) & 0 \\ 0 & 0 & 1 \end{bmatrix} \left\{\vec{C}\right\}_B \tag{4.19}$$

Continuing with the Analysis

The moment resulting from the inertial body has been developed. Now expressions for the moments produced by the external forces are required. These can be attained by analysis of figure 4.2.

$${}^O\vec{\tau}_{CM,forces} = -\vec{F}_{ten} r_{CM/P} \sin(\phi + \xi) + \vec{F}_{thru} r_{CM/P} \cos(\delta + \xi) \tag{4.20}$$

Setting the moments from the inertial body and the external forces equal to each other yields the completed moment equation.

$$I_{zz}\left(\ddot{\theta} + \ddot{\phi}\right)\vec{k} = -\vec{F}_{ten} r_{CM/P} \sin(\phi + \xi) + \vec{F}_{thru} r_{CM/P} \cos(\delta + \xi) \tag{4.21}$$

In order to develop an equation based on the sum of the forces the acceleration has to be determined.

$${}^O\vec{a}_{CM/O} = {}^O\vec{a}_{P/O} + {}^O\vec{a}_{CM/P} \tag{4.22}$$

$$\vec{r}_{P/O} = r_{P/O}\cos(\theta)\vec{i}_O + r_{P/O}\sin(\theta)\vec{j}_O \tag{4.23}$$

$${}^O\vec{v}_{P/O} = -r_{P/O}\dot{\theta}\sin(\theta)\vec{i}_O + r_{P/O}\dot{\theta}\cos(\theta)\vec{j}_O \tag{4.24}$$

$${}^O\vec{a}_{P/O} = r_{P/O}(-\ddot{\theta}\sin(\theta) - \dot{\theta}^2\cos(\theta))\vec{i}_O \tag{4.25}$$

$$+ \; r_{P/O}(\ddot{\theta}\cos(\theta) - \dot{\theta}^2\sin(\theta))\vec{j}_O$$

$$\vec{r}_{CM/P} = r_{CM/P}\cos(\phi + \xi)\vec{i}_P + r_{CM/P}\sin(\phi + \xi)\vec{j}_P \tag{4.26}$$

$${}^P\vec{v}_{CM/P} = -r_{CM/P}\dot{\phi}\sin(\phi + \xi)\vec{i}_P + r_{CM/P}\dot{\phi}\cos(\phi + \xi)\vec{j}_P \tag{4.27}$$

$${}^P\vec{a}_{CM/P} = r_{CM/P}(-\ddot{\phi}\sin(\phi + \xi) - \dot{\phi}^2\cos(\phi + \xi))\vec{i}_P \tag{4.28}$$

$$+ \quad r_{CM/P}(\ddot{\phi}\cos(\phi+\xi) - \dot{\phi}^2\sin(\phi+\xi))\vec{j}_P$$

Now the transport theorem is used to find the velocity and acceleration of the body with respect to the inertial frame.

$$\begin{aligned} {}^O\vec{v}_{CM/P} &= {}^P\vec{v}_{CM/P} + {}^O\vec{\omega}^P \times \vec{r}_{CM/P} && (4.29)\\ &= -r_{CM/P}(\dot{\phi}+\dot{\theta})\sin(\phi+\xi)\vec{i}_P && (4.30)\\ &+ r_{CM/P}(\dot{\phi}+\dot{\theta})\cos(\phi+\xi)\vec{j}_P \end{aligned}$$

$$\begin{aligned} {}^O\vec{a}_{CM/P} &= {}^P\vec{a}_{CM/P} + {}^O\vec{\alpha}^P \times \vec{r}_{CM/P} && (4.31)\\ &+ 2{}^O\vec{\omega}^P \times {}^P\vec{v}_{CM/P} + {}^O\vec{\omega}^P \times ({}^O\vec{\omega}^P \times \vec{r}_{CM/P})\\ &= (r_{CM/P}(-\ddot{\phi}\sin(\phi+\xi) - \dot{\phi}^2\cos(\phi+\xi) && (4.32)\\ &- \ddot{\theta}\sin(\phi+\xi) - 2\dot{\theta}\dot{\phi}\cos(\phi+\xi)\\ &- \dot{\theta}^2\cos(\phi+\xi)))\vec{i}_P\\ &+ (r_{CM/P}(\ddot{\phi}\cos(\phi+\xi)\\ &- \dot{\phi}^2\sin(\phi+\xi) + \ddot{\theta}\cos(\phi+\xi)\\ &- 2\dot{\theta}\dot{\phi}\sin(\phi+\xi) - \dot{\theta}^2\sin(\phi+\xi)))\vec{j}_P \end{aligned}$$

Now the acceleration terms can be substituted into equation 4.22.

$$\begin{aligned} {}^O\vec{a}_{CM/O} &= r_{P/O}(-\ddot{\theta}\sin(\theta) - \dot{\theta}^2\cos(\theta))\vec{i}_O && (4.33)\\ &+ r_{P/O}(\ddot{\theta}\cos(\theta) - \dot{\theta}^2\sin(\theta))\vec{j}_O\\ &+ [(r_{CM/P}(-\ddot{\phi}\sin(\phi+\xi) - \dot{\phi}^2\cos(\phi+\xi)\\ &- \ddot{\theta}\sin(\phi+\xi) - 2\dot{\theta}\dot{\phi}\cos(\phi+\xi)\\ &- \dot{\theta}^2\cos(\phi+\xi)))\vec{i}_P\\ &+ (r_{CM/P}(\ddot{\phi}\cos(\phi+\xi)\\ &- \dot{\phi}^2\sin(\phi+\xi) + \ddot{\theta}\cos(\phi+\xi)\\ &- 2\dot{\theta}\dot{\phi}\sin(\phi+\xi) - \dot{\theta}^2\sin(\phi+\xi)))\vec{j}_P]_O \end{aligned}$$

The components in the P frame have to be converted to the inertial frame to be used in the force equation. This topic was covered in the previous section. In this case the example vector $\vec{C}$ would be replaced by ${}^{O}\vec{a}_{CM/P}$.

The next step is to develop expressions for the external forces acting on the system. The magnitude of the tension is itself fairly complicated. It will be dependent on several more factors than just the angular velocity and length of the tether. Between the moment equation 4.21 and summing the forces along the x and y axes there are 3 equations to work with. Two values fully define the system, $\ddot{\theta}$ and $\ddot{\phi}$. F_{ten} will be treated as a third variable to solve. Its direction can be determined since its force acts along the tether. From the definition of a unit vector an expression for the force from the tension in the tether can be found.

$$\vec{F}_{ten} = -F_{ten}\frac{\vec{r}_{Q/O}}{r_{Q/O}} = -F_{ten}\frac{r_{Q/O}\cos(\theta)\vec{i}_O + r_{Q/O}\sin(\theta)\vec{j}_O}{r_{Q/O}} \tag{4.34}$$

The force from the thrust can be any function of time. It is assumed that the force is oriented toward point P, the body frame. However, it can be oriented at any angle in that frame, as can be seen in the free body diagram in figure 4.2 represented by the angle δ. It has to undergo a rotation sequence in order to be in the inertial frame. The angle it rotates through for the transformation is $\theta + \phi$.

$$\vec{F}_{thru,x} = F_{thru}(\sin(\delta)\cos(\theta+\phi) - \cos(\delta)\sin(\theta+\phi))\vec{i}_O \tag{4.35}$$

$$\vec{F}_{thru,y} = F_{thru}(\sin(\delta)\sin(\theta+\phi) + \cos(\delta)\cos(\theta+\phi))\vec{j}_O \tag{4.36}$$

Every term is now available to be substituted in to the equations for the sum of the forces 4.15. The final equations of motion are listed here together in their complete form.

$$I_{zz}\left(\ddot{\theta}+\ddot{\phi}\right)\vec{k} = -\vec{F}_{ten}r_{CM/P}\sin(\phi+\xi) + \vec{F}_{thru}r_{CM/P}\cos(\delta+\xi) \tag{4.37}$$

$$\begin{aligned} m_{tot}{}^{O}\vec{a}_{CM/O,x} &= -F_{ten}\frac{r_{Q/O}\cos(\theta)\vec{i}_O}{r_{Q/O}} \\ &+ F_{thru}(\sin(\delta)\cos(\theta+\phi) - \cos(\delta)\sin(\theta+\phi))\vec{i}_O \end{aligned} \tag{4.38}$$

$$m_{tot}{}^{O}\vec{a}_{CM/O,y} = -F_{ten}\frac{r_{Q/O}\sin(\theta)\vec{j}_O}{r_{Q/O}} \tag{4.39}$$

$$+ \quad F_{thru}(\sin(\delta)\sin(\theta+\phi) + \cos(\delta)\cos(\theta+\phi))\vec{j}_O$$

Now there are 3 equations with 3 unknowns, $\ddot{\theta}, \ddot{\phi}$, and F_{ten}. MatLab was used to solve for expressions for them. They are listed for each case in the appendix.

4.2.3 Data Analysis

To test a system values representing the system need to be assumed. Those values were the total mass, moment of inertia about the z axis, the angle of the center of mass, the angle of the thrust fan, and the lengths $r_{Q/O}$ and $r_{Q/O}$. MatLab was used to solve the equations of motion for $\ddot{\phi}$ and $\ddot{\theta}$. Then, a second program in MatLab used its ode45 routine to numerically solve the equations using the assumed values. The graphs in figure 4.3 show ϕ and θ with respect to time. They also list the values that were assumed for the sample trial. For a stable system the angular velocity of the craft around the reference frame should continually increase. The parabolic shape of θ is a sign of this acceleration. ϕ continually oscillates as it tries to reach equilibrium.

When testing other values certain trends were noticeable. Once the peak overshoot became greater than 90° the system became unstable. This occurs because after that the force from the thrust is pushing it in the other direction. For a given set of initial conditions, increasing the thrust makes the system more unstable, while increasing the inertia makes the system more stable. The angle of the thruster also affects the stability. As the angle δ (which dictates the direction of the thrust force) becomes smaller, the the system becomes more unstable. It also causes the disturbance to damp out slower.

4.3 Effect of Moving the Tether Away from the Body Axes

4.3.1 Physical Description

In this model the tether can be attached anywhere on the body, rather than solely at the geometric center. The system shown in 4.4 begins to resemble the

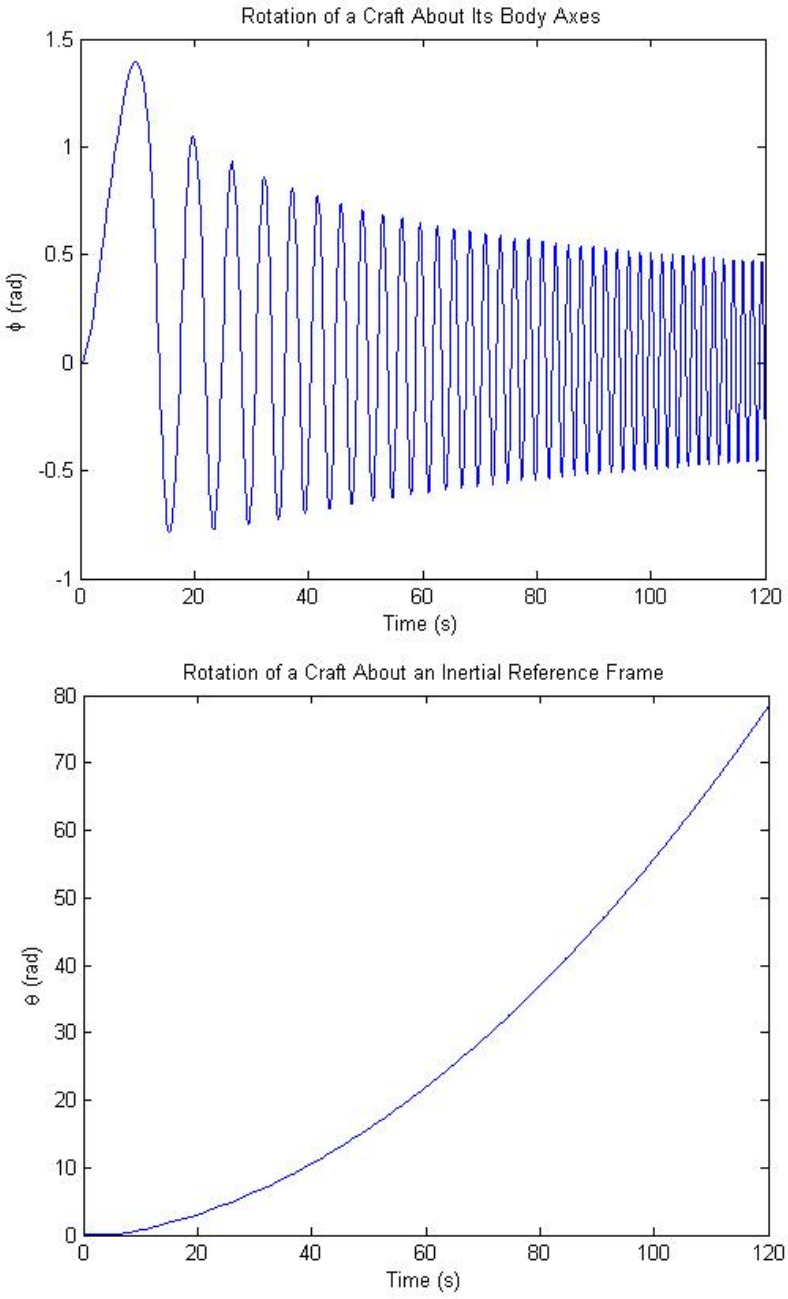

Figure 4.3: Motion of the Simplified System
$m_{tot} = 5kg, I_{zz} = 4kgm^2, r_{Q/O} = 10m, r_{CM/P} = 0.75m, \xi = 0, \delta = \frac{60\pi}{180} rad, F_{thru} = 1N$

completed model. However, the effects of friction and changes in the length of the tether are still not considered.

4.3.2 Equations of Motion of the System

The procedure for the analysis is the same as for the previous example. However, terms will change to accommodate the additional vector, $\vec{r}_{P/Q}$. Both of the moments from the inertial body and from the thrust force remain unchanged when taken about the center of mass. However, the moment resulting from the external force of the tension in the tether needs to be revised based on the free body diagram.

$$\overset{O}{O}\vec{\tau}_{CM,tension} = -\vec{F}_{ten}\left[r_{CM/P}\sin(\phi+\xi) + r_{P/Q}\sin(\phi)\right] \tag{4.40}$$

This can easily substitute the tension term in equation 4.37.

$$\begin{aligned} I_{zz}\left(\ddot{\theta}+\ddot{\phi}\right)\vec{k} &= -\vec{F}_{ten}\left[(r_{CM/P}\sin(\phi+\xi) + r_{P/Q}\sin(\phi)\right] \\ &+ \vec{F}_{thru} r_{CM/P}\cos(\delta+\xi) \end{aligned} \tag{4.41}$$

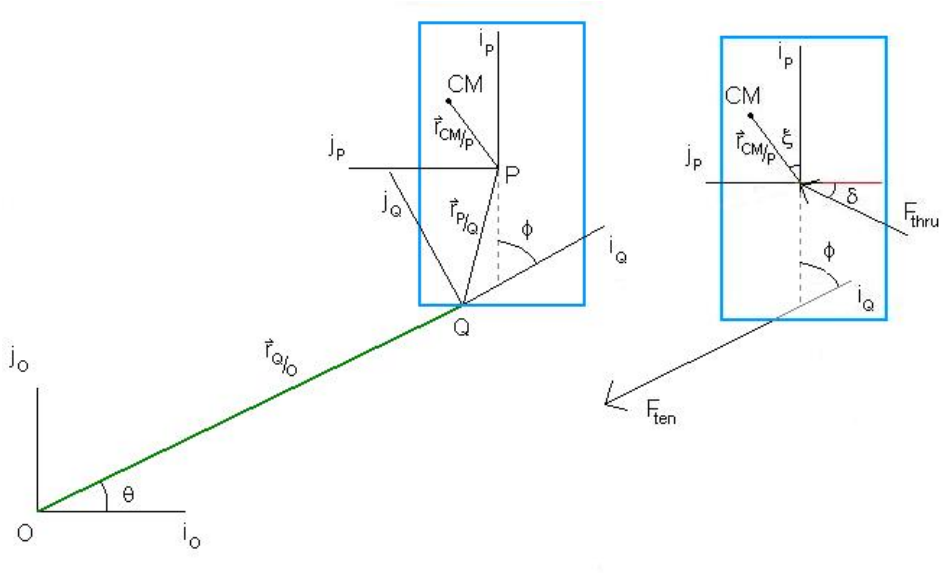

Figure 4.4: Model and Free Body Diagram of the Second System

The acceleration term for the force equations needs considerable changes.

$$\left\{{}^{O}\vec{a}_{CM/O}\right\}_O = \left\{{}^{O}\vec{a}_{Q/O}\right\}_O + \left\{{}^{O}\vec{a}_{P/Q}\right\}_O + \left\{{}^{O}\vec{a}_{CM/P}\right\}_O \tag{4.42}$$

$$\begin{aligned}
\vec{r}_{Q/O} &= r_{Q/O}\cos(\theta)\vec{i}_O + r_{Q/O}\sin(\theta)\vec{j}_O && (4.43)\\
{}^{O}\vec{v}_{Q/O} &= -r_{Q/O}\dot{\theta}\sin(\theta)\vec{i}_O + r_{Q/O}\dot{\theta}\cos(\theta)\vec{j}_O && (4.44)\\
{}^{O}\vec{a}_{Q/O} &= r_{Q/O}(-\ddot{\theta}\sin(\theta) - \dot{\theta}^2\cos(\theta))\vec{i}_O && (4.45)\\
&+ r_{Q/O}(\ddot{\theta}\cos(\theta) - \dot{\theta}^2\sin(\theta))\vec{j}_O
\end{aligned}$$

$$\begin{aligned}
\vec{r}_{P/Q} &= r_{P/Q}\cos(\phi)\vec{i}_Q + r_{P/Q}\sin(\phi)\vec{j}_Q && (4.46)\\
{}^{Q}\vec{v}_{P/Q} &= -r_{P/Q}\dot{\phi}\sin(\phi)\vec{i}_Q + r_{P/Q}\dot{\phi}\cos(\phi)\vec{j}_Q && (4.47)\\
{}^{Q}\vec{a}_{P/Q} &= r_{P/Q}(-\ddot{\phi}\sin(\phi) - \dot{\phi}^2\cos(\phi))\vec{i}_Q && (4.48)\\
&+ r_{P/Q}(\ddot{\phi}\cos(\phi) - \dot{\phi}^2\sin(\phi))\vec{j}_Q
\end{aligned}$$

Now the transfer function is used to get the velocity and acceleration with respect to the inertial frame.

$$\begin{aligned}
{}^{O}\vec{v}_{P/Q} &= {}^{Q}\vec{v}_{P/Q} + {}^{O}\vec{\omega}^{Q} \times \vec{r}_{P/Q} && (4.49)\\
&= -r_{P/Q}(\dot{\phi}+\dot{\theta})\sin(\phi)\vec{i}_Q + r_{P/Q}(\dot{\phi}+\dot{\theta})\cos(\phi)\vec{j}_Q && (4.50)
\end{aligned}$$

$$\begin{aligned}
{}^{O}\vec{a}_{P/Q} &= {}^{Q}\vec{a}_{P/Q} + {}^{O}\vec{\alpha}^{Q} \times \vec{r}_{P/Q} && (4.51)\\
&+ 2{}^{O}\vec{\omega}^{Q} \times^{Q} \vec{v}_{P/Q} + {}^{O}\vec{\omega}^{Q} \times ({}^{O}\vec{\omega}^{Q} \times \vec{r}_{P/Q})\\
&= r_{P/Q}(-\ddot{\phi}\sin(\phi) - \dot{\phi}^2\cos(\phi) - \ddot{\theta}\sin(\phi) && (4.52)\\
&- 2\dot{\theta}\dot{\phi}\cos(\phi) - \dot{\theta}^2\cos(\phi))\vec{i}_Q\\
&+ r_{P/Q}(\ddot{\phi}\cos(\phi) - \dot{\phi}^2\sin(\phi) + \ddot{\theta}\cos(\phi)\\
&- 2\dot{\theta}\dot{\phi}\sin(\phi) - \dot{\theta}^2\sin(\phi))\vec{j}_Q
\end{aligned}$$

The next set of equations considers the distance $\vec{r}_{CM/P}$. It is simpler since frame

CM rotates with frame P making $\{{}^P\vec{v}_{CM/P}\}_P$ and $\{{}^P\vec{a}_{CM/P}\}_P$ equal to 0.

$$\vec{r}_{CM/P} = r_{CM/P}\cos(\xi)\vec{i}_P + r_{CM/P}\sin(\xi)\vec{j}_P \tag{4.53}$$

The velocity and acceleration with respect to the O frame is not equal to 0. However, it is simplified.

$$\begin{aligned} {}^O\vec{v}_{CM/P} &= {}^O\vec{\omega}^P \times \vec{r}_{CM/P} && (4.54)\\ &= -r_{CM/P}(\dot{\phi}+\dot{\theta})\sin(\xi)\vec{i}_P && (4.55)\\ &+ r_{CM/P}(\dot{\phi}+\dot{\theta})\cos(\xi)\vec{j}_P \end{aligned}$$

$$\begin{aligned} {}^O\vec{a}_{CM/P} &= {}^O\vec{\alpha}^P \times \vec{r}_{CM/P} && (4.56)\\ &+ {}^O\vec{\omega}^P \times ({}^O\vec{\omega}^P \times \vec{r}_{CM/P})\\ &= (r_{CM/P}(-(\ddot{\phi}+\ddot{\theta})\sin(\xi) - (\dot{\phi}+\dot{\theta})^2\cos(\xi)))\vec{i}_P && (4.57)\\ &+ (r_{CM/P}((\ddot{\phi}+\ddot{\theta})\cos(\xi) - (\dot{\phi}+\dot{\theta})^2\sin(\xi)))\vec{j}_P \end{aligned}$$

Now these terms can be substituted into equation 4.42 for the acceleration. This expression can be compared to equation 4.33 for the acceleration of the most simplified case on page 30.

$$\begin{aligned} {}^O\vec{a}_{CM/O} &= r_{Q/O}(-\ddot{\theta}\sin(\theta) - \dot{\theta}^2\cos(\theta))\vec{i}_O && (4.58)\\ &+ r_{Q/O}(\ddot{\theta}\cos(\theta) - \dot{\theta}^2\sin(\theta))\vec{j}_O\\ &+ [r_{P/Q}(-\ddot{\phi}\sin(\phi) - \dot{\phi}^2\cos(\phi) - \ddot{\theta}\sin(\phi)\\ &- 2\dot{\theta}\dot{\phi}\cos(\phi) - \dot{\theta}^2\cos(\phi))\vec{i}_Q\\ &+ r_{P/Q}(\ddot{\phi}\cos(\phi) - \dot{\phi}^2\sin(\phi) + \ddot{\theta}\cos(\phi)\\ &- 2\dot{\theta}\dot{\phi}\sin(\phi) - \dot{\theta}^2\sin(\phi))\vec{j}_Q]_O\\ &+ [(r_{CM/P}(-(\ddot{\phi}+\ddot{\theta})\sin(\xi) - (\dot{\phi}+\dot{\theta})^2\cos(\xi)))\vec{i}_P\\ &+ (r_{CM/P}((\ddot{\phi}+\ddot{\theta})\cos(\xi) - (\dot{\phi}+\dot{\theta})^2\sin(\xi)))\vec{j}_P]_O \end{aligned}$$

The expressions for the external forces are the same as previously, due to how the reference frames were set up. Now all the terms are available to summarize

the equations of motion of the system.

$$I_{zz}\left(\ddot{\theta}+\ddot{\phi}\right)\vec{k} = -\vec{F}_{ten}\left[r_{CM/P}\sin(\phi+\xi)+r_{P/Q}\sin(\phi)\right] \quad (4.59)$$
$$+ \vec{F}_{thru}r_{CM/P}\cos(\delta+\xi)$$

$$m_{tot}{}^{O}\vec{a}_{CM/O,x} = -F_{ten}\frac{r_{Q/O}\cos(\theta)\vec{i}_O}{r_{Q/O}} \quad (4.60)$$
$$+ F_{thru}(\sin(\delta)\cos(\theta+\phi)-\cos(\delta)\sin(\theta+\phi))\vec{i}_O$$

$$m_{tot}{}^{O}\vec{a}_{CM/O,y} = -F_{ten}\frac{r_{Q/O}\sin(\theta)\vec{j}_O}{r_{Q/O}} \quad (4.61)$$
$$+ F_{thru}(\sin(\delta)\sin(\theta+\phi)+\cos(\delta)\cos(\theta+\phi))\vec{j}_O$$

In these equations, the expressions for ${}^{O}\vec{a}_{CM/O}$ are its components found in equation 4.58.

4.3.3 Data Analysis

The extra distance between where the tether is attached and the geometric center of the body tends to provide additional stability. Figure 4.5 shows the angles that define the system. The same values and time span were used to better compare the difference. The only new value, $\vec{r}_{P/Q}$, was set to 0.1m.

It makes sense that the graph of ϕ has the same form as the previous example. A vector could be defined such that,

$$\vec{r}_{CM/Q} = \vec{r}_{P/Q}+\vec{r}_{CM/P} \quad (4.62)$$

If this is the case, the system is essentially the same as in the simplest form; $\vec{r}_{CM/Q}$ is just extended. The main difference is that the torque from the tension about the center of mass has a greater moment arm.

4.4 Allowing the Tether to Change Lengths

Most tethered systems need the ability to reel in or out. Therefore, it is important to develop an understanding of what effects this feature has. It will affect design decisions such as the maximum reel in or out rate, and size and power of motors.

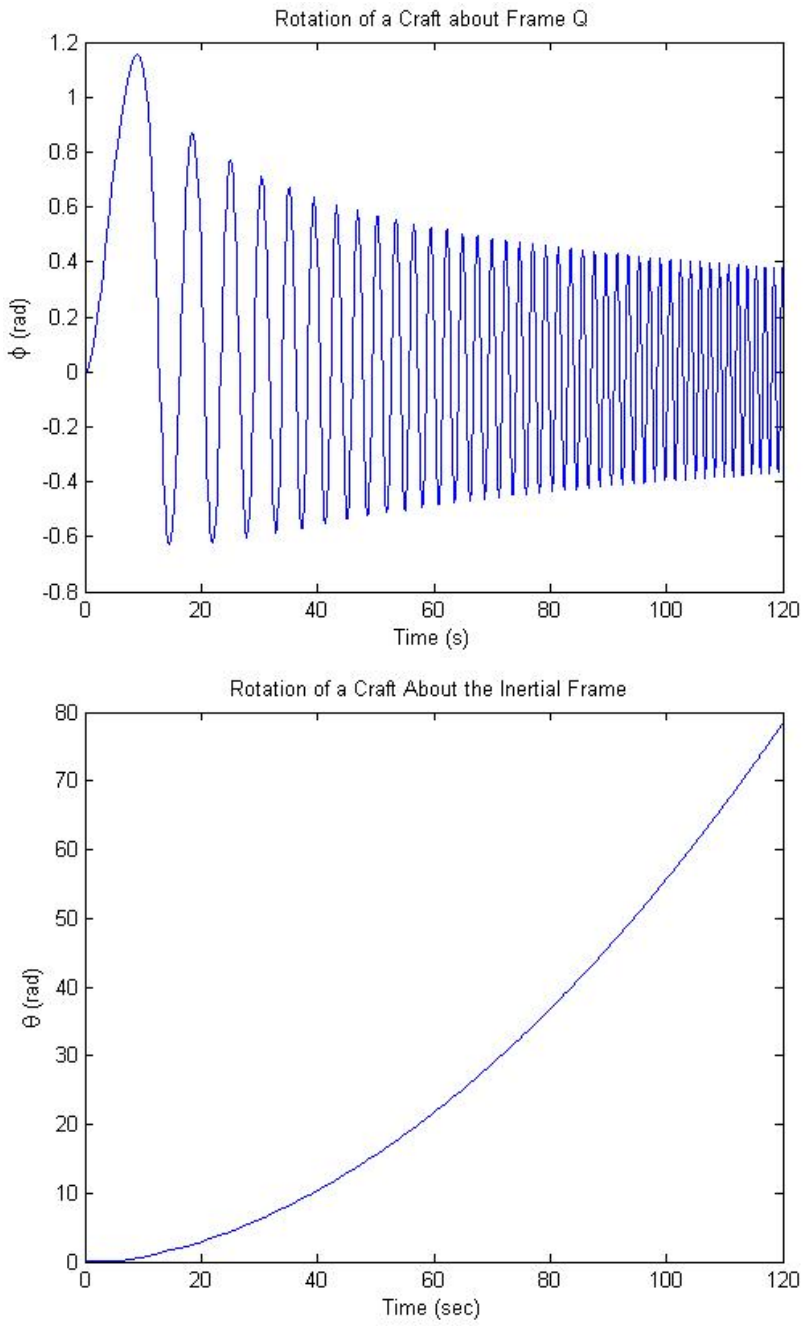

Figure 4.5: Motion of the Second System
$m_{tot} = 5kg, I_{zz} = 4kgm^2, r_{Q/O} = 10m, r_{CM/P} = 0.75m, \xi = 0$
$\delta = \frac{60\pi}{180} rad, F_{thru} = 1N), r_{P/Q} = 0.1m$

4.4.1 Physical Description

The system is identical to the previous example. This implies that the external forces and moments will be unaffected. However, the acceleration will change.

4.4.2 Equations of Motion of the System

The only term to examine is ${}^{O}\vec{a}_{CM/O}$. More specifically, ${}^{O}\vec{a}_{Q/O}$ is the only term to be affected.

$$\left\{{}^{O}\vec{a}_{CM/O}\right\}_O = \left\{{}^{O}\vec{a}_{Q/O}\right\}_O + \left\{{}^{O}\vec{a}_{P/Q}\right\}_O + \left\{{}^{O}\vec{a}_{CM/P}\right\}_O \tag{4.63}$$

$$\vec{r}_{Q/O} = r_{Q/O}\cos(\theta)\vec{i}_O + r_{Q/O}\sin(\theta)\vec{j}_O \tag{4.64}$$

$$\begin{aligned} {}^{O}\vec{v}_{Q/O} &= (\dot{r}_{Q/O}\cos(\theta) - r_{Q/O}\dot{\theta}\sin(\theta))\vec{i}_O \\ &+ (\dot{r}_{Q/O}\sin(\theta) + r_{Q/O}\dot{\theta}\cos(\theta))\vec{j}_O \end{aligned} \tag{4.65}$$

$$\begin{aligned} {}^{O}\vec{a}_{Q/O} &= (\ddot{r}_{Q/O}\cos(\theta) - 2\dot{r}_{Q/O}\dot{\theta}\sin(\theta) \\ &- r_{Q/O}\ddot{\theta}\sin(\theta) - r_{Q/O}\dot{\theta}^2\cos(\theta))\vec{i}_O \end{aligned} \tag{4.66}$$

$$\begin{aligned} &+ (\ddot{r}_{Q/O}\sin(\theta) + 2\dot{r}_{Q/O}\dot{\theta}\cos(\theta) \\ &+ r_{Q/O}\ddot{\theta}\cos(\theta) - r_{Q/O}\dot{\theta}^2\sin(\theta))\vec{j}_O \end{aligned} \tag{4.67}$$

This can now replace ${}^{O}\vec{a}_{Q/O}$ in equation 4.58.

$$\begin{aligned} {}^{O}\vec{a}_{CM/O} &= (\ddot{r}_{Q/O}\cos(\theta) - 2\dot{r}_{Q/O}\dot{\theta}\sin(\theta) \\ &- r_{Q/O}\ddot{\theta}\sin(\theta) - r_{Q/O}\dot{\theta}^2\cos(\theta))\vec{i}_O \end{aligned} \tag{4.68}$$

$$\begin{aligned} &+ (\ddot{r}_{Q/O}\sin(\theta) + 2\dot{r}_{Q/O}\dot{\theta}\cos(\theta) \\ &+ r_{Q/O}\ddot{\theta}\cos(\theta) - r_{Q/O}\dot{\theta}^2\sin(\theta))\vec{j}_O \\ &+ [r_{P/Q}(-\ddot{\phi}\sin(\phi) - \dot{\phi}^2\cos(\phi) - \ddot{\theta}\sin(\phi) \\ &- 2\dot{\theta}\dot{\phi}\cos(\phi) - \dot{\theta}^2\cos(\phi))\vec{i}_Q \\ &+ r_{P/Q}(\ddot{\phi}\cos(\phi) - \dot{\phi}^2\sin(\phi) + \ddot{\theta}\cos(\phi) \\ &- 2\dot{\theta}\dot{\phi}\sin(\phi) - \dot{\theta}^2\sin(\phi))\vec{j}_Q]_O \\ &+ [(r_{CM/P}(-(\ddot{\phi} + \ddot{\theta})\sin(\xi) - (\dot{\phi} + \dot{\theta})^2\cos(\xi)))\vec{i}_P \end{aligned} \tag{4.69}$$

$$+ \quad (r_{CM/P}((\ddot{\phi}+\ddot{\theta})\cos(\xi) - (\dot{\phi}+\dot{\theta})^2\sin(\xi)))\vec{j}_P]_O$$

The final equations of motion look exactly like the previous example with the new acceleration, equation 4.68, inserted.

$$\begin{aligned} I_{zz}\left(\ddot{\theta}+\ddot{\phi}\right)\vec{k} &= -\vec{F}_{ten}\left[r_{CM/P}\sin(\phi+\xi) + r_{P/Q}\sin(\phi)\right] \qquad (4.70)\\ &+ \vec{F}_{thru} r_{CM/P}\cos(\delta+\xi) \\ m_{tot}{}^O\vec{a}_{CM/O,x} &= -F_{ten}\frac{r_{Q/O}\cos(\theta)\vec{i}_O}{r_{Q/O}} \qquad (4.71)\\ &+ F_{thru}(\sin(\delta)\cos(\theta+\phi) - \cos(\delta)\sin(\theta+\phi))\vec{i}_O \\ m_{tot}{}^O\vec{a}_{CM/O,y} &= -F_{ten}\frac{r_{Q/O}\sin(\theta)\vec{j}_O}{r_{Q/O}} \qquad (4.72)\\ &+ F_{thru}(\sin(\delta)\sin(\theta+\phi) + \cos(\delta)\cos(\theta+\phi))\vec{j}_O \end{aligned}$$

Since this is probably the most interesting scenerio, a few variations of $r_{Q/O}, \dot{r}_{Q/O}$, and $\ddot{r}_{Q/O}$ will be tested. The first uses all the same conditions as for the previous scenerio; $r_{Q/O} = 10m, \dot{r}_{Q/O} = 0, \ddot{r}_{Q/O} = 0$. This demonstrates that when the derivatives of the length of the tether are 0 that the model does follow the same motion as previously predicted.

4.4.3 Data Analysis

The next two figures show the difference between the effects of reeling in and reeling out the tether. The acceleration for both of them are 0. The reel in rate is -0.05$\frac{m}{s}$, and the reel out rate is 0.05$\frac{m}{s}$. Both cases initially start at a tether length of 10m. This implies that at the end of 2 minutes the tether is at a new length of 4m and 16m, respectively.

It is observed that reeling in provides extra stability. While reeling out decreases it. Also, by observing θ, it is seen that reeling in increased the angular velocity about the inertial frame. This agrees with the familiar experience of spinning in a chair with your arms out. When your arms are brought in, the moment of inertia is decreased caused a greater angular velocity. As a final case, the acceleration term is used. It is set to 0.00042$\frac{m}{s^2}$ while the initial velocity is set

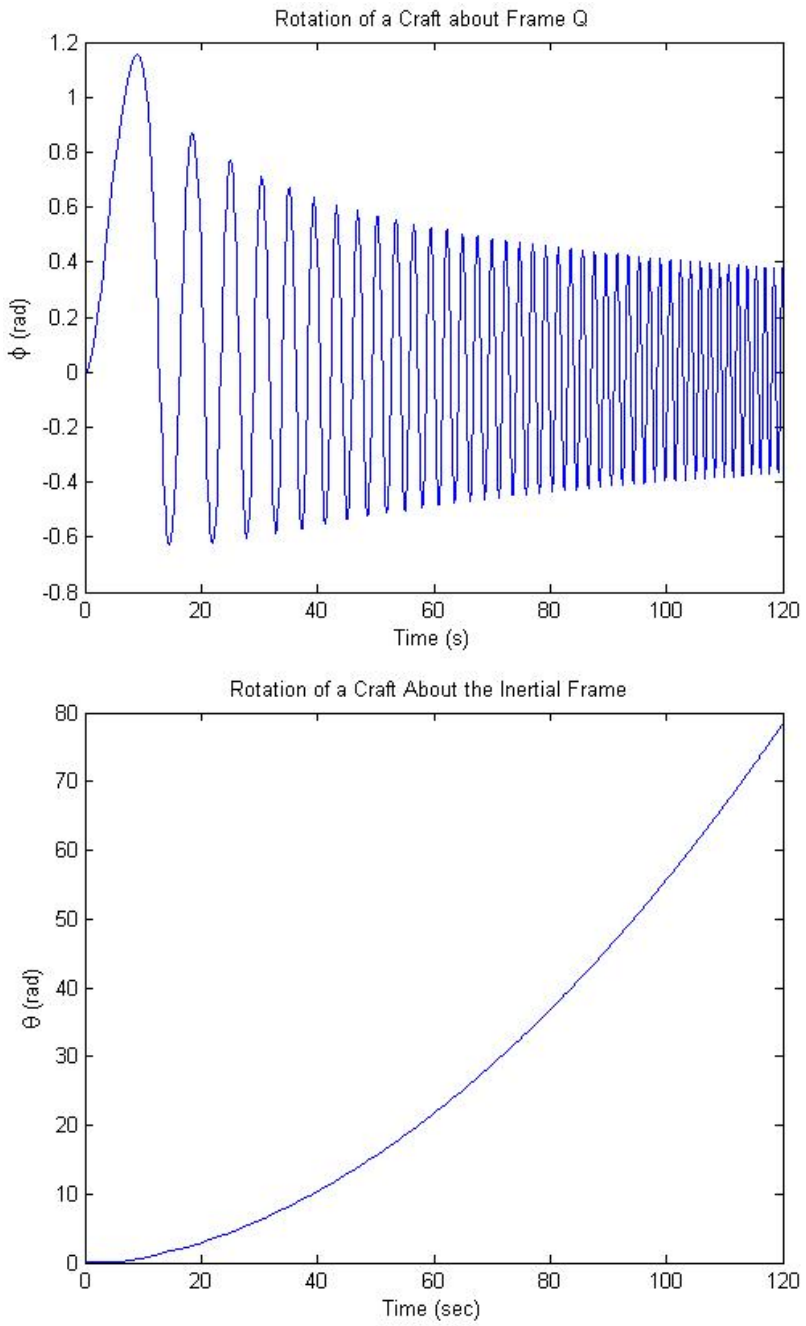

Figure 4.6: Motion of the Completed System without Friction: Case 1
$m_{tot} = 5kg, I_{zz} = 4kgm^2, r_{CM/P} = 0.75m, \xi = 0, \delta = \frac{60\pi}{180} rad, F_{thru} = 1N$
$r_{P/Q} = 0.1m, r_{Q/O} = 10m, \dot{r}_{Q/O} = 0, \ddot{r}_{Q/O} = 0$

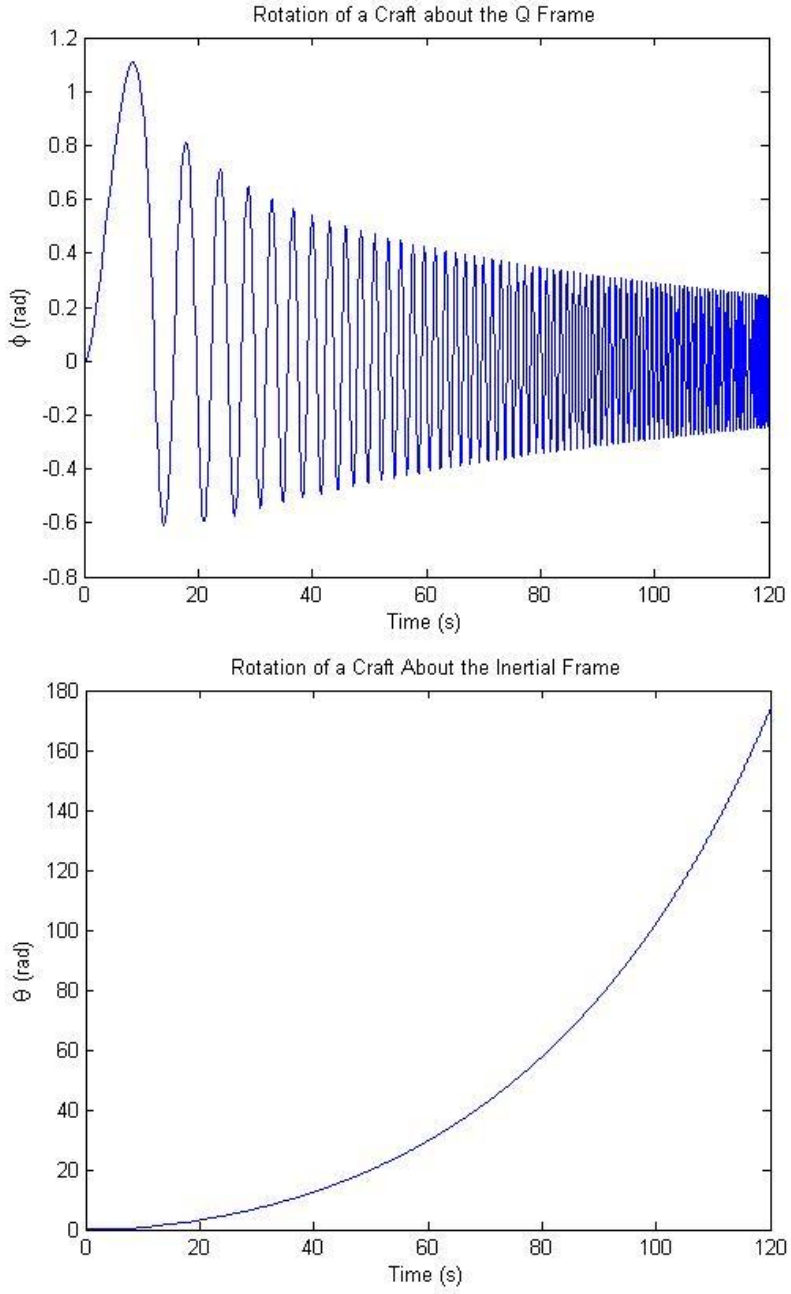

Figure 4.7: Motion of the Completed System without Friction: Case 2
$m_{tot} = 5kg, I_{zz} = 4kgm^2, r_{CM/P} = 0.75m, \xi = 0, \delta = \frac{60\pi}{180} rad, F_{thru} = 1N$
$r_{P/Q} = 0.1m, r_{Q/O} = (-0.05t + 10)m, \dot{r}_{Q/O} = -0.05\frac{m}{s}, \ddot{r}_{Q/O} = 0$

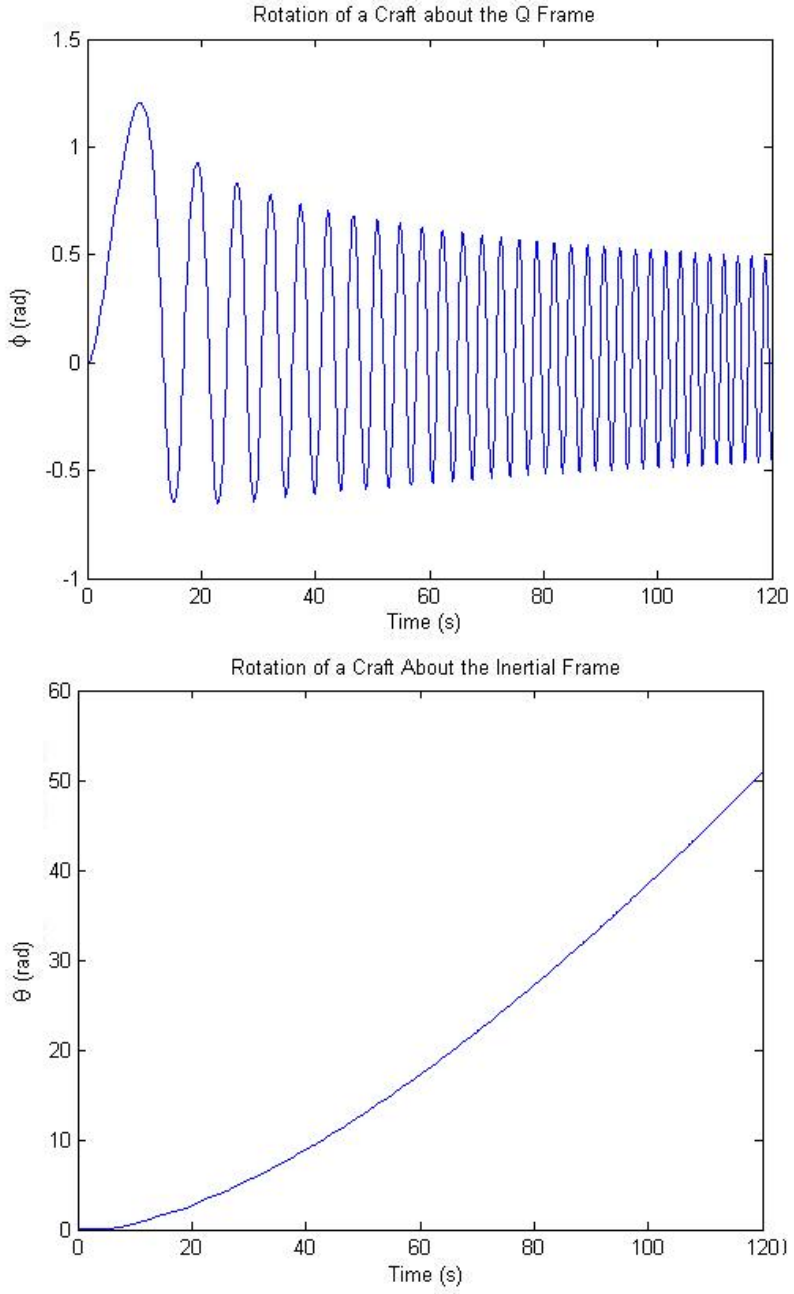

Figure 4.8: Motion of the Completed System without Friction: Case 3
$m_{tot} = 5kg, I_{zz} = 4kgm^2, r_{CM/P} = 0.75m, \xi = 0, \delta = \frac{60\pi}{180} rad, F_{thru} = 1N$
$r_{P/Q} = 0.1m, r_{Q/O} = (0.05t + 10)m, \dot{r}_{Q/O} = 0.05\frac{m}{s}, \ddot{r}_{Q/O} = 0$

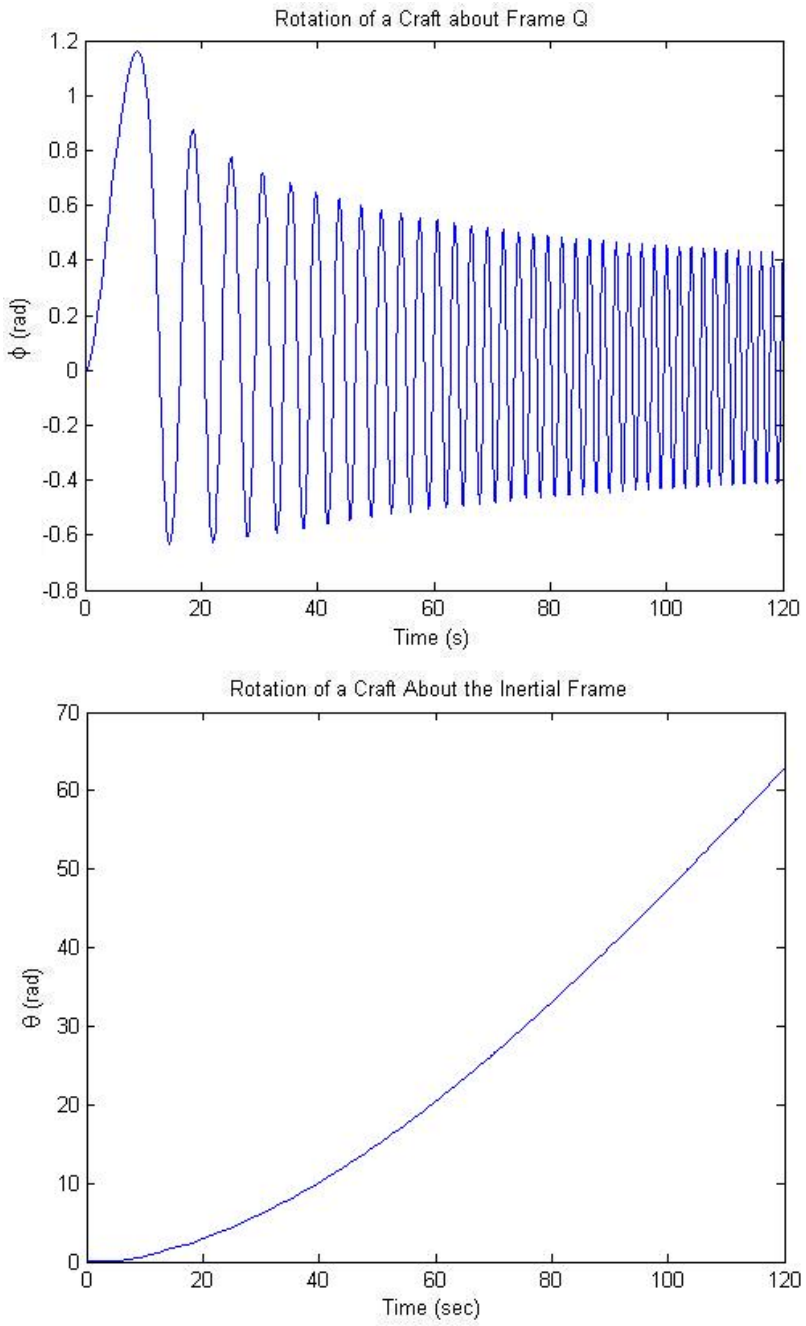

Figure 4.9: Motion of the Completed System without Friction: Case 4
$m_{tot} = 5kg, I_{zz} = 4kgm^2, r_{CM/P} = 0.75m, \xi = 0, \delta = \frac{60\pi}{180} rad, F_{thru} = 1N$
$r_{P/Q} = 0.1m, r_{Q/O} = (0.00042t^2 + 10)m, \dot{r}_{Q/O} = 0.00042t\frac{m}{s}, \ddot{r}_{Q/O} = 0.00042\frac{m}{s}$

to 0. Those values were chosen to contrast with figure 4.8. In 2 minutes with this acceleration the final length of the tether is 16m. Between the two, the graph of ϕ does not change much. However, at the end of the time period, θ of the constant acceleration case was around 10° further.

4.5 Adding Friction

4.5.1 Physical Description

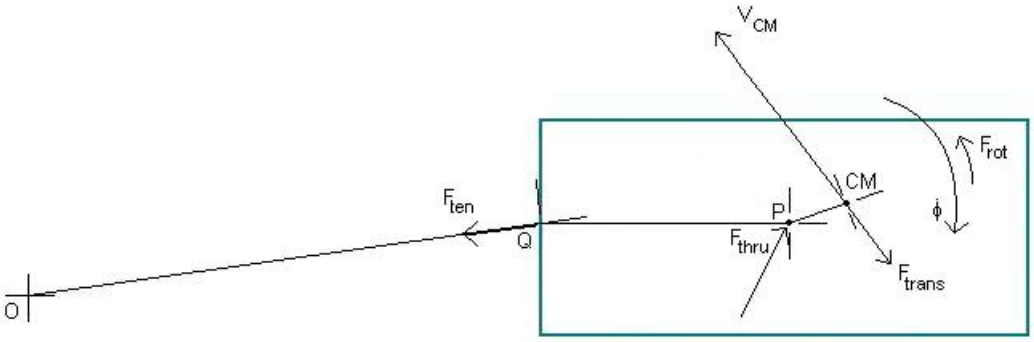

Figure 4.10: Free Body Diagram Including Friction

The next element to be considered is friction. A body may experience different kinds of friction. Kinetic and viscous effects are considered for this application. It is likely that the edge of skirt of the hovercraft will touch the surface. This would result in some kinetic friction. However, it is much less than the typical kinetic friction coefficient times the normal force of the sliding object since the majority of the hovercraft is being suspended by a cushion of air. It is suspected that kinetic friction will have very little effect overall and can be neglected for this experiment.

4.5.2 Developing Expressions for Friction

The main cause of friction results from viscous influences. The shear stress and force for a flat plate are assumed to apply to the hovercraft. They are given by

White (2003).

$$\vec{\tau} = \mu\frac{d\vec{u}}{dy} = \mu\frac{\vec{V}}{h} \tag{4.73}$$

$$d\vec{F} = \vec{\tau}dA, \vec{F} = \int d\vec{F} = \pi\mu\frac{\vec{V}}{h}\int r^2 dr = \frac{\pi\mu r^3\vec{V}}{3h} \tag{4.74}$$

The equations are developed from the Navier-Stokes equations by assuming Couette flow. In Couette flow one flat plate slides over a stationary flat plate with a fluid in between. One assumption of Couette flow is that the moving plate has a constant velocity. This implies that the acceleration of the hovercraft is assumed to be small enough to be neglected.

To clarify these values, μ is the viscosity of air, the units of the velocity (V) are in rad/sec, h is the average distance that the hovercraft is suspended above the surface, and r is the average value of the radius of the skirt of the hovercraft. The only value that changes greatly is the velocity. Since the others all form a product they can be simplified to a constant. Also, it should be noted that a circular hovercraft was assumed. However, the main point is that in the end the expression does not have to change; the constant can simply be adjusted.

Another issue is that the friction, kinetic and viscous, has to be implemented into the equations of motion. Determining whether they should be included in the moment equation or the sum of the forces equation needs to be resolved through experimentation in the end. Since it has been decided that the kinetic friction for the hovercraft is small enough to be neglected, this analysis focuses on the viscous damping.

The expression for the viscous damping forces was determined in equation 4.74. However, the velocity term can be considered in two different ways. First, if the hovercraft were purely spinning about its center of mass a moment would be created which would act against the motion of the rotation. In this scenario the velocity term is $\dot{\vec{\phi}}$. The force is then multiplied by the average radius of the hovercraft to produce the resultant moment.

$$\vec{M} = \sum_{i=1}^{n}\vec{F_i}\times\vec{d_i} = \frac{\pi\mu r^3\vec{V}}{3h}\times\vec{r_i} = C_{rot}\dot{\vec{\phi}}r_{avg} = C_{rot}\dot{\vec{\phi}} \tag{4.75}$$

The viscous friction can also be applied to the sum of the forces equations. Even if the hovercraft is not rotating about its center of mass it will always rotate about the inertial center which can be considered as a translation. The expression for the force is derived differently. For a translating flat plate the force applied by a fluid along the surface of the plate is constant which implies that the integral drops out. The direction is specified using the definition of a unit vector and acknowledging that it acts to oppose the velocity of the center of mass with respect to the inertial reference frame.

$$\vec{\tau} = \mu\frac{d\vec{u}}{dy} = \mu\frac{{}^{O}v_{CM/O}}{h}\frac{{}^{O}\vec{v}_{CM/O}}{{}^{O}v_{CM/O}} \tag{4.76}$$

$$\vec{F} = \vec{\tau}A = \mu\frac{{}^{O}v_{CM/O}}{h}\pi r^2\frac{{}^{O}\vec{v}_{CM/O}}{{}^{O}v_{CM/O}} = C_{trans}\,{}^{O}\vec{v}_{CM/O} \tag{4.77}$$

To determine the values of the constants experimentation is needed. Comments on this matter are presented in the Data Analysis section.

4.5.3 Equations of Motion of the System

A more basic expression for the velocity can be acquired by combining equations 4.44, 4.50, and 4.55 on page 35.

$$\{{}^{O}\vec{v}_{CM/O}\}_O = \{{}^{O}\vec{v}_{Q/O}\}_O + \{{}^{O}\vec{v}_{P/Q}\}_O + \{{}^{O}\vec{v}_{P/Q}\}_O \tag{4.78}$$

$$\begin{aligned} {}^{O}\vec{v}_{CM/O} &= -r_{Q/O}\dot{\theta}\sin(\theta)\vec{i}_O + r_{Q/O}\dot{\theta}\cos(\theta)\vec{j}_O \\ &+ \{-r_{P/Q}(\dot{\phi}+\dot{\theta})\sin(\phi)\vec{i}_Q \\ &+ r_{P/Q}(\dot{\phi}+\dot{\theta})\cos(\phi)\vec{j}_Q\}_O \\ &+ \{-r_{CM/P}(\dot{\phi}+\dot{\theta})\sin(\xi)\vec{i}_P \\ &+ r_{CM/P}(\dot{\phi}+\dot{\theta})\cos(\xi)\vec{j}_P\}_O \end{aligned} \tag{4.79}$$

(4.80)

For simplicity in the equations of motion, the components of the force are shortened to ${C_{trans}}^{O}\vec{v}_{CM/O,x}$ and ${C_{trans}}^{O}\vec{v}_{CM/O,y}$

$$\begin{aligned} I_{zz}\left(\ddot{\theta}+\ddot{\phi}\right)\vec{k} &= -\vec{F}_{ten}\left[r_{CM/P}\sin(\phi+\xi)+r_{P/Q}\sin(\phi)\right] && (4.81)\\ &+ \vec{F}_{thru}r_{CM/P}\cos(\delta+\xi)\\ &- C_{rot}\dot{\vec{\phi}}\\ {m_{tot}}^{O}\vec{a}_{CM/O,x} &= -F_{ten}\frac{r_{Q/O}\cos(\theta)\vec{i}_O}{r_{Q/O}} && (4.82)\\ &+ F_{thru}(\sin(\delta)\cos(\theta+\phi)-\cos(\delta)\sin(\theta+\phi))\vec{i}_O\\ &- {C_{trans}}^{O}\vec{v}_{CM/O,x}\\ {m_{tot}}^{O}\vec{a}_{CM/O,y} &= -F_{ten}\frac{r_{Q/O}\sin(\theta)\vec{j}_O}{r_{Q/O}} && (4.83)\\ &+ F_{thru}(\sin(\delta)\sin(\theta+\phi)+\cos(\delta)\cos(\theta+\phi))\vec{j}_O\\ &- {C_{trans}}^{O}\vec{v}_{CM/O,y} && (4.84)\end{aligned}$$

4.5.4 Data Analysis

The following three sets of figures show the results of adding friction to the theoretical model. The first shows that setting the friction equal to zero results in an identical motion to previous models. This simply helps to validates that the friction was implemented into the equations of motion correctly. It also acts as a control or standard to compare the other figures. The second and third sets incorporate only the rotational and then translational viscous damping, respectively.

When contrasting the first and second sets of images some very large differences are apparent. First, the addition of viscous rotational friction causes the rotation of the hovercraft about its center of mass to damp out almost entirely after a minute. Also, the force from the thrust is now used more effectively. This is observed in the second graph by observing that the final velocity with the friction is almost 5 times greater. Also noted is that the velocity still increased linearly on average. It is unusual to think of friction as allowing an object to travel faster. However, it makes since in this case because the friction is going

into damping the rotation of the hovercraft about its own body axes rather than slowing the entire system.

The third set of graphs which model the viscous friction as a translating force also offer striking differences. The most unexpected is that the motion about the body axes still damped out significantly. More expected is that the acceleration of the hovercraft about the inertial reference frame decreased.

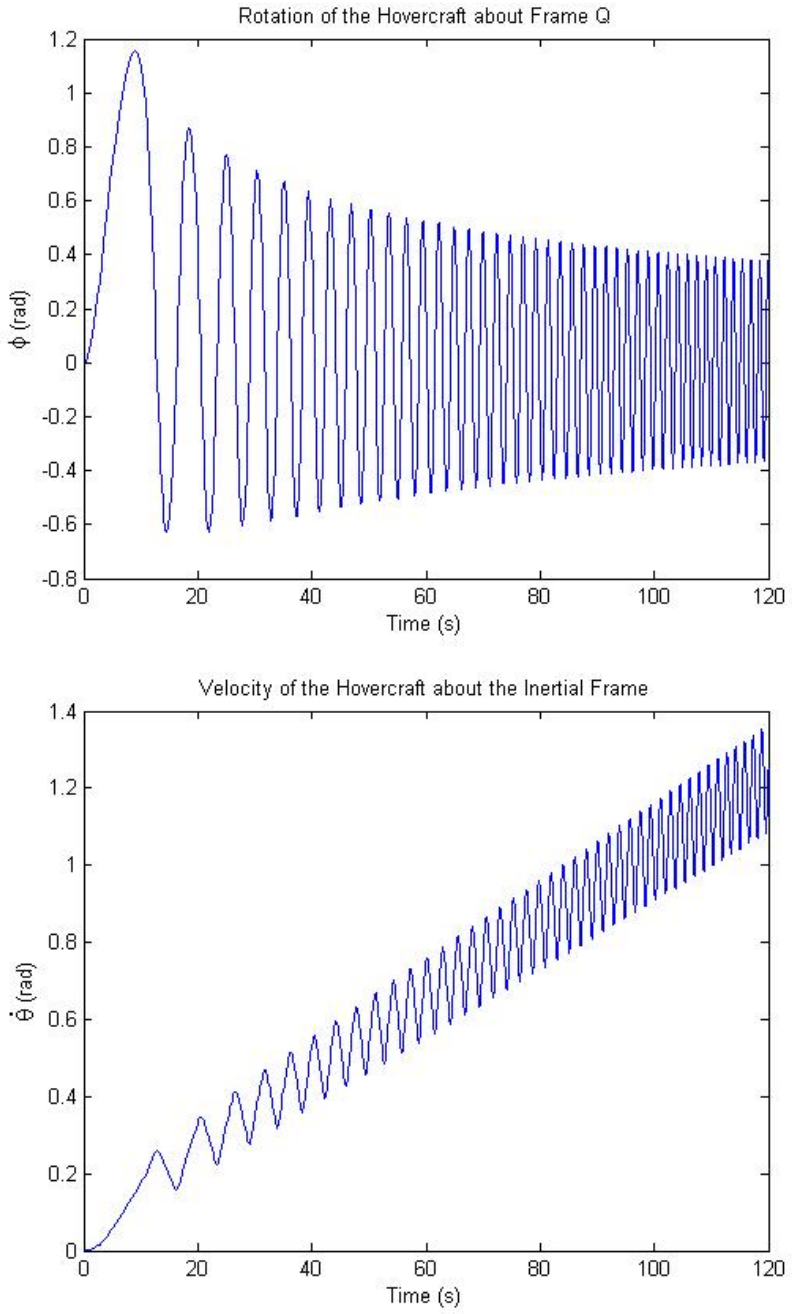

Figure 4.11: Motion of the Completed System without Friction
$m_{tot} = 5kg, I_{zz} = 4kgm^2, r_{CM/P} = 0.75m, \xi = 0, \delta = \frac{60\pi}{180} rad, F_{thru} = 1N$
$r_{P/Q} = 0.1m, r_{Q/O} = 10m, \dot{r}_{Q/O} = 0, \ddot{r}_{Q/O} = 0, C_{rot} = 0, C_{trans} = 0$

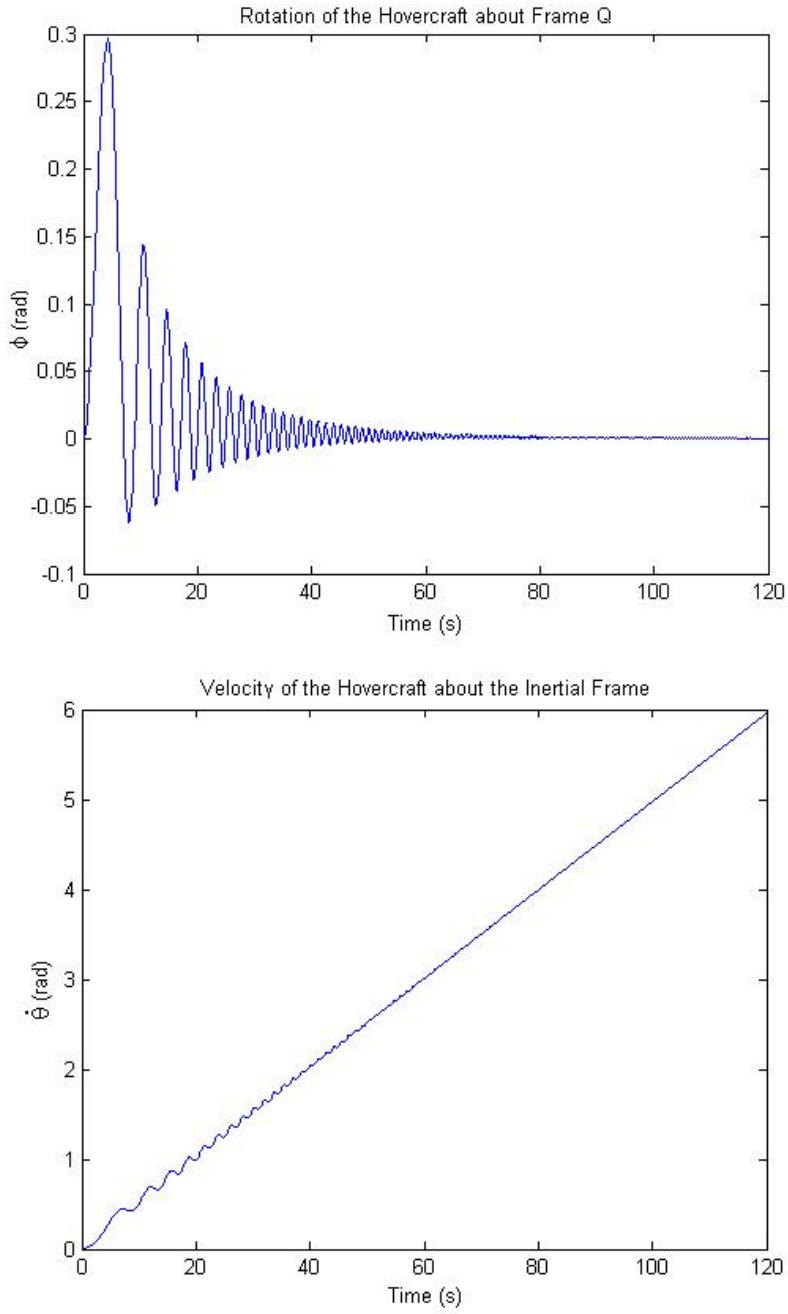

Figure 4.12: Motion of the Completed System with Viscous Rotational Friction
$m_{tot} = 5kg, I_{zz} = 4kgm^2, r_{CM/P} = 0.75m, \xi = 0, \delta = \frac{60\pi}{180}rad, F_{thru} = 1N$
$r_{P/Q} = 0.1m, r_{Q/O} = 10m, \dot{r}_{Q/O} = 0, \ddot{r}_{Q/O} = 0, C_{rot} = 0.3, C_{trans} = 0$

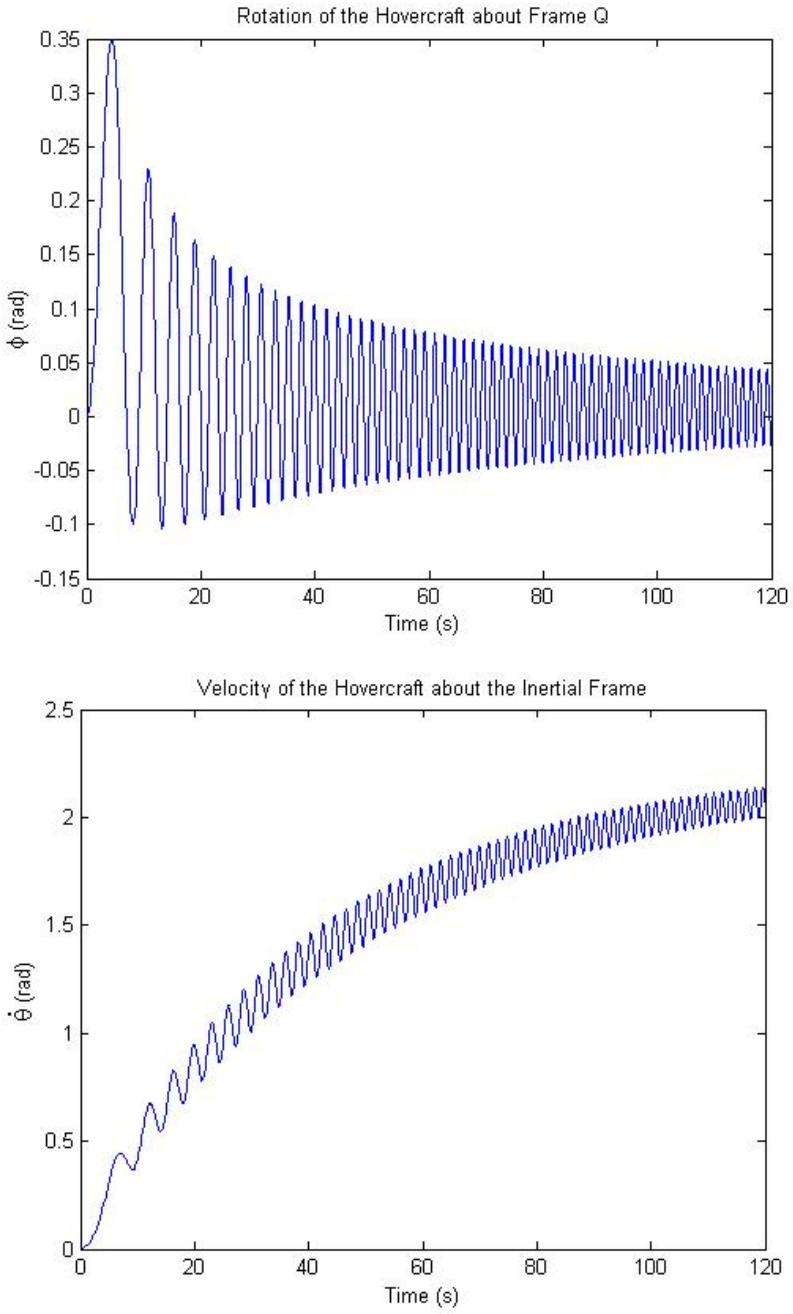

Figure 4.13: Motion of the Completed System with Viscous Translational Friction
$m_{tot} = 5kg, I_{zz} = 4kgm^2, r_{CM/P} = 0.75m, \xi = 0, \delta = \frac{60\pi}{180}rad, F_{thru} = 1N$
$r_{P/Q} = 0.1m, r_{Q/O} = 10m, \dot{r}_{Q/O} = 0, \ddot{r}_{Q/O} = 0, C_{rot} = 0, C_{trans} = 0.3$

Chapter 5

Comparing the Experimental and Analytic Results

Appendix B contains the results of the various setups. An explanation of the charts is given on the first page of the appendix. This chapter compares the experimental results to the analytic results, detailing the successes and pitfalls of the experimentation.

In order to study the similarities between the experimental and analytical results a suitable friction term must be developed. The most realistic would be rather complicated. The ducted fan motor, in addition to providing the air pressure for lift, also creates an oscillation which would affect the friction. Sen (1993) Instead, a simpler model was devised after consideration of the experiments.

Before each setup the hovercraft was balanced by altering the positions of bodies on it and by bending the structure of the craft as described in a previous chapter. In this initial state, with 0 velocity, the initial friction was assumed to be 0. However, as the hovercraft develops velocity, a friction can develop if all the applied forces are not in plane with the center of mass. The figure below demonstrates the effect of the tether. Even though the thrust force is not shown it would have the same effect at a different angle further complicating the actual result. The torque developed would be:

$$\vec{T} = \vec{F}_{ten} \times \vec{e} \tag{5.1}$$

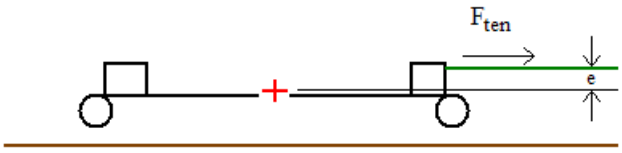

Figure 5.1: Torque Resulting from Out of Plane Forces

Also, the amount of friction developed for a given amount of torque would also form some unknown distribution with velocity. So the following expressions can be stated depending on whether the force is above or below the center of mass.[1] A is a coefficient which describes the proportion that the friction varies with velocity and B describes the shape of the distribution. In the torque equation, d is the distance from the center to the edge of the skirt contacting the ground.

$$|F| = F_{ten} \times e \left(A\dot{\theta}\right)^B = CF_{ten}\dot{\theta}^B \tag{5.2}$$

$$\vec{T} = \pm \left(|F|\, d\right) \vec{k_z} \tag{5.3}$$

Another component of the friction is due to damping. It seemed from the experiments that any rotational damping was negligible. However, the translational damping does need to be accounted. If it is assumed to be symmetrically applied about the center of mass, then it does not contribute to rotational damping and an expression for it can be simply stated.

$$|F| = DF_{ten}\dot{\theta} \tag{5.4}$$

In order to determine where the center of mass is located a plumb line method was used. The hovercraft was suspended by a point on its edge. A plumb line is dropped at the same point where the hovercraft is suspended. The mass is evenly distributed on both sides of the line, otherwise it would shift for equilibrium. The

[1] The direction is described in the MatLab code so that only the magnitude of the force needs to be defined.

center of mass is determined by hanging it at different locations and marking the intersection of the plumb lines.

The inertia was determined using a data logger and analyzer called Data Studio. The hovercraft was fastened to a spinning platform. A mass is tied to the spinning apparatus and allowed to fall. The inertia can be evaluated from the acceleration of the falling mass. A larger mass gives more accurate results by minimizing the effects of friction. The inertia of the rotating equipment must be determined first. Then, it can be subtracted from the inertia of the hovercraft and equipment together. The equation for the inertia is shown below. r is the radius of the pulley attaching the falling mass to the spinning apparatus. α is the angular acceleration of the of the spinning apparatus which was automatically recorded into Data Studio by an attached rotation sensor.

$$I = \frac{(mg + m\alpha r)r}{\alpha} \tag{5.5}$$

Now, with all the required data, the MatLab program can be used to evaluate the analytic motion. The following charts, from setup 18, compare one of the more ideal results. The red line shows the analytic results, while the green line shows one typical trial of the experimental data. The other yellow lines are the other experimental trials. They are there to show similarities between the experimental trials, but lighter in order to see details of the typical trial; the green line. The actual configuration of this particular setup is described in the appendix. However, to discuss the trends from the setup the actual setup information is not required.

In general, it is observed that the two charts are very similar. The attitude of the hovercrafts increases to about 50° and levels off. The frequencies increase with time. The range of attitude angles is similar. Also, the analytic angle of the tether closely matches the experimental values.

However, a major difference which has presented itself is that the frequency of the analytic solution is larger over time than the experimental results. A Nyquist chart is shown below of the frequency of the attitude of the hovercraft. It is observed that the analytic peak frequency is 0.65Hz while each of the experimental

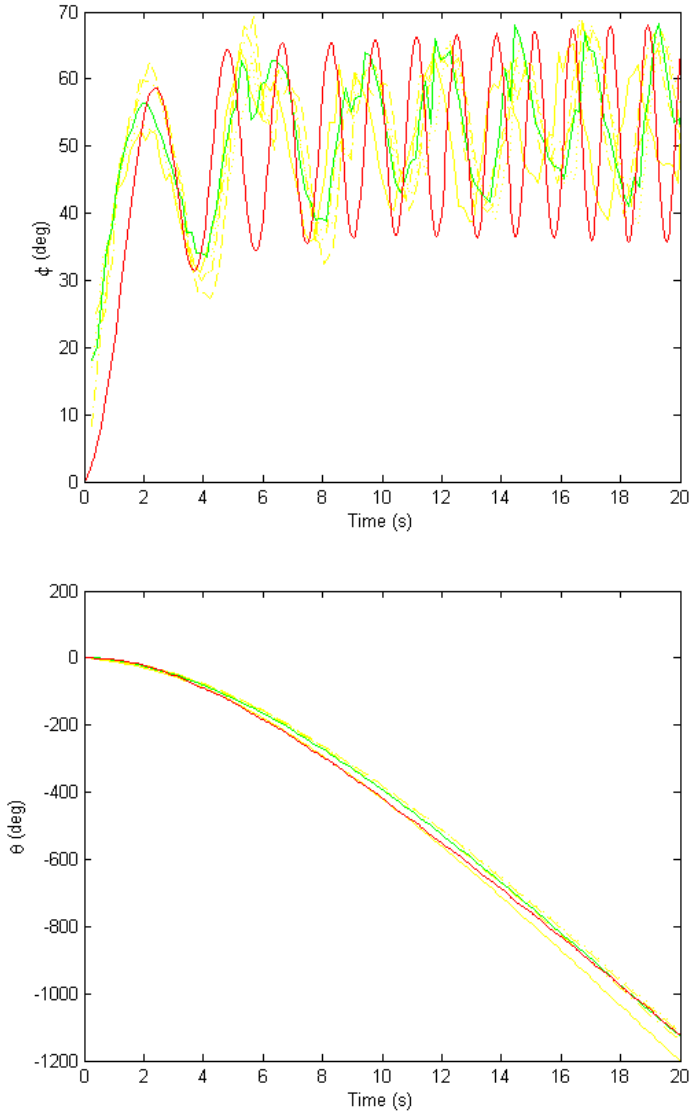

Figure 5.2: Attitude of the Hovercraft and Angle of the Tether Respectively

frequencies peak at about 0.4Hz. One possible explanation for this is that the friction terms are actually more complicated than the terms developed by the assumptions. It can be observed in the original chart of the attitude, especially in the initial oscillations, that certain oscillations are damped out which would effectively increase the peak frequency.

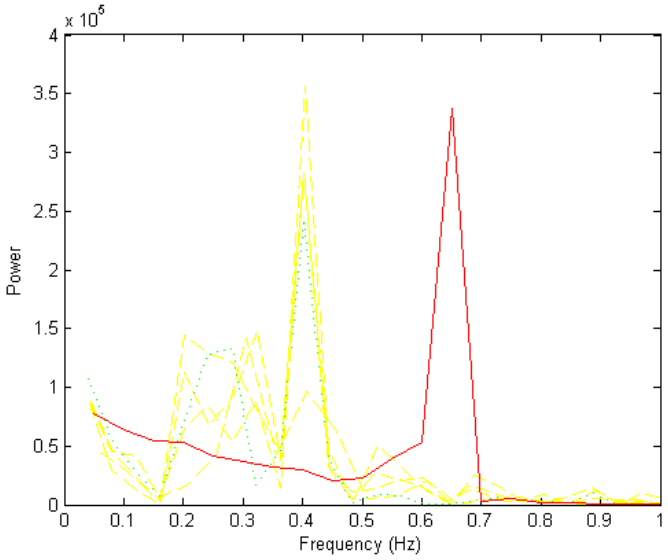

Figure 5.3: Nyquist Frequency for Attitude of Setup 18

Other unusual phenomena occur on a less frequent basis. The following figures are from setup 15. This behavior may be the result of the imprecise layout of the hovercraft. The methods utilize through these trials have the virtue of versatility. However, every feature may be a centimeter or a few degrees off. For example, while the center of mass was actually observed and recorded, the distance that the thrust vector is from the center of mass is still uncertain since the thrust fan is placed on the hovercraft at a preselected angle from an inexact geometric center.

Another likely culprit to the unusual motion may still be the uncertain friction terms. By greatly exaggerating the damping coefficient for setup 15 the analytic result begins to acquire some of the unusual attributes of its experimental counterpart. The large fluctuations in θ become apparent. The frequency of ϕ becomes significantly smaller, and its envelop develops a wavy, almost sinusoidal flow.

The reel in and out setups typify both the attributes and shortcomings of the experiment.

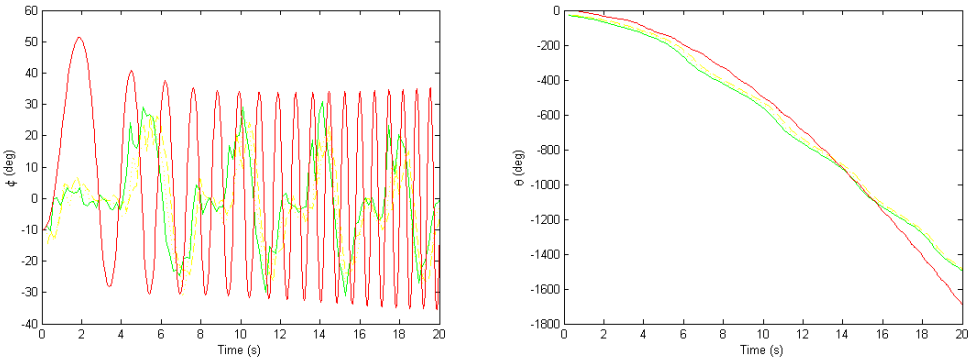

Figure 5.4: Attitude of the Hovercraft and Angle of the Tether Respectively for Setup 15

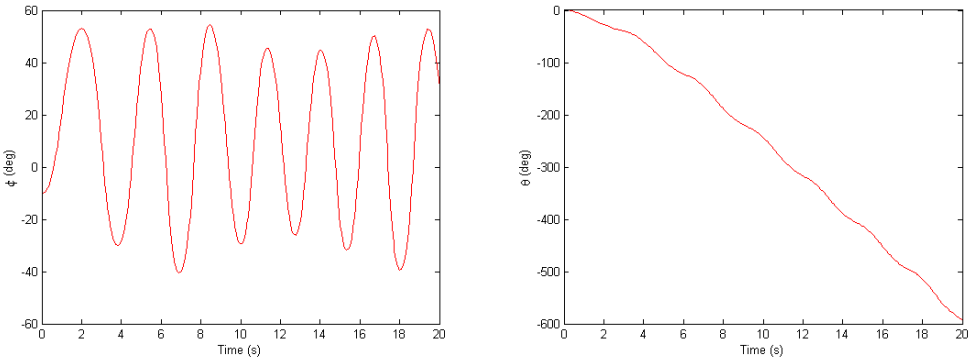

Figure 5.5: Analytic Result of Setup 15 if the Frictional Damping Coefficient is Greatly Exaggerated

Chapter 6

Conclusions

Recently tethered bodies have found several new applications in the space industry which have made their study all that much more important. Each application has its own demands which may require its own analysis.

In this study, a general motion was observed. The angle about the inertial reference frame increased parabolically and became a linear progression as a constant thrust was applied. The rotation about the body axis, the attitude of the hovercraft, took on the shape of an enveloping sine wave. The frequency of the sine wave tended to increase with time. These observations were confirmed in both the analytic and experimental observations. Also, the range of the attitude and the average value of the attitude were approximately equivalent.

The experimental and analytic results differ in the scale of the frequency. In general, the analytic frequency was always greater. Also, occasional experimental setups tended to yield unusual envelopes. The primary reason for these differences is believed to be design imperfections in the hovercraft. Also, the actual friction terms required for the analytic results can be difficult to account for appropriately. Oscillations created by the lift fans and a friction which varies with velocity complicate the friction expression. The experimental apparatus can be used to gauge the trends of the analytic analysis. However, to improve the accuracy of the results a more precise hovercraft design is desired.

As previously mentioned there are several factors that affect the motion of tethered satellites. Several resources are available to research the specific topic. A few are Bachmann *et al.* (1991), Pirozhenko (1989), and Gwaltney (1992).

References

Bachmann, S., Modi, V. & Misra, A. (1991). Dynamics and control of a space station based tethered elevator system. *Spaceflight*. 59

Bekey, I. (1997). Tethering a new technique for payload deployment. *Aerospace America*, **35**, 36–40. 4

Carroll, J. (1985). *Guidebook for Analysis of Tether Applications*. Springfield, Va.: National Aeronautics and Space Administration; National Technical Information Service, distributor. 3

Chobotov, V. (1963). Gravity-Gradient Excitation of a Rotating Cable-Counterweight Space Station in Orbit. *Journal of Applied Mechanics, December*, 547–554. 3

Doty, P., Rupp, C. & Smith, H. (1995). First and second flights of the Small Expendable Deployer System. *1995 AIAA Space Programs and Technologies Conference*. 3

Freescale (2002). MC9S12C Family Device Users Guide. *Motorola*, **1.11**. 15

Ginsberg, J.H. (1998). *Advanced Engineering Dynamics*. Cambridge University Press. 23, 26

Gwaltney, M., D. Greene (1992). Ground-Based Implementation and Verification of Control Laws for Tethered Satellites. *Journal of Guidance, Control, and Dynamics*, **15**, 271–273. 59

Higuchi, K., Natori, M., Iwasa, T., Abe, M. & f Tokyo, U. (1997). A ground experiment of motion control of retrieving space tether. *AIAA/ASME/ASCE/AHS/ASC Structures, Structural Dynamics, and Materials Conference and Exhibit, 38 th, and AIAA/ASME/AHS Adaptive Structures Forum, Kissimmee, FL*, 714–719. 5, 22

Jin, Z., Waydo, S., Wildanger, E., Lammers, M., Scholze, H., Foley, P., Held, D. & Murray, R. (2004). MVWT-II: the second generation Caltech Multi-Vehicle Wireless Testbed. *American Control Conference, 2004. Proceedings of the 2004*, **6**, 5321–5326. 16

Johnson, L. & Herrmann, M. (1998). *International Space Station Electrodynamic Tether Reboost Study*. Springfield, VA: National Aeronautics and Space Administration, Marshall Space Flight Center; National Technical Information Service, distributor. 3

Lavis, D. (1985). Air Cushion Craft. *Naval Engineers Journal*, **97**, 262–264. 16, 17

Misra, A. & Modi, V. (1982). Dynamics and control of tether connected two-body systems-A brief review. *International Astronautical Federation, International Astronautical Congress, 33rd, Paris, France, Sept. 27-Oct. 2, 1982, 25 p.*. 2

Modi, V., Lakshmanan, P. & Misra, A. (1990). Offset control of tethered satellite systems: Analysis and experimental verification. *Acta Astronautica*, **21**, 283–294. 6

Modi, V., Pradhan, S., Chu, M., Tyc, G. & Misra, A. (1996). Experimental investigation of the dynamics of spinning tethered bodies. *Acta Astronautica*, **39**, 487–495. 7

Modi, V., Pradhan, S. & Misra, A. (1997). Controlled dynamics of flexible orbiting tethered systems- Analysis and experiments. *Journal of Vibration and Control*, **3**, 459–497. 4

NASA (2000). The Tethered Satellite System Reflight. *http://liftoff.msfc.nasa.gov/Shuttle/sts-75/tss-1r/brochure/*. 3

Padgett, D.A. (2006). *Nullcline Analysis as a Tethered Satellite Mission Design Tool*. Master's thesis, North Carolina State University. 2

Pengelley, C. (1966). Preliminary Survey of Dynamic Stability of Cable-Connected Spinning Space Station. *Journal of Spacecraft and Rockets*, **3**, 1456–1462. 2

Penzo, P. & Mayer, H. (1986). Tethers and asteroids for artificial gravity assist in the solar system. *Journal of Spacecraft and Rockets*, **23**, 79–82. 4

Pirozhenko, A. (1989). Spatial motion of two bodies with an elastic non-restraining coupling. *International Applied Mechanics*, **25**, 1153–1159. 59

Purdy, W., Coffey, S., Barnds, W., Kelm, B. & Davis, M. (1997). TiPS- Results of a tethered satellite experiment. *Astrodynamics 1997*, 3–23. 3

Schultz, F., Vigneron, F. & Jablonski, A. (2002). Horizontally-configured ground-test method for tethered satellites. *Canadian Aeronautics and Space Journal*, **48**, 97–106. 5

Sen, M. (1993). Dynamic analysis of a hemispherical dome levitated by an air jet. *Applied mathematical modelling*, **17**, 226–235. 53

Sorensen, K. (2003). Momentum eXchange Electrodynamic Reboost (MXER) Tether Technology Assessment Group Final Report. *NASA/MSFC In-Space Propulsion Technology Office, Huntsville, AL*. 4

Tai, C. & Loh, H. (1965). Planar Motion of Rotating Cable-Connected Space Station in Orbit. *Journal of Spacecraft and Rockets*, **2**, 889–901. 2

Thomson, W.T. (1986). *Introduction to Space Dynamics*. General Publishing Company, Ltd. 26

Trivailo, P., Williams, P. & Blanksby, C. (2002). Assessment of the Use of Tether Technology in the Future Exploration of Mars. *The* 2^{nd} *Australian Mars Exploration Conference, 12-14 July*. 3, 4

Tsiolkovskii, K. (1961). A Way to Stars. 1

TUI (2006). "http://www.tethers.com/orbittoorbit.html". *Tethers*. 9

Tyc, G., Vigneron, F., Jablonski, A., Han, R., Modi, V. & Misra, A. (1996). Flight dynamics results from the OEDIPUS-C tether mission. *AIAA/AAS Astrodynamics Conference, San Diego, CA*, 39–50. 4

Wells, H.G. (2004). *The First Men In The Moon*. 1^{st} World Library. 1

White, F.M. (2003). *Fluid Mechanics*. The McGraw-Hill Co., Inc. 46

Appendix

Appendix A

MatLab Files

The following files demonstrate how MatLab was used to determine the motion of the final system and to acquire the information from the experiments.

A.1 Deriving Equations for $\ddot{\vec{\theta}}$ and $\ddot{\vec{\phi}}$

```
%  th    - theta
%  phi   - phi
%  lam   - angle of the thrust fan
%  Izz   - moment of inertia about the Z axis
%  m     - mass of the hovercraft
%  Fthru - Force from the thrust fan
%  Ffric - Force due to friction
%  Ften  - Force due to the tension in the tether
%  rqo   - the length of Q with respect to O
%  iota  - the angle of the center of mass with respect to the P
```

```
%          axis
%
%  A anb B are used as shortened expressions for the unit vector
%        components
%        of Ffric.  Their actual expressions are substituted in
%        after ddth
%        and ddphi are determined.

syms ddth dth th ddphi dphi phi lam Izz m FthruFten rqo rcmp rpq
syms iota ddrqo drqo Ffric A B

Rqoi = abs(rqo).*cos(th);
Rqoj = abs(rqo).*sin(th);

oAqoi = ddrqo.*cos(th) - 2.*drqo.*dth.*sin(th) + abs(rqo).*(-ddth
        .*sin(th) - dth.^2.*cos(th));
oAqoj = ddrqo.*sin(th) + 2.*drqo.*dth.*cos(th) + abs(rqo).*(ddth.*
        cos(th) - dth.^2.*sin(th));

oApqi = (abs(rpq).*((-ddphi.*sin(phi) - dphi.^2.*cos(phi)) - ddth
        .*sin(phi) - 2.*dth.*(dphi).*cos(phi) - dth.^2.*cos(phi
        )).*cos(th)) - (abs(rpq).*((ddphi.*cos(phi) - dphi.^2.*sin
        (phi)) + ddth.*cos(phi) - 2.*dth.*(dphi).*sin(phi) - dth.^
        2.*sin(phi)).*sin(th));
oApqj = (abs(rpq).*((-ddphi.*sin(phi) - dphi.^2.*cos(phi)) - ddth
```

```
        .*sin(phi) - 2.*dth.*(dphi).*cos(phi) - dth.^2.*cos(phi
        )).*sin(th)) + (abs(rpq).*((ddphi.*cos(phi) - dphi.^2.*sin
        (phi)) + ddth.*cos(phi) - 2.*dth.*(dphi).*sin(phi) - dth.^
        2.*sin(phi)).*cos(th));

oAcmpi = (abs(rcmp).*(-(ddphi + ddth).*sin(iota) - (dth + dphi).^2
         .*cos(iota))).*cos(th + phi) - (abs(rcmp).*((ddth + ddphi
         ).*cos(iota) - (dth + dphi).^2.*sin(iota)).*sin(th + phi
         ));
oAcmpj = (abs(rcmp).*(-(ddphi + ddth).*sin(iota) - (dth + dphi).^2
         .*cos(iota))).*sin(th + phi) + (abs(rcmp).*((ddth + ddphi
         ).*cos(iota) - (dth + dphi).^2.*sin(iota)).*cos(phi + th
         ));

E1 = Izz.*(ddphi + ddth) + Ften.*(abs(rpq).*sin(phi) + abs(rcmp).*
     sin(phi + iota)) + Fthru.*(cos(lam + iota).*abs(rcmp))

E2 = m.*(oAqoi + oApqi + oAcmpi) + Ften.*(Rqoi/abs(rqo)) - Fthru.*
     (-sin(lam).*cos(th + phi) - cos(lam).*sin(th + phi)) + Ffric
     .*A

E3 = m.*(oAqoj + oApqj + oAcmpj) + Ften.*(Rqoj/abs(rqo)) - Fthru.*
     (-sin(lam).*sin(th + phi) + cos(lam).*cos(th + phi)) + Ffric
     .*B
```

A.2 Numerically Solving with Ode45

This is actually two separate M-files. The first is called simple5_ode45. It simply calls the function in single quotes and tells MatLab to solve it using ode45.

```
%  simple5_ode45
[time,X] = ode45('simple5_equation', [0 100], [0; 0; 0; 0]);
```

The second file is a function containing expressions for the angular accelerations in state space form. In this case, many of the expressions if left in their complete form would have taken up several pages. These expressions have been cut down to a single line. Any that end in "..." have been shortened. Also, in the first MatLab file, reference was made to expressions "A" and "B". This is where their actual formulas are substituted back into the final expressions.

```
function dx = simple2_ode45(t,x)
dx = zeros(4,1);


rqo = 10;%.01*t + 10;
drqo = 0.000001;%.01;
ddrqo = 0;


m = 2;
iota = 0;
lam = 60*pi/180;
Izz = .08333;
rcmp = .01;
rpq = .1;
```

```
Fthru = 1;
Ffric = .01*m + .11.*(((drqo.*cos(x(3))-abs(rqo).*x(4) ...

A = ((drqo.*cos(x(3))-abs(rqo).*x(4).*sin(x(3)) ...

B = ((drqo.*sin(x(3))+abs(rqo).*x(4).*cos(x(3)) ...

% --- simplified5 ---
dx(1) = x(2);
dx(2) = (-4*sin(x(3))*sin(x(1)+iota)*x(4)*x(2) ...
dx(3) = x(4);
dx(4) = ((-2*m*drqo*x(4)*sin(x(3))*abs(rpq)*sin(x(1)) ...
```

A.3 Acquiring the Experimental Data

This program makes reference to an excel file which was used to develop a trend line equation using geometry in order to correctly study the images taken at an angle. This file can be found on the Nonlinear Dynamics and Space Systems Laboratory on the NC States's Mechanical Engineering website. The address is *http://www.mae.ncsu.edu/research/ndssl/index.asp*.

```
%--------------------------------------------------------------------------
% This file finds an object in an image by subtracting out a background
% image.  The position is stored in two arrays "x_position" and "y_position".
% The angle is stored in an array called "angle".
%--------------------------------------------------------------------------
```

```
% characteristics of the files
%   A,B,C,D come from the trend line equation found in the Excel file
%   "image_perspective_example". They are of the form Ax^3+Bx^2+Cx+D

m_max = 400;%480;
trial_file = trial_4_20_25_1_3(1:m_max,:,:,:);   %day6_trial2_p1;
bg_image = bg_4_20(1:m_max,:,:);   %day9_bg;
time_test = time_4_20_25_1_3;   %time1;
number_of_frames = 95;
%camera_angle = 51;
%x_inertial = 355;   %366;
%y_inertial = 206;   %176;
x_inertial_in = 110;
y_inertial_in = 120;   %113

A = -0.000001174;
B = 0.001522205;
C = 0.042201668;
D = -1.656588812;

level_coefficient = .6; % <-- affects how the images are subtracted

%             side walls
%    (x1,y1) /          \ (x3,y3)      hor1 --------------wall
%           /            \
%          /              \
%         /                \           hor2 --------------black line
%   (x2,y2)                 (x4,y4)          --------------black line
```

```
x1 = 128;                                   hor1 = 58;
y1 = 63;
                                            hor2 = 280;
x2 = 26;
y2 = 282;

x3 = 580;
y3 = 57;

x4 = 682;
y4 = 276;

% declaring variables

faulty = zeros(number_of_frames,1);
position_pix = zeros(1,2,number_of_frames);

x_position = zeros(number_of_frames,1);
y_position = zeros(number_of_frames,1);
angle_pix = zeros(number_of_frames,1);
i = 1;
k = 0;
z = 0;

% reducing the background image

for j = 1:1:number_of_frames
   trial(:,:,1,j) = imsubtract(trial_file(:,:,1,j),bg_image(:,:,1));
end
```

```
%trial(:,:,2:3) = [];

for j = 1:1:number_of_frames
   trial(:,:,:,j) = imadjust(trial(:,:,:,j));
end

level = level_coefficient;   graythresh(trial(:,:,:,:));
trial(:,:,:,:) = im2bw(trial(:,:,:,:),level);
trial(:,:,:,:) = trial(:,:,:,:).*255;



% finding the actual object based on size/color criteria

for j = 1:1:number_of_frames
    [labeled, numObjects] = bwlabel(~trial(:,:,i,j),8);
    properties = regionprops(labeled,'Area');

    for a = 1:1:numObjects
        if (properties(a).Area > 700) || (properties(a).Area < 50)
            for m = 1:1:m_max
                for n = 1:1:720
                    if (labeled(m,n) == a)
                        trial(m,n,1,j) = 255;
                    end
                end
            end
        end
    end
end
```

```
for j = 1:1:number_of_frames
    for m = 1:1:m_max
        for n = 1:1:720
            if trial(m,n,1,j) == 0
                trial(m,n,1,j) = 255;
            elseif trial(m,n,1,j) == 255
                trial(m,n,1,j) = 0;
            end
        end
    end
end

trial = uint8(trial./255);

%  getting information from the image

hor1_revised = hor1-(A*hor1^3 + B*hor1^2 + C*hor1 + D)
               - mod(A*hor1^3 + B*hor1^2 + C*hor1 + D,1);
hor2_revised = hor2-(A*hor2^3 + B*hor2^2 + C*hor2 + D)
               - mod(A*hor2^3 + B*hor2^2 + C*hor2 + D,1);

for j = 1:1:number_of_frames

  labeled = double(trial(:,:,1,j));
   % if numObjects > 1
   %      faulty(j) = 1;
  %       i = i + 1;
  %  elseif numObjects == 1
         position1 = regionprops(labeled,'Centroid');
         position_pix(:,:,j) = [position1.Centroid];
```

```
        wall1 = (position_pix(1,2,j)
                - (y1 - ((y2-y1)/(x2-x1))*x1))/((y2-y1)/(x2-x1));
        % x = (y-b)/m
        wall2 = (position_pix(1,2,j)
                - (y3 - ((y4-y3)/(x4-x3))*x3))/((y4-y3)/(x4-x3));
        m_prime = (A*position_pix(1,2,j)^3 + B*position_pix(1,2,j)^2
        + C*position_pix(1,2,j) + D)
        - mod(A*position_pix(1,2,j)^3 + B*position_pix(1,2,j)^2
        + C*position_pix(1,2,j) + D,1);

        x_position(j,1) = 221.5*((wall1-position_pix(1,1,j))/(wall1-wall2));
        % in inches
        y_position(j,1) = 169.75*((hor1_revised -
        (position_pix(1,2,j)-m_prime))/(hor1_revised - hor2_revised));
        % in inches
%   else                  231.5
%   end

   test_image = zeros(m_max,720);
 %  if numObjects == 1
       for m = (position_pix(1,2,j)
               -mod(position_pix(1,2,j),1)-20):1:(position_pix(1,2,j)
               -mod(position_pix(1,2,j),1)+20)
          for n = (position_pix(1,1,j)
          -mod(position_pix(1,1,j),1)-25):1:(position_pix(1,1,j)
          -mod(position_pix(1,1,j),1)+25)
              if trial(m,n,1,j) ~= 0
               wall1 = (m - (y1 - ((y2-y1)/(x2-x1))*x1))/((y2-y1)/(x2-x1));
               wall2 = (m - (y3 - ((y4-y3)/(x4-x3))*x3))/((y4-y3)/(x4-x3));
               % x = (y-b)/m
```

```
                    m_prime = (A*m^3 + B*m^2 + C*m + D)
                              - mod(A*m^3 + B*m^2 + C*m + D,1);
                  % ^-- This needs to be altered when the camera moves

                    m_position(j) = 221.5*((wall1 - n)/(wall1 - wall2));
                    % in inches
                    n_position(j) = 231.5*((hor1_revised
                                    - (m-m_prime))/(hor1_revised
                                    - hor2_revised));
                    % in inches

                    test_image(n_position(j)-mod(n_position(j),1)
                               ,m_position(j)-mod(m_position(j),1)) = 255;
                else
                end
            end
        end
        test_image = uint8(test_image./255);
        labeled = double(test_image(:,:));
        angle_hc = regionprops(labeled,'Orientation');
        angle_pix(j,1) = [angle_hc.Orientation];
        test_image = test_image.*255;

   %else
   %end
end

%  deriving theta

for j = 1:1:number_of_frames
```

```
    theta(j,1) = ((atan((y_inertial_in - y_position(j))
                /(x_position(j) - x_inertial_in))) - k*pi)*180/pi;
    angle(j,1) = angle_pix(j,1) - z*180;
    if j>1
        if theta(j,1) > (theta(j-1,1)+80)
            k = k + 1;
            theta(j,1) = ((atan((y_inertial_in-y_position(j))/(x_position(j)
                        - x_inertial_in))) - k*pi)*180/pi;
        else
        end
        if angle_pix(j,1) > (angle_pix(j-1,1)+80)
            z = z + 1;
            angle(j,1) = angle_pix(j,1) - z*180;
        else
        end
        if angle_pix(j,1) < (angle_pix(j-1,1)-80)
            z = z - 1;
            angle(j,1) = angle_pix(j,1) - z*180;
        else
        end
    else
    end
end



i = 1;
for j = 1:1:number_of_frames
    if faulty(j) == 0
        time4(i,1) = time_test(j,1);
        x_position4(i,1) = x_position(j,1);
```

```
        y_position4(i,1) = y_position(j,1);
        angle_pix4(i,1) = angle_pix(j,1);
        theta4(i,1) = theta(j,1);
        angle4(i,1) = angle(j,1);
        phi = theta4-angle4;
        %length4(i,1) = sqrt((y_position1(i,1) - y_inertial_in).^2
                        + (x_position1(i,1) - x_inertial_in).^2);
        i = i + 1;
    else
    end
end
```

```
clear x1 x2 x3 x4 y1 y2 y3 y4 hor1 hor2 number_of_frames camera_angle;
clear x_inertial y_inertial x_inertial_in y_inertial_in i j position_pix;
clear m_prime wall1 wall2 properties position1 k theta angle A B C D;
clear numObjects m_position n_position m n level_coefficient angle_hc a;
clear background level m_max labeled ans z hor1_revised hor2_revised;
clear angle_pix1 trial_file bg_image time_test
% some of these may be better not to clear
clear x_position y_position angle_pix  faulty test_image trial;
```

Appendix B

Results

This section presents the results of the experiment and compares them to the theoretical analysis. The beginning of each set of results summarizes the configuration for that particular setup; tether length, thrust fan angle, etc. For each setup there were multiple trials[1] The first shows theta; the angle the tether makes with the absolute horizontal. The second graph compares the experimental phi, the angle the hovercraft makes with the tether. Voltage applied at the lift fans would tend to affect the results. As such, for these graphs, the trials are color coded by the order that they were conducted; red, green, blue, indigo, then violet.

The next couple of graphs compare the experimental and analytic results. The analytic result is always a solid, red line. It is overlayed on the experimental trials. The majority of the experimental trials are yellow. In order to better recognize the similarities and differences of the experimental versus the analytic results, one of the trials is a solid, green line to distinguish it from the experimental grouping. This may also be useful to pick out details of the experimental results that were lost in the jumble of the previous set of graphs.

The majority of the setups focus on a constant tether length. The position is actually described as the distance, in inches, of the hovercraft center from the far left corner of the squash court. A graph of the hovercraft position would simply be a circle and is generally

[1]Typically there would be 5 trials. However, some may contain fewer due to errors in the experiment.

considered not worthwhile to show. However, for the final graphs which demonstrate the effects of reeling in and out, the position is more interesting and shows the change in length and was included.

B.1 Setup 1

Table B.1: Configuration of Setup 1

Length of Tether	1.278m
Length of $r_{P/Q}$	.2m
Angle of Tether Attachment	0°
Offset of Center of Mass	.005m
Offset Angle of Center of Mass	30°
Mass of Hovercraft	1.1233kg
Inertia of Hovercraft	$.0175kgm^2$
Angle of Thrust Fan	15°
Thrust Force	.421N
Friction Expression	$.02\dot{\theta} + .3\dot{\theta}$
Rotational Friction Expression	$-0.004\dot{\theta}$

The first 6 setups only vary the thrust fan angle. Throughout this set the trends discussed in chapter 8 can be seen. The analytic θ matches closely to the experimental. Also, the range and average of ϕ for the trials is similar. However, the frequency of ϕ for the analytic results is significantly greater than for the experimental.

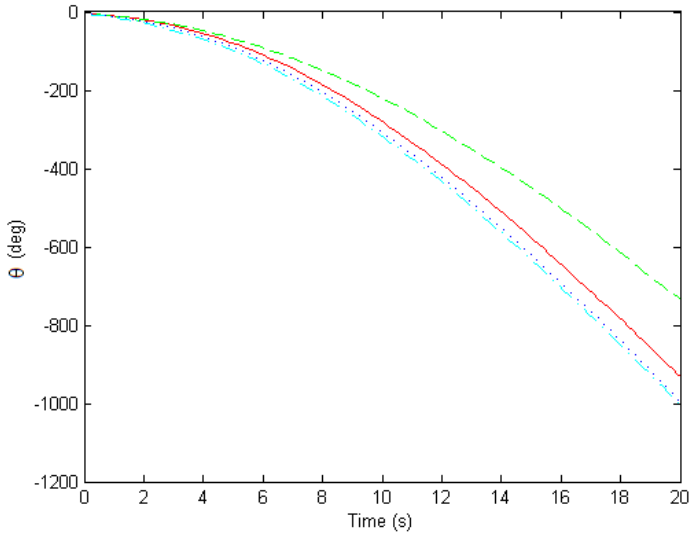

Figure B.1: Angle of the Hovercraft with the Inertial Frame for Setup 1

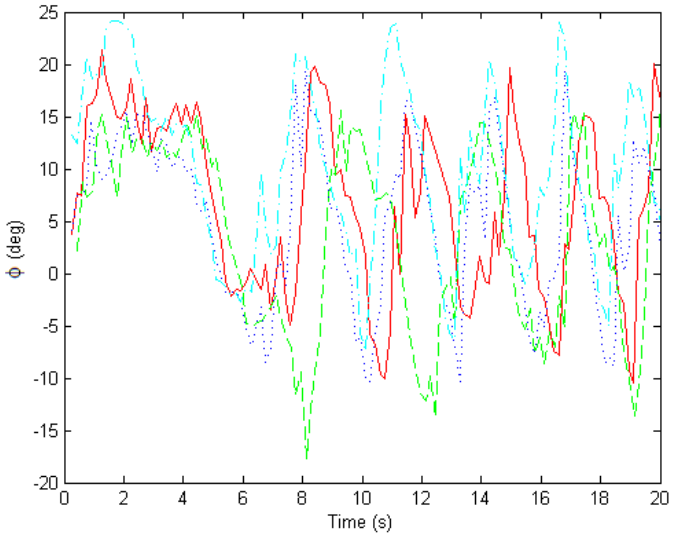

Figure B.2: Attitude of the Hovercraft for Setup 1

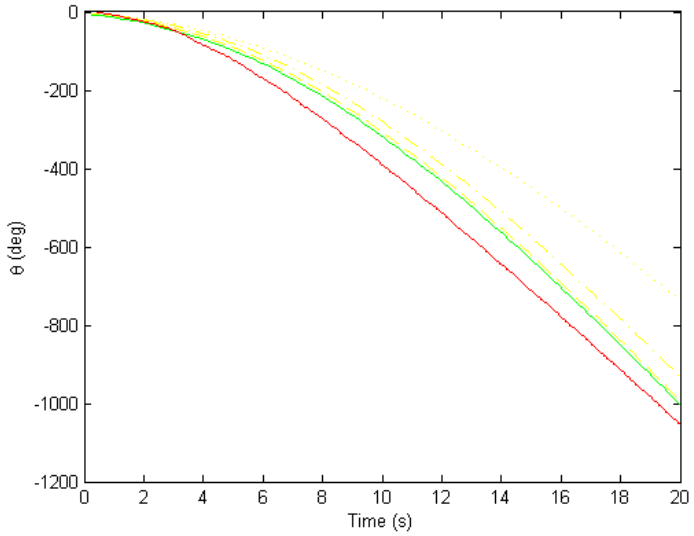

Figure B.3: Comparison of the Analytical and Experimental Results of Tether Angle for Setup 1

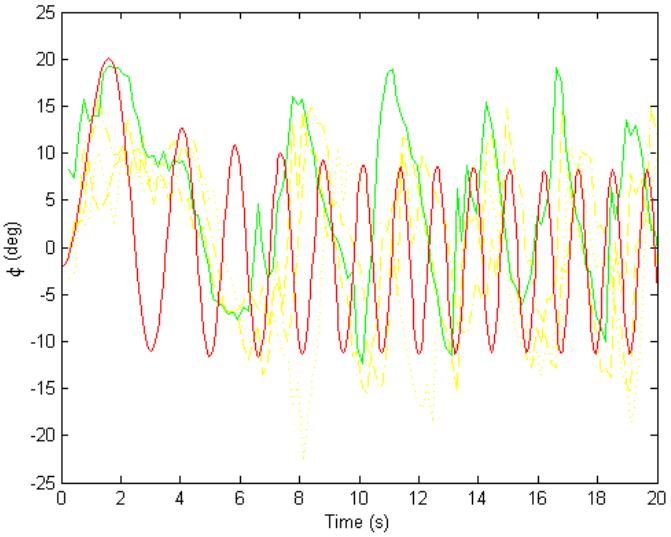

Figure B.4: Comparison of the Analytical and Experimental Results of Hovercraft Attitude for Setup 1

B.2 Setup 2

Table B.2: Configuration of Setup 2

Length of Tether	1.278m
Length of $r_{P/Q}$	0.2m
Angle of Tether Attachment	0°
Offset of Center of Mass	0.01m
Offset Angle of Center of Mass	-150°
Mass of Hovercraft	1.1233kg
Inertia of Hovercraft	$.0172kgm^2$
Angle of Thrust Fan	30°
Thrust Force	0.421N
Friction Expression	$.03\dot{\theta} + 0.2\dot{\theta}$
Rotational Friction Expression	$-0.006\dot{\theta}$

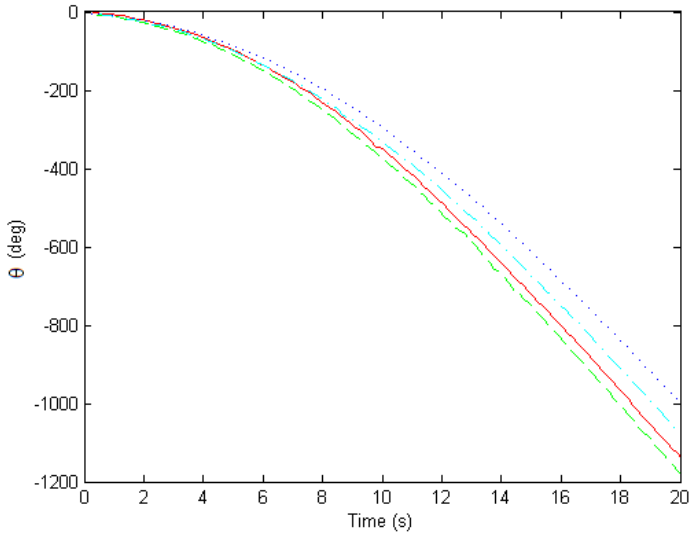

Figure B.5: Angle of the Hovercraft with the Inertial Frame for Setup 2

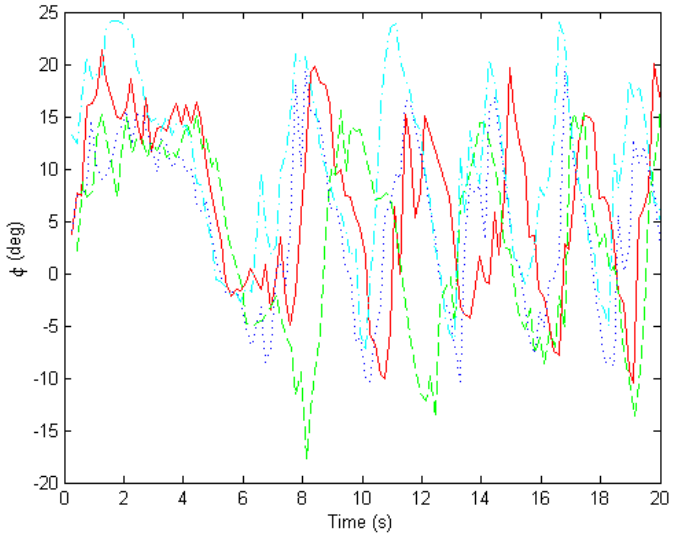

Figure B.6: Attitude of the Hovercraft for Setup 2

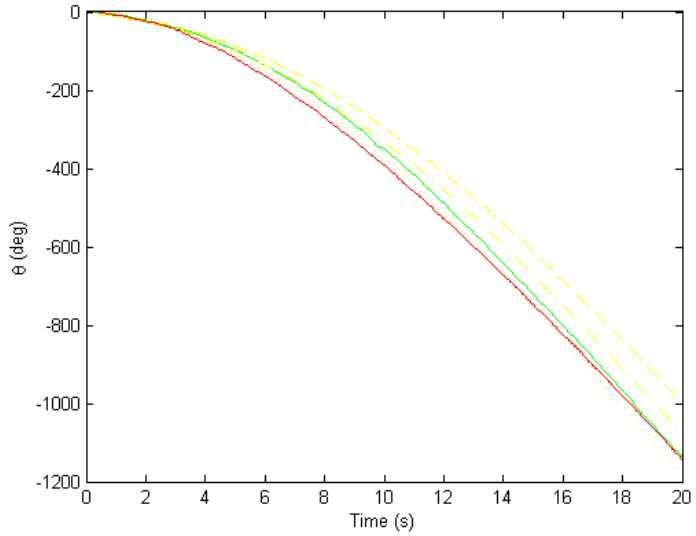

Figure B.7: Comparison of the Analytical and Experimental Results of Tether Angle for Setup 2

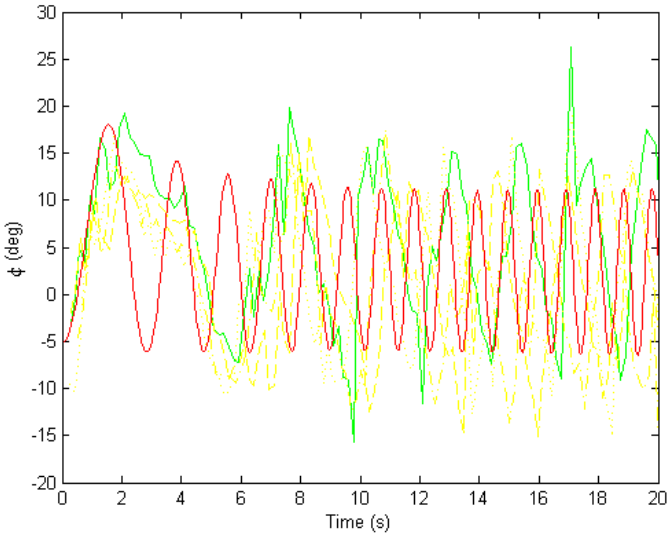

Figure B.8: Comparison of the Analytical and Experimental Results of Hovercraft Attitude for Setup 2

B.3 Setup 3

Table B.3: Configuration of Setup 3

Length of Tether	1.278m
Length of $r_{P/Q}$	0.2m
Angle of Tether Attachment	$0°$
Offset of Center of Mass	0.02m
Offset Angle of Center of Mass	$-170°$
Mass of Hovercraft	1.1233kg
Inertia of Hovercraft	$.0172kgm^2$
Angle of Thrust Fan	$45°$
Thrust Force	0.421N
Friction Expression	$.03\dot{\theta} + 0.1\dot{\theta}$
Rotational Friction Expression	$-0.006\dot{\theta}$

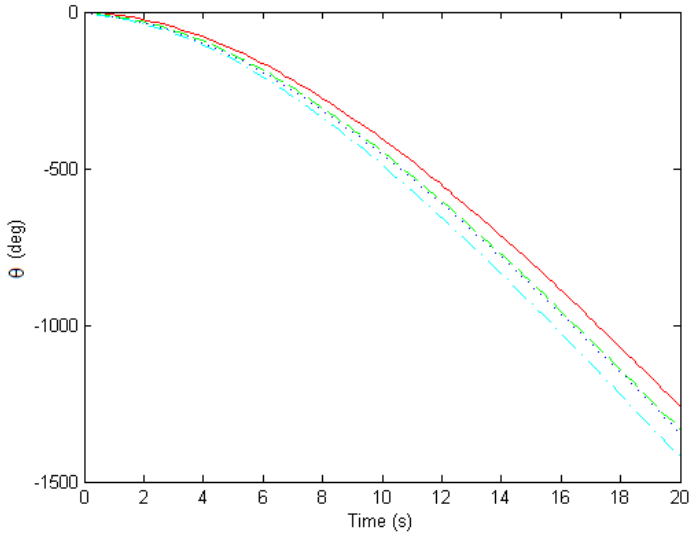

Figure B.9: Angle of the Hovercraft with the Inertial Frame for Setup 3

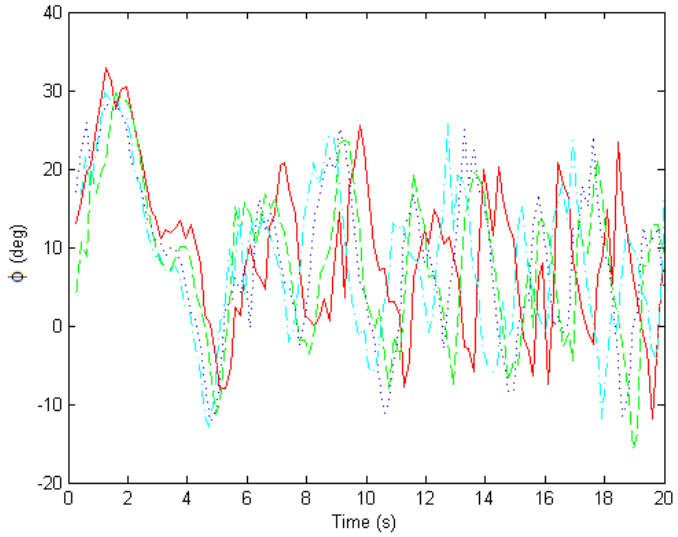

Figure B.10: Attitude of the Hovercraft for Setup 3

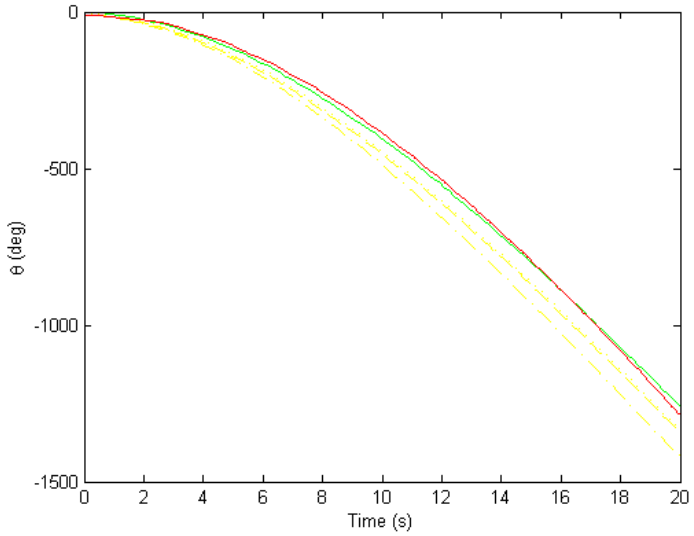

Figure B.11: Comparison of the Analytical and Experimental Results of Tether Angle for Setup 3

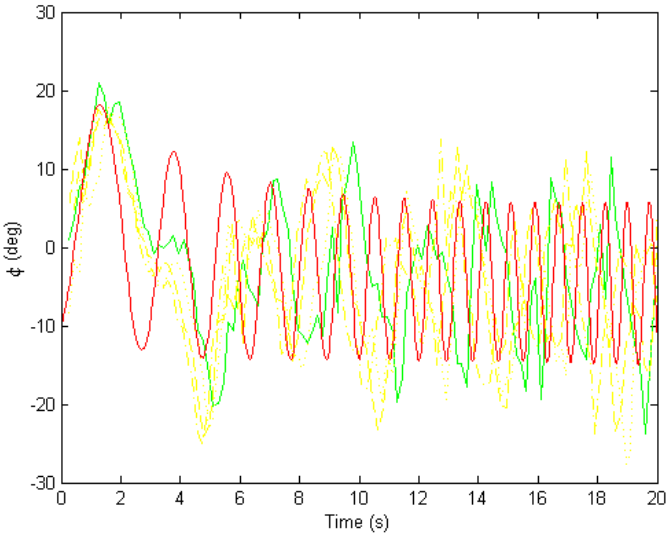

Figure B.12: Comparison of the Analytical and Experimental Results of Hovercraft Attitude for Setup 3

B.4 Setup 4

Table B.4: Configuration of Setup 4

Length of Tether	1.278m
Length of $r_{P/Q}$	0.2m
Angle of Tether Attachment	0°
Offset of Center of Mass	0.015m
Offset Angle of Center of Mass	$-175°$
Mass of Hovercraft	1.1233kg
Inertia of Hovercraft	$.0169kgm^2$
Angle of Thrust Fan	60°
Thrust Force	0.421N
Friction Expression	$.03\dot{\theta} + 0.13\dot{\theta}$
Rotational Friction Expression	$-0.006\dot{\theta}$

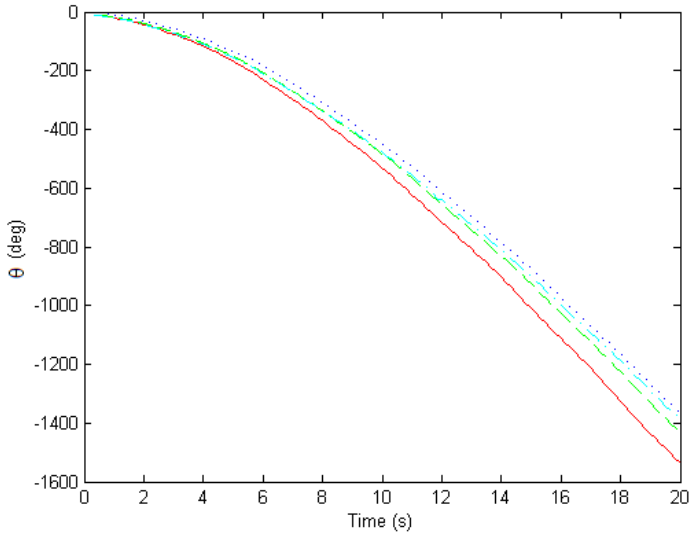

Figure B.13: Angle of the Hovercraft with the Inertial Frame for Setup 4

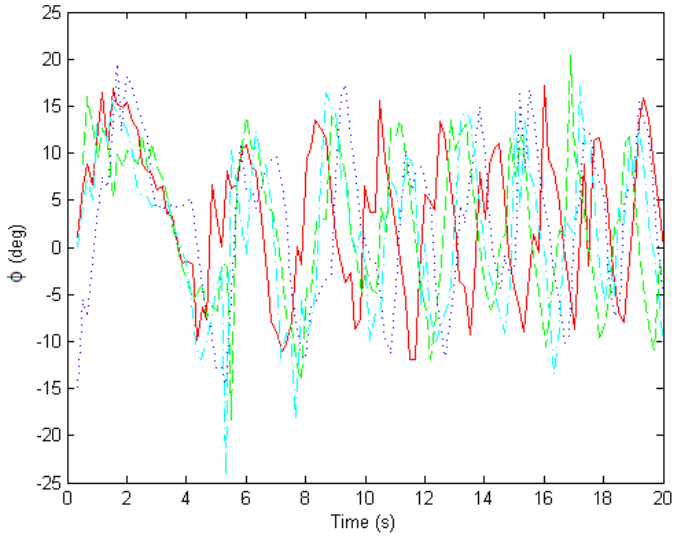

Figure B.14: Attitude of the Hovercraft for Setup 4

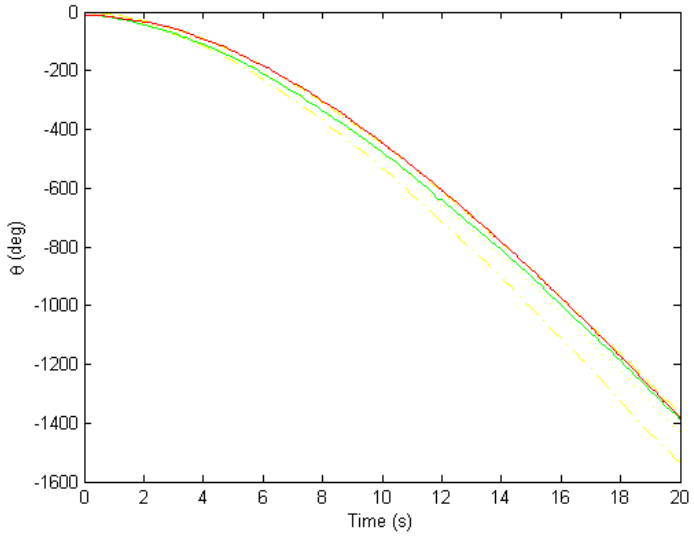

Figure B.15: Comparison of the Analytical and Experimental Results of Tether Angle for Setup 4

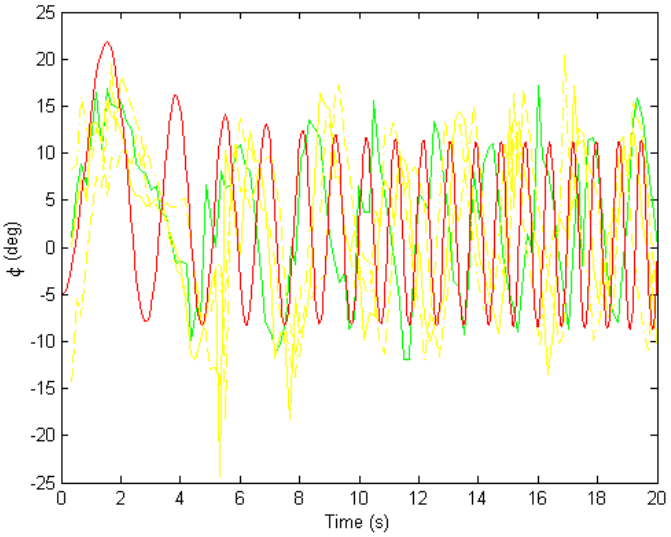

Figure B.16: Comparison of the Analytical and Experimental Results of Hovercraft Attitude for Setup 4

B.5 Setup 5

Table B.5: Configuration of Setup 5

Length of Tether	1.278m
Length of $r_{P/Q}$	0.2m
Angle of Tether Attachment	0°
Offset of Center of Mass	0.02m
Offset Angle of Center of Mass	-100°
Mass of Hovercraft	1.1233kg
Inertia of Hovercraft	$.0168kgm^2$
Angle of Thrust Fan	75°
Thrust Force	0.421N
Friction Expression	$.03\dot{\theta} + 0.2\dot{\theta}$
Rotational Friction Expression	$-0.006\dot{\theta}$

This trial is particularly useful for discussing the damping of certain oscillations of the hovercraft attitude discussed in Chapter 8. The analytic θ is a nearly perfect match with three of the experimental trials. However, the peak frequency of ϕ is still greater in the analytic results. It can be observed, especially in the second crest of the analytic attitude, that there is an experimental crest which matches the frequency but is significantly smaller compared to the surrounding crests. This damped oscillation is repeated throughout the time scale. If they were all of equal magnitude then the peak frequencies would be similar.

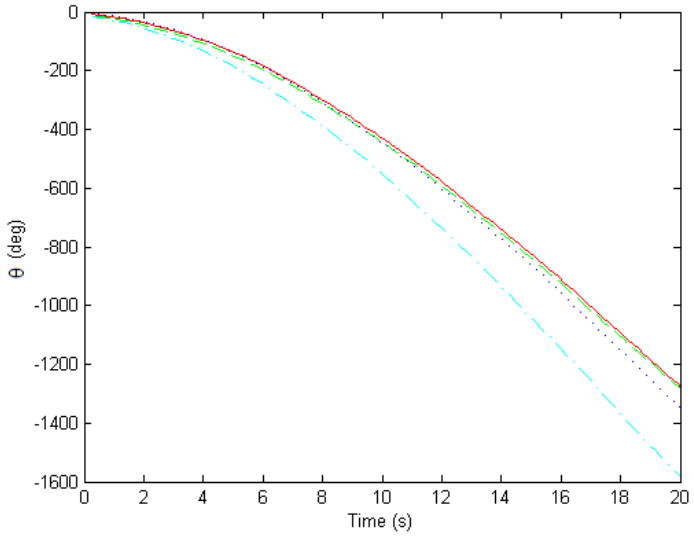

Figure B.17: Angle of the Hovercraft with the Inertial Frame for Setup 5

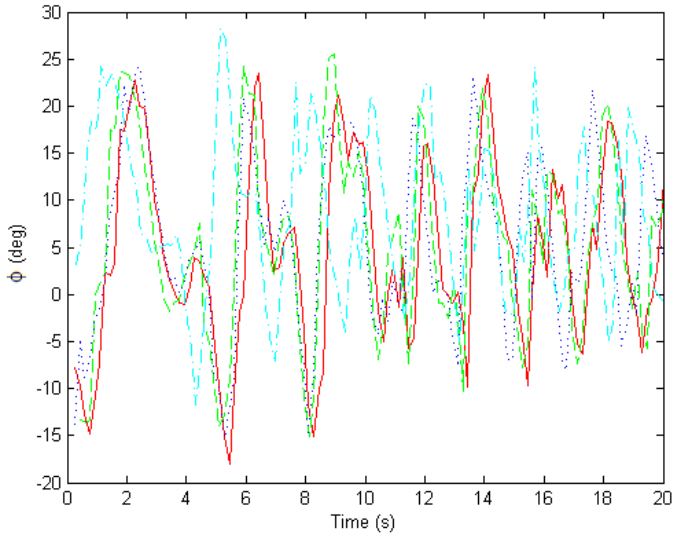

Figure B.18: Attitude of the Hovercraft for Setup 5

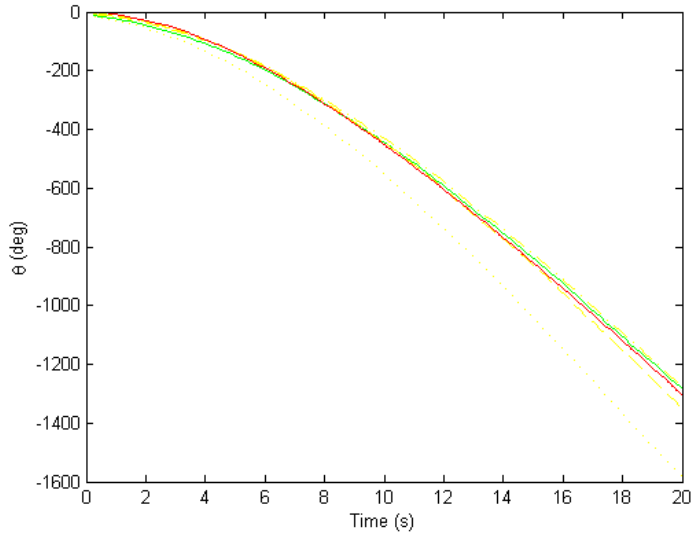

Figure B.19: Comparison of the Analytical and Experimental Results of Tether Angle for Setup 5

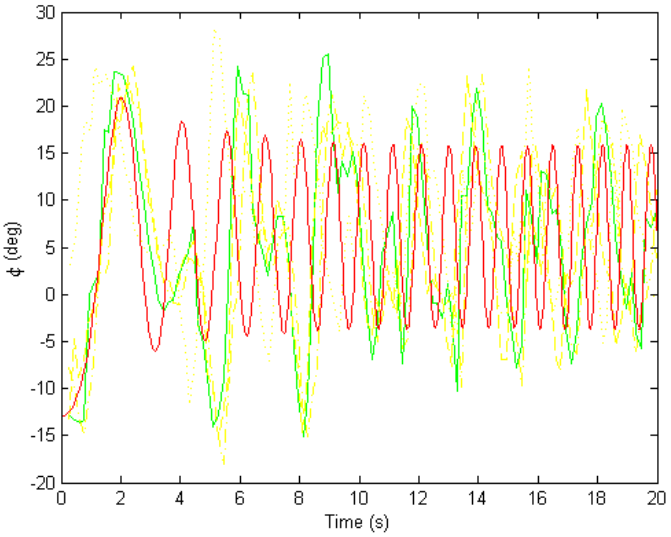

Figure B.20: Comparison of the Analytical and Experimental Results of Hovercraft Attitude for Setup 5

B.6 Setup 6

Table B.6: Configuration of Setup 6

Length of Tether	1.278m
Length of $r_{P/Q}$	0.2m
Angle of Tether Attachment	0°
Offset of Center of Mass	0.015m
Offset Angle of Center of Mass	-135°
Mass of Hovercraft	1.1233kg
Inertia of Hovercraft	$.0168kgm^2$
Angle of Thrust Fan	15°
Thrust Force	0.421N
Friction Expression	$.03\dot{\theta} + 0.2\dot{\theta}$
Rotational Friction Expression	$-0.006\dot{\theta}$

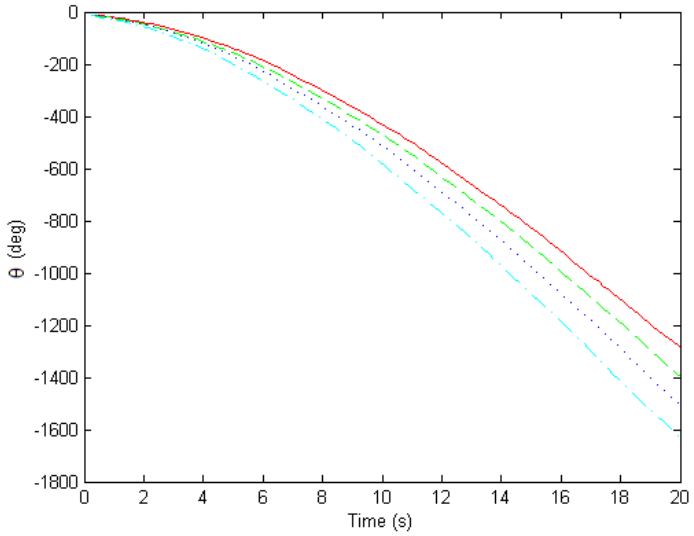

Figure B.21: Angle of the Hovercraft with the Inertial Frame for Setup 6

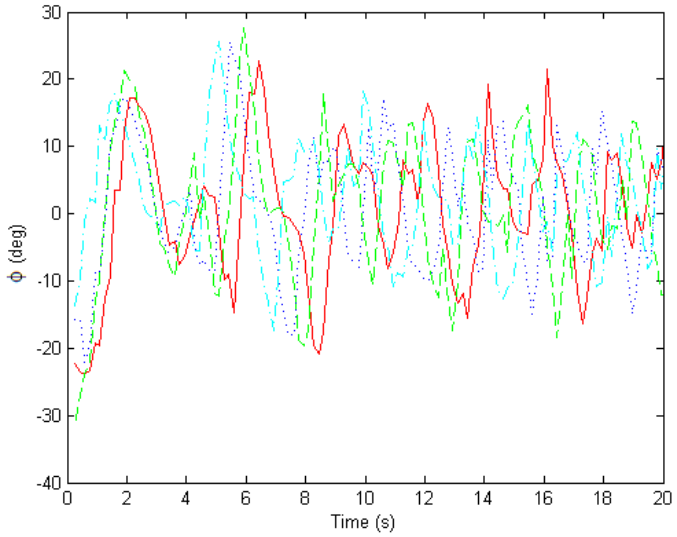

Figure B.22: Attitude of the Hovercraft for Setup 6

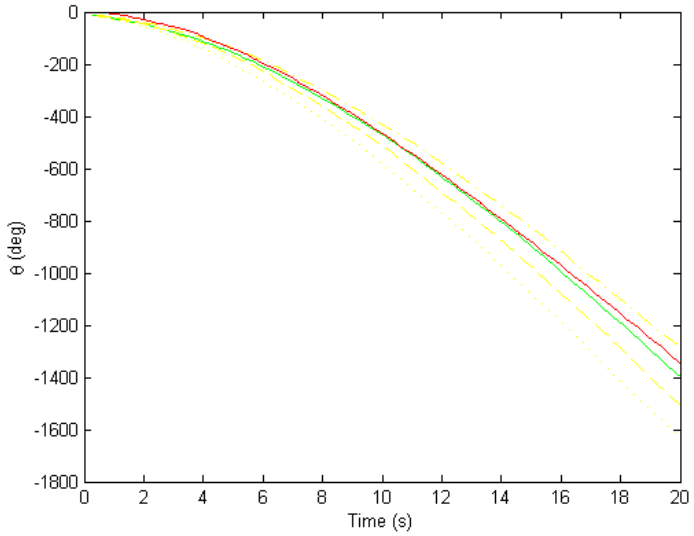

Figure B.23: Comparison of the Analytical and Experimental Results of Tether Angle for Setup 6

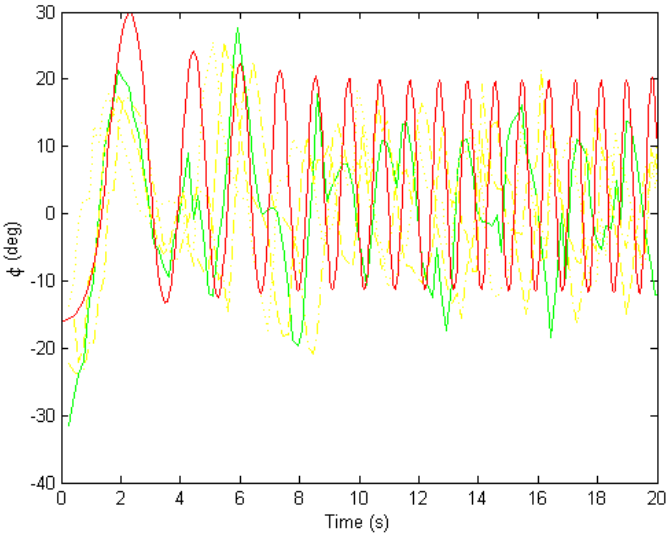

Figure B.24: Comparison of the Analytical and Experimental Results of Hovercraft Attitude for Setup 6

B.7 Setup 7

Table B.7: Configuration of Setup 7

Length of Tether	0.533m
Length of $r_{P/Q}$	0.2m
Angle of Tether Attachment	0°
Offset of Center of Mass	0.02m
Offset Angle of Center of Mass	−90°
Mass of Hovercraft	1.1233kg
Inertia of Hovercraft	$.0175kgm^2$
Angle of Thrust Fan	15°
Thrust Force	0.421N
Friction Expression	$.08\dot{\theta} + 0.27\dot{\theta}$
Rotational Friction Expression	$-0.011\dot{\theta}$

The next six setups repeat the same angle configuration for a different length of tether.

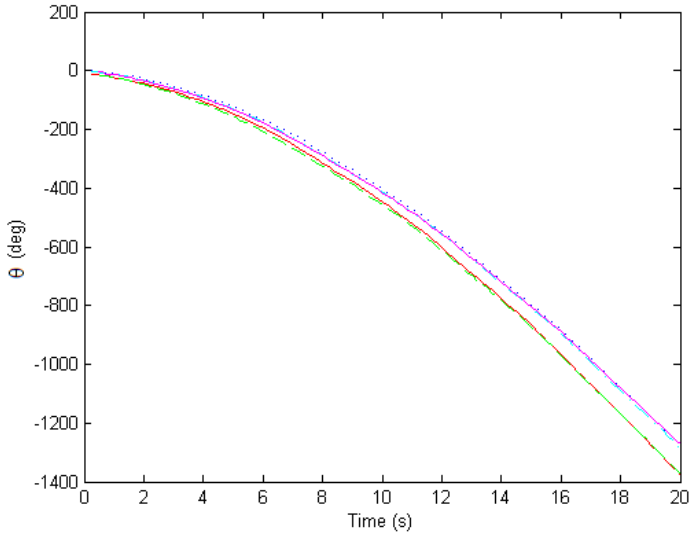

Figure B.25: Angle of the Hovercraft with the Inertial Frame for Setup 7

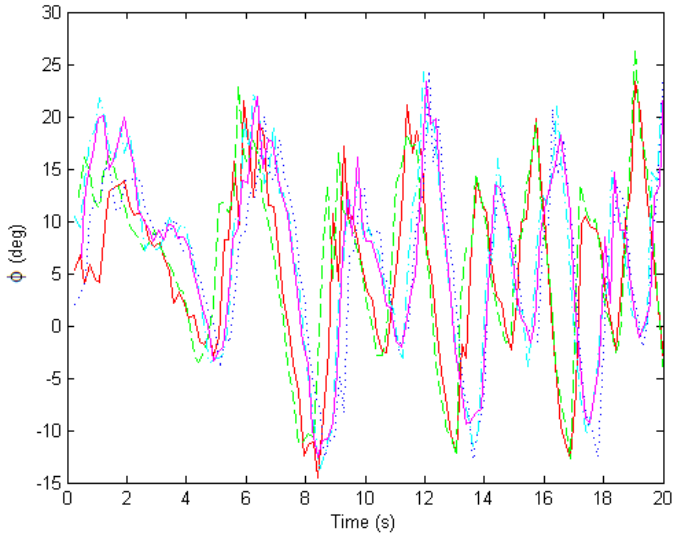

Figure B.26: Attitude of the Hovercraft for Setup 7

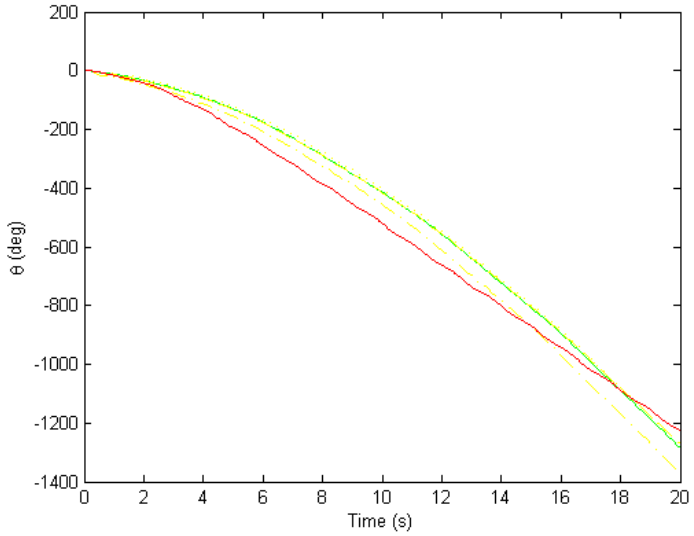

Figure B.27: Comparison of the Analytical and Experimental Results of Tether Angle for Setup 7

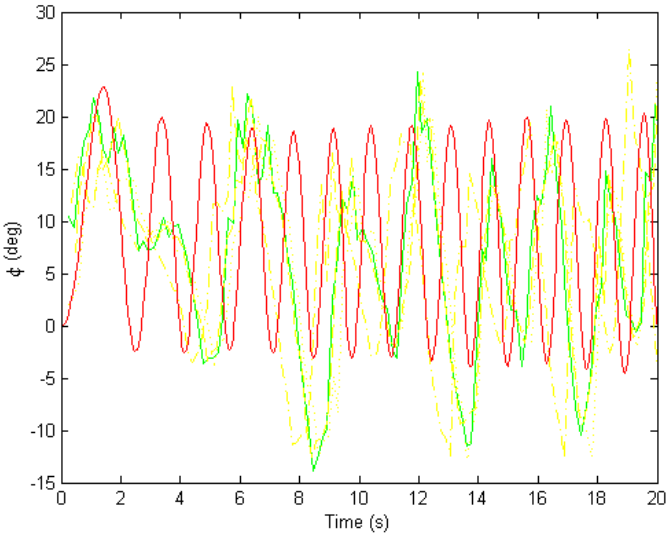

Figure B.28: Comparison of the Analytical and Experimental Results of Hovercraft Attitude for Setup 7

B.8 Setup 8

Table B.8: Configuration of Setup 8

Length of Tether	0.533m
Length of $r_{P/Q}$	0.2m
Angle of Tether Attachment	0°
Offset of Center of Mass	0.02m
Offset Angle of Center of Mass	-45°
Mass of Hovercraft	1.1233kg
Inertia of Hovercraft	$.0172kgm^2$
Angle of Thrust Fan	30°
Thrust Force	0.421N
Friction Expression	$.035\dot{\theta} + 0.213\dot{\theta}$
Rotational Friction Expression	$-0.007\dot{\theta}$

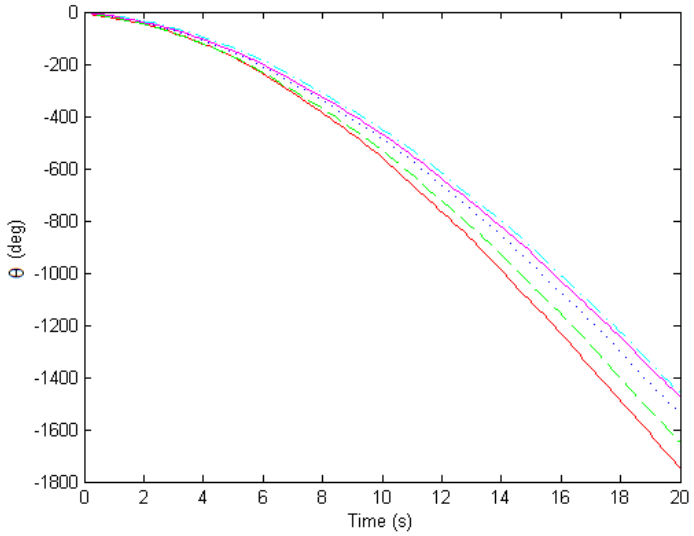

Figure B.29: Angle of the Hovercraft with the Inertial Frame for Setup 8

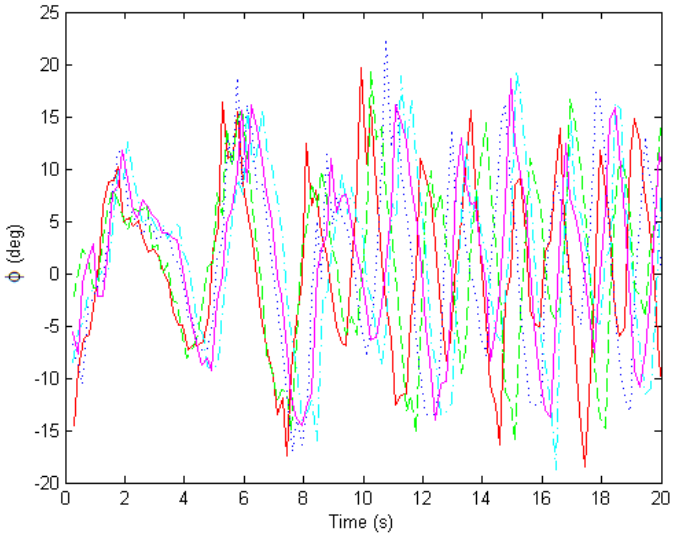

Figure B.30: Attitude of the Hovercraft for Setup 8

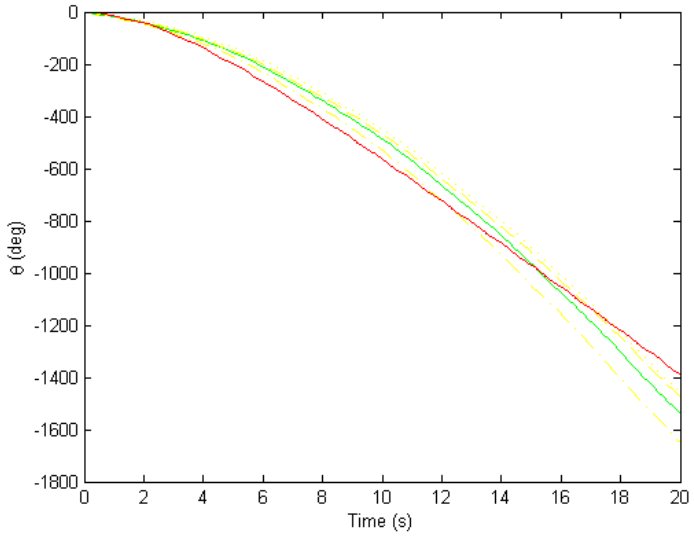

Figure B.31: Comparison of the Analytical and Experimental Results of Tether Angle for Setup 8

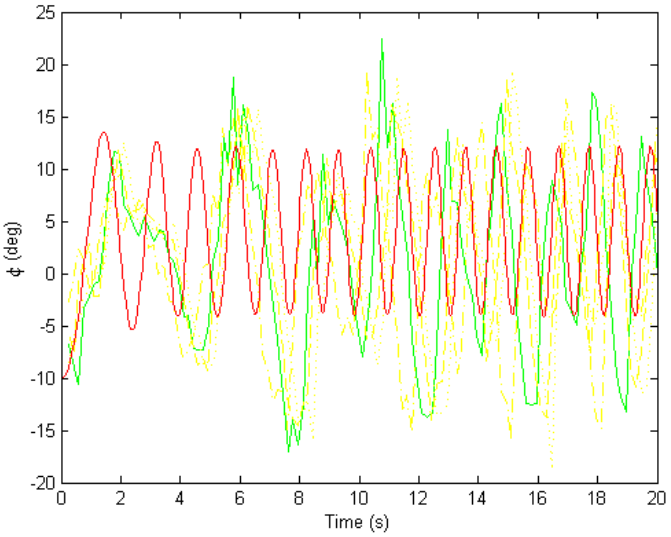

Figure B.32: Comparison of the Analytical and Experimental Results of Hovercraft Attitude for Setup 8

B.9 Setup 9

Table B.9: Configuration of Setup 9

Length of Tether	0.533m
Length of $r_{P/Q}$	0.2m
Angle of Tether Attachment	$0°$
Offset of Center of Mass	0.01m
Offset Angle of Center of Mass	$-45°$
Mass of Hovercraft	1.1233kg
Inertia of Hovercraft	$.0172kgm^2$
Angle of Thrust Fan	$45°$
Thrust Force	0.421N
Friction Expression	$.032\dot{\theta} + 0.160\dot{\theta}$
Rotational Friction Expression	$-0.006\dot{\theta}$

Setups 9, 10, and 11 exhibit a behavior unlike the others in the set. It appears that the experiments drag longer in the beginning of their motion. The most likely reason for this behavior is that the balance was off.

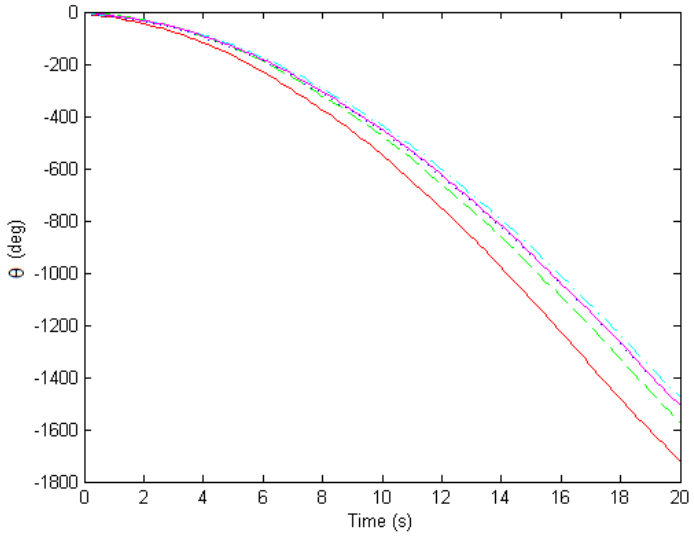

Figure B.33: Angle of the Hovercraft with the Inertial Frame for Setup 9

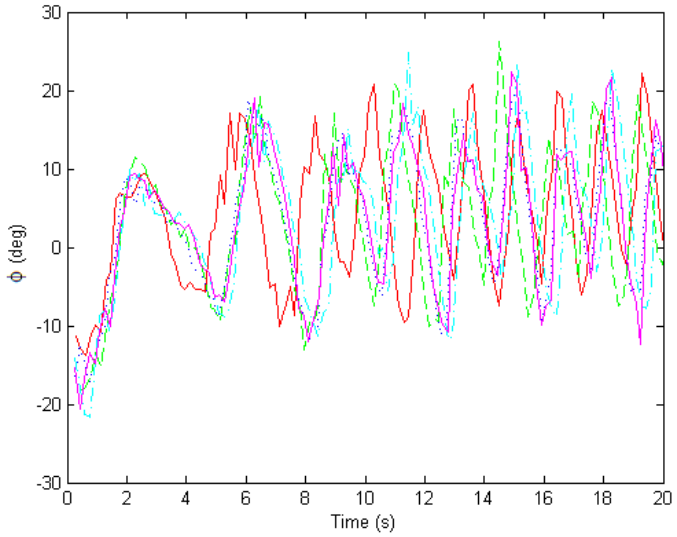

Figure B.34: Attitude of the Hovercraft for Setup 9

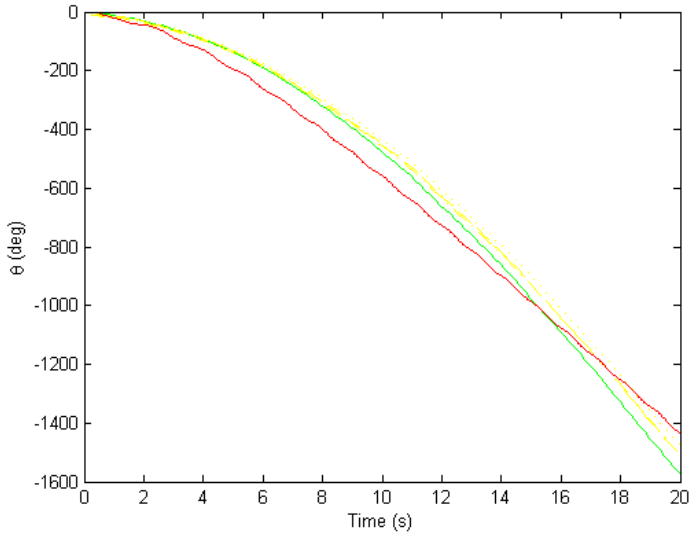

Figure B.35: Comparison of the Analytical and Experimental Results of Tether Angle for Setup 9

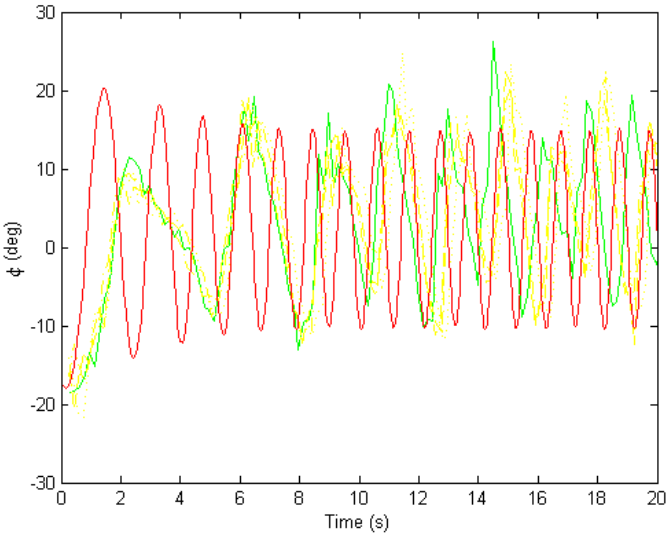

Figure B.36: Comparison of the Analytical and Experimental Results of Hovercraft Attitude for Setup 9

B.10 Setup 10

Table B.10: Configuration of Setup 10

Length of Tether	0.533m
Length of $r_{P/Q}$	0.2m
Angle of Tether Attachment	0°
Offset of Center of Mass	0.01m
Offset Angle of Center of Mass	-120°
Mass of Hovercraft	1.1233kg
Inertia of Hovercraft	$.0169kgm^2$
Angle of Thrust Fan	60°
Thrust Force	0.421N
Friction Expression	$.043\sqrt{\dot{\theta}} + 0.091\dot{\theta}$
Rotational Friction Expression	$-0.009\sqrt{\dot{\theta}}$

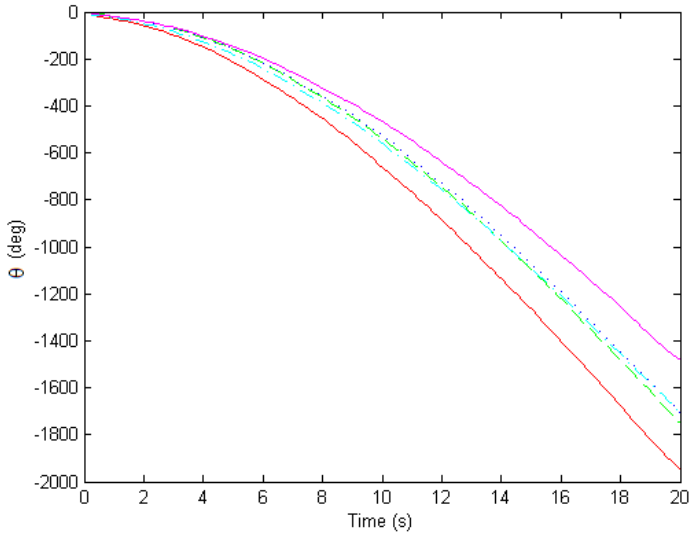

Figure B.37: Angle of the Hovercraft with the Inertial Frame for Setup 10

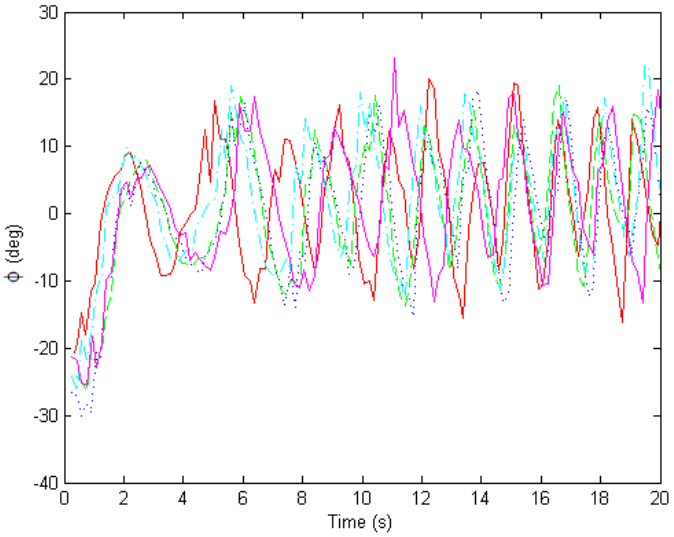

Figure B.38: Attitude of the Hovercraft for Setup 10

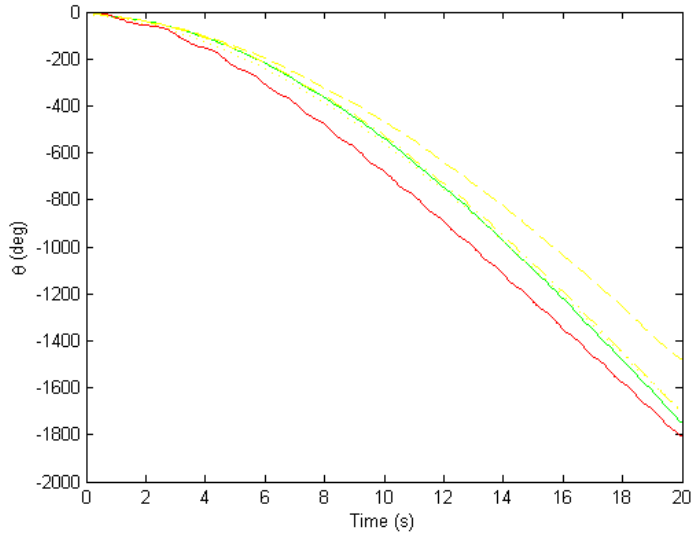

Figure B.39: Comparison of the Analytical and Experimental Results of Tether Angle for Setup 10

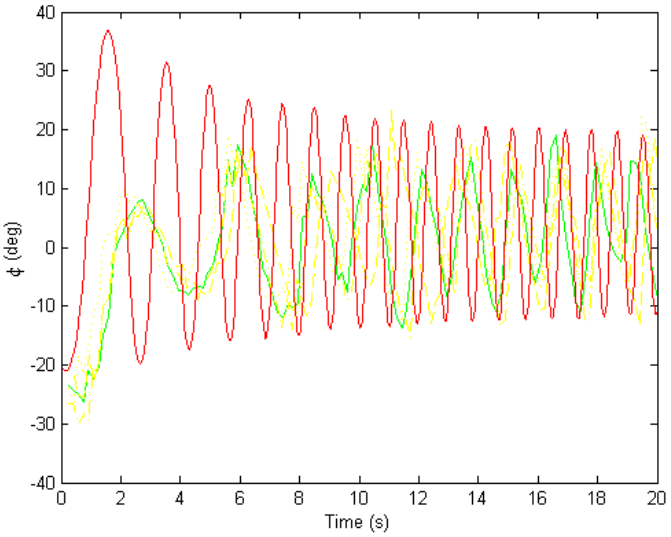

Figure B.40: Comparison of the Analytical and Experimental Results of Hovercraft Attitude for Setup 10

B.11 Setup 11

Table B.11: Configuration of Setup 11

Length of Tether	0.533m
Length of $r_{P/Q}$	0.2m
Angle of Tether Attachment	0°
Offset of Center of Mass	0.01m
Offset Angle of Center of Mass	-135°
Mass of Hovercraft	1.1233kg
Inertia of Hovercraft	$.0168kgm^2$
Angle of Thrust Fan	75°
Thrust Force	0.421N
Friction Expression	$.053\sqrt{\dot{\theta}} + 0.107\dot{\theta}$
Rotational Friction Expression	$-0.011\sqrt{\dot{\theta}}$

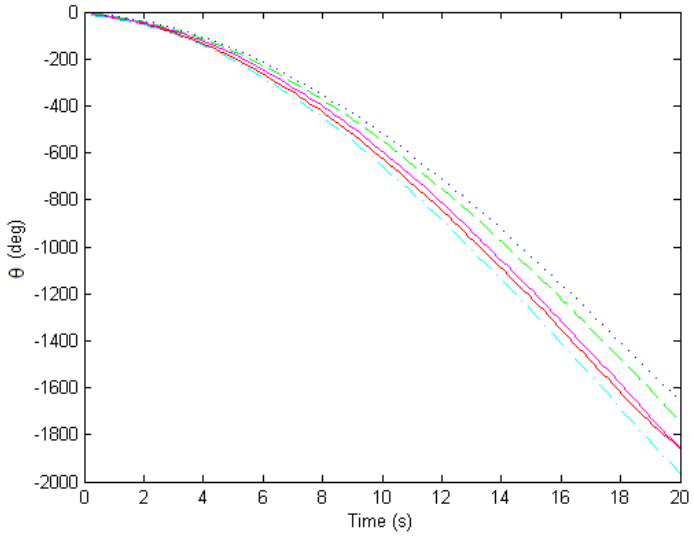

Figure B.41: Angle of the Hovercraft with the Inertial Frame for Setup 11

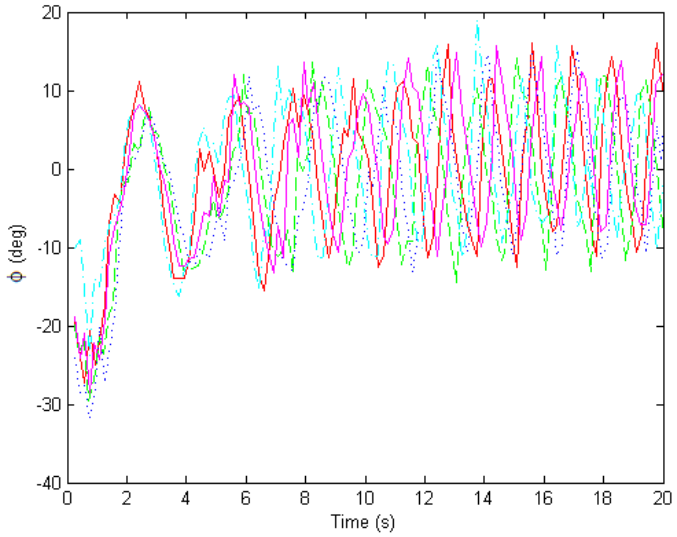

Figure B.42: Attitude of the Hovercraft for Setup 11

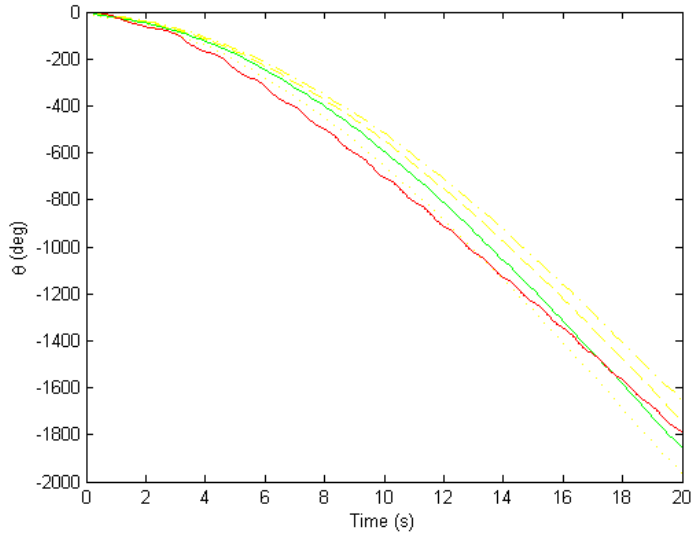

Figure B.43: Comparison of the Analytical and Experimental Results of Tether Angle for Setup 11

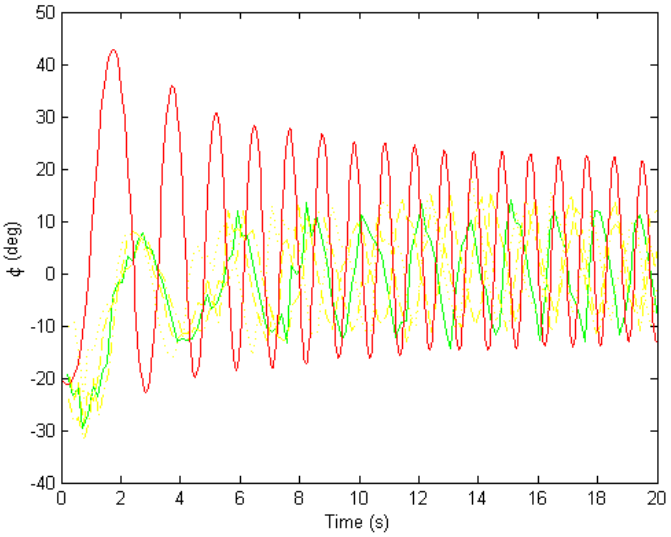

Figure B.44: Comparison of the Analytical and Experimental Results of Hovercraft Attitude for Setup 11

B.12 Setup 12

Table B.12: Configuration of Setup 12

Length of Tether	0.533m
Length of $r_{P/Q}$	0.2m
Angle of Tether Attachment	0°
Offset of Center of Mass	0.02m
Offset Angle of Center of Mass	0°
Mass of Hovercraft	1.1233kg
Inertia of Hovercraft	$.0168kgm^2$
Angle of Thrust Fan	90°
Thrust Force	0.421N
Friction Expression	$.053\sqrt{\dot{\theta}} + 0.107\dot{\theta}$
Rotational Friction Expression	$-0.011\sqrt{\dot{\theta}}$

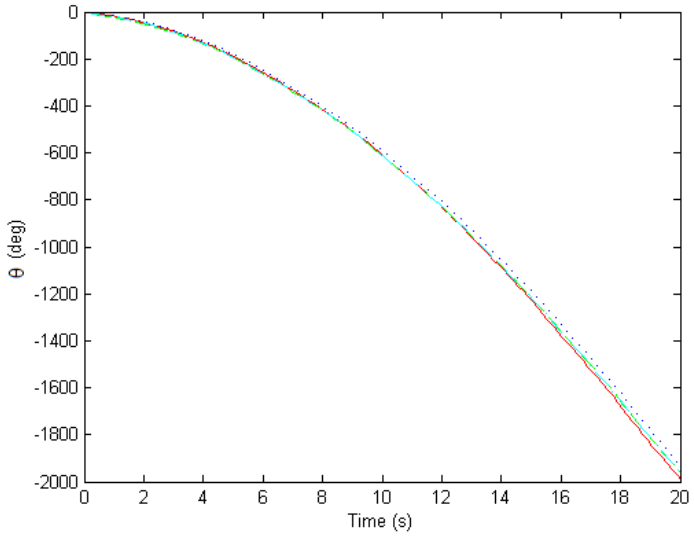

Figure B.45: Angle of the Hovercraft with the Inertial Frame for Setup 12

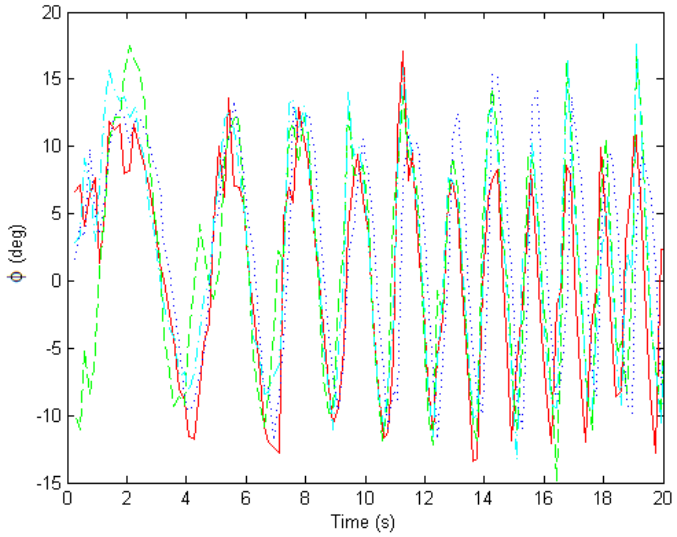

Figure B.46: Attitude of the Hovercraft for Setup 12

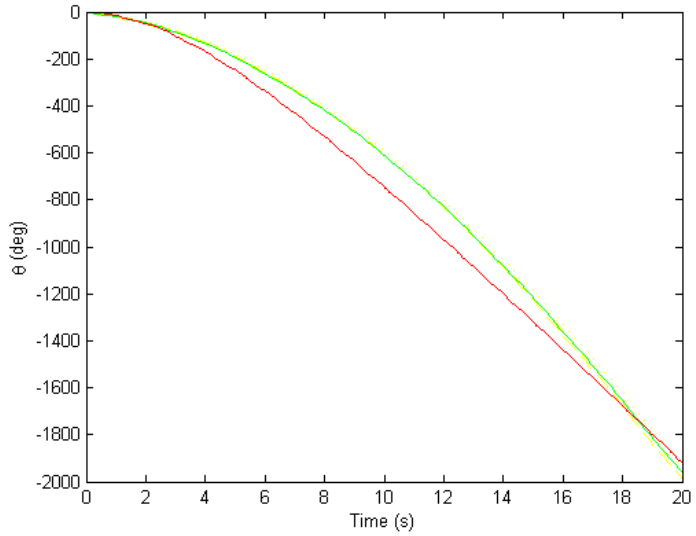

Figure B.47: Comparison of the Analytical and Experimental Results of Tether Angle for Setup 12

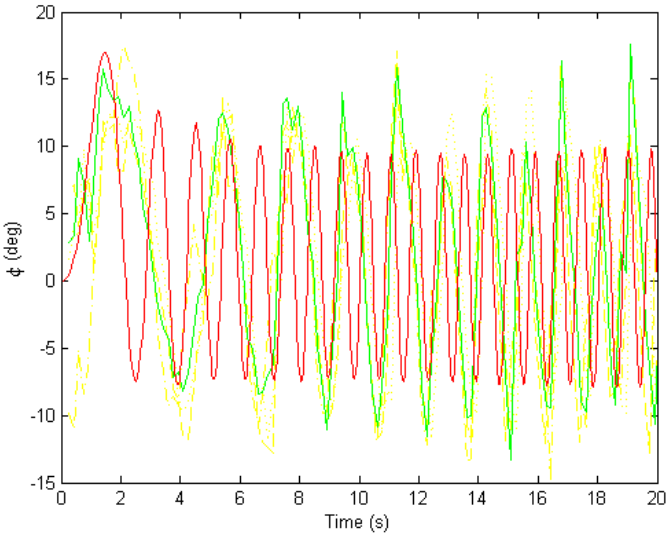

Figure B.48: Comparison of the Analytical and Experimental Results of Hovercraft Attitude for Setup 12

B.13 Setup 13

Table B.13: Configuration of Setup 13

Length of Tether	1.270m
Length of $r_{P/Q}$	0.20m
Angle of Tether Attachment	0°
Offset of Center of Mass	0.01m
Offset Angle of Center of Mass	135°
Mass of Hovercraft	1.0223kg
Inertia of Hovercraft	$.0164kgm^2$
Angle of Thrust Fan	30°
Thrust Force	0.421N
Friction Expression	$.051\sqrt{\dot{\theta}} + 0.16\dot{\theta}$
Rotational Friction Expression	$-0.010\sqrt{\dot{\theta}}$

For the next three setups the servo, the heaviest single component, was removed. The trials test a few of the previous angles at the original tether length with a smaller mass.

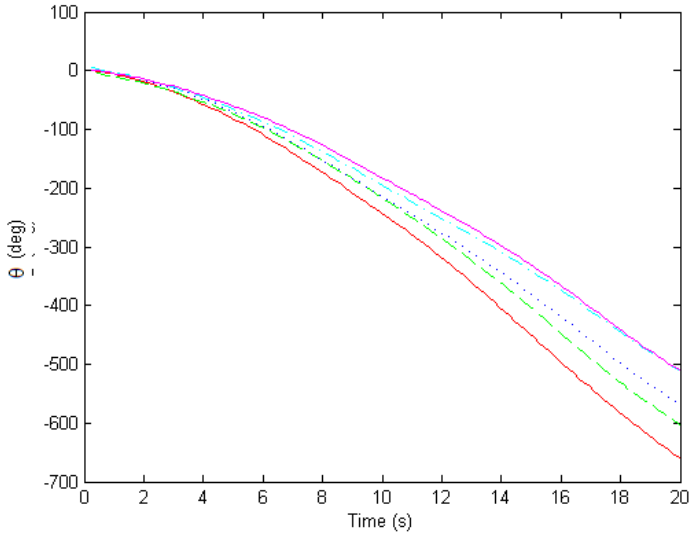

Figure B.49: Angle of the Hovercraft with the Inertial Frame for Setup 13

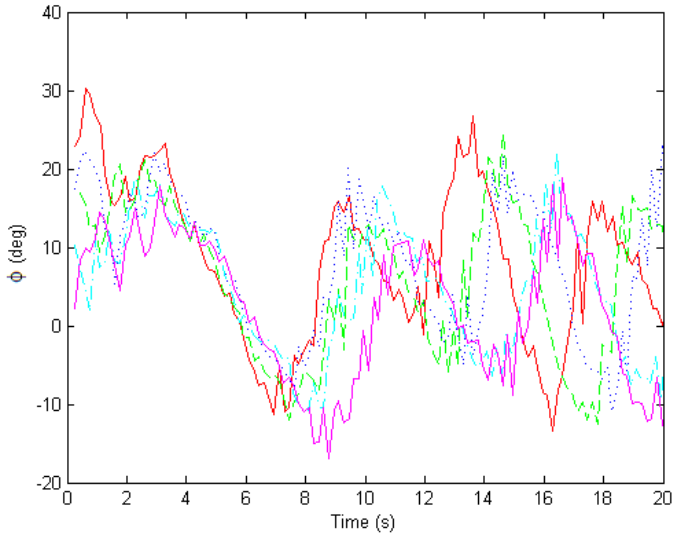

Figure B.50: Attitude of the Hovercraft for Setup 13

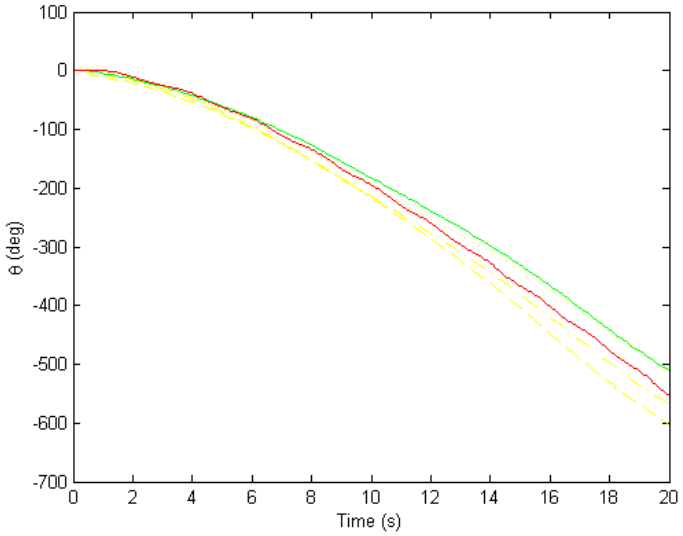

Figure B.51: Comparison of the Analytical and Experimental Results of Tether Angle for Setup 13

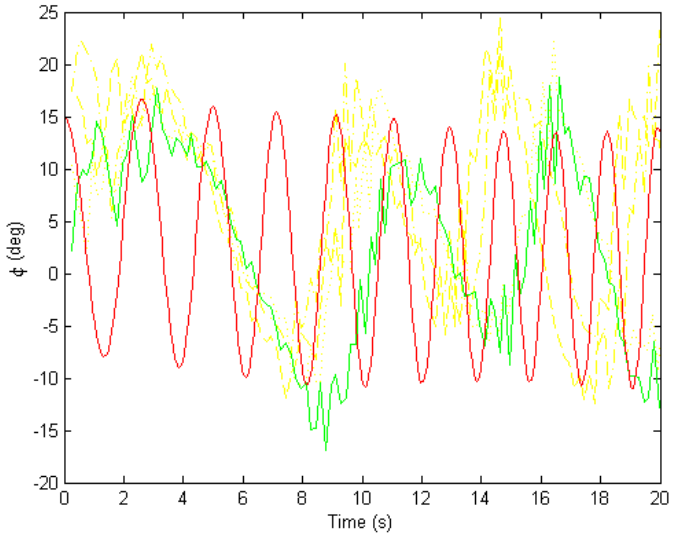

Figure B.52: Comparison of the Analytical and Experimental Results of Hovercraft Attitude for Setup 13

B.14 Setup 14

Table B.14: Configuration of Setup 14

Length of Tether	1.270m
Length of $r_{P/Q}$	0.20m
Angle of Tether Attachment	0°
Offset of Center of Mass	0.01m
Offset Angle of Center of Mass	150°
Mass of Hovercraft	1.0223kg
Inertia of Hovercraft	$.0161kgm^2$
Angle of Thrust Fan	60°
Thrust Force	0.421N
Friction Expression	$.146\sqrt{\dot{\theta}} + 0.007\dot{\theta}$
Rotational Friction Expression	$-0.03\sqrt{\dot{\theta}}$

Setups 14 and 15 were conducted on a separate day from setup 13. They also exhibit a highly unusual behavior confusing the results.

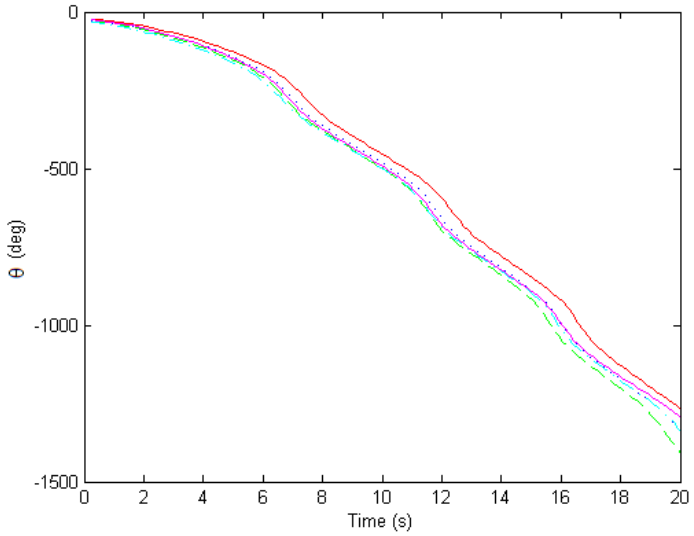

Figure B.53: Angle of the Hovercraft with the Inertial Frame for Setup 14

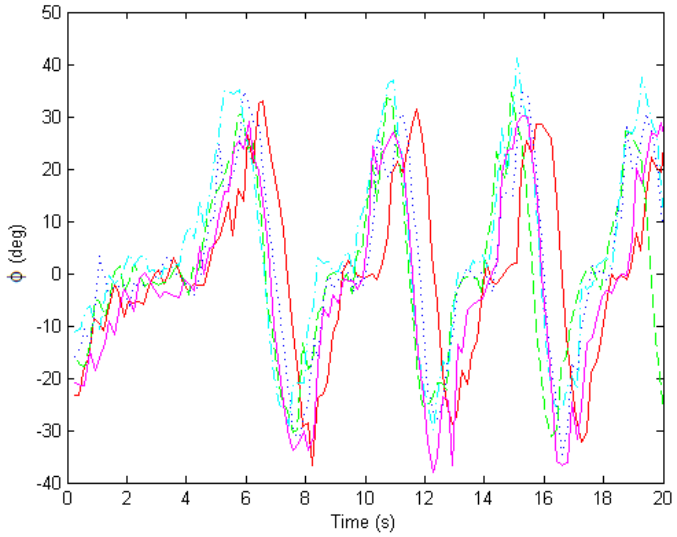

Figure B.54: Attitude of the Hovercraft for Setup 14

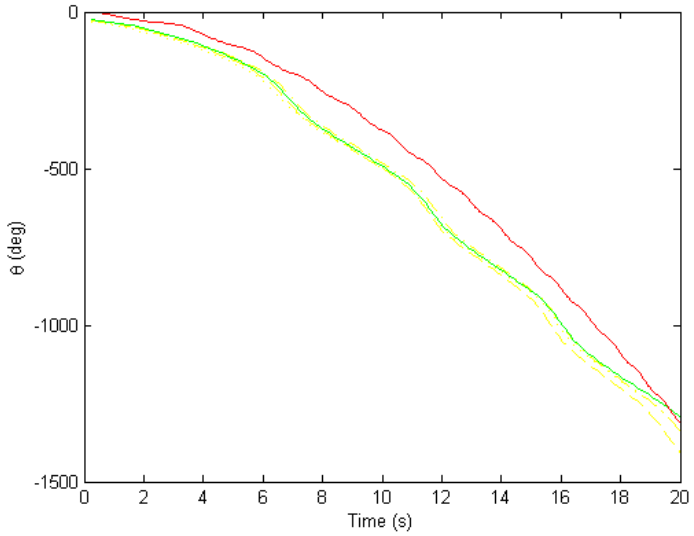

Figure B.55: Comparison of the Analytical and Experimental Results of Tether Angle for Setup 14

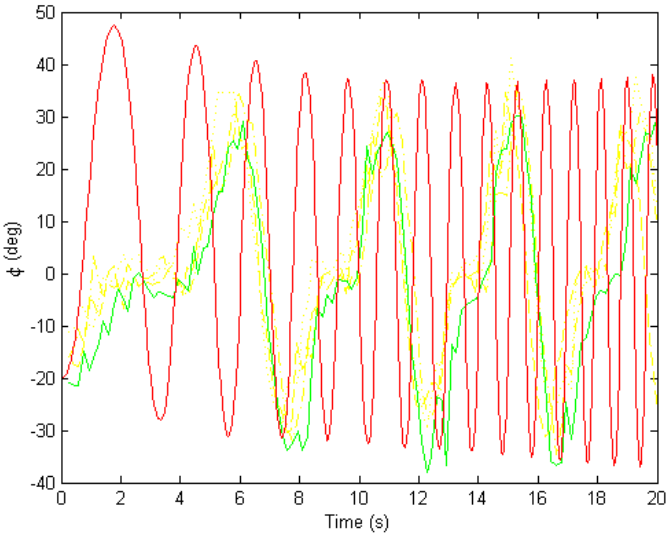

Figure B.56: Comparison of the Analytical and Experimental Results of Hovercraft Attitude for Setup 14

B.15 Setup 15

Table B.15: Configuration of Setup 15

Length of Tether	1.270m
Length of $r_{P/Q}$	0.20m
Angle of Tether Attachment	0°
Offset of Center of Mass	0.01m
Offset Angle of Center of Mass	150°
Mass of Hovercraft	1.0223kg
Inertia of Hovercraft	$.0160kgm^2$
Angle of Thrust Fan	90°
Thrust Force	0.421N
Friction Expression	$.146\sqrt{\dot{\theta}} + 0.007\dot{\theta}$
Rotational Friction Expression	$-0.03\sqrt{\dot{\theta}}$

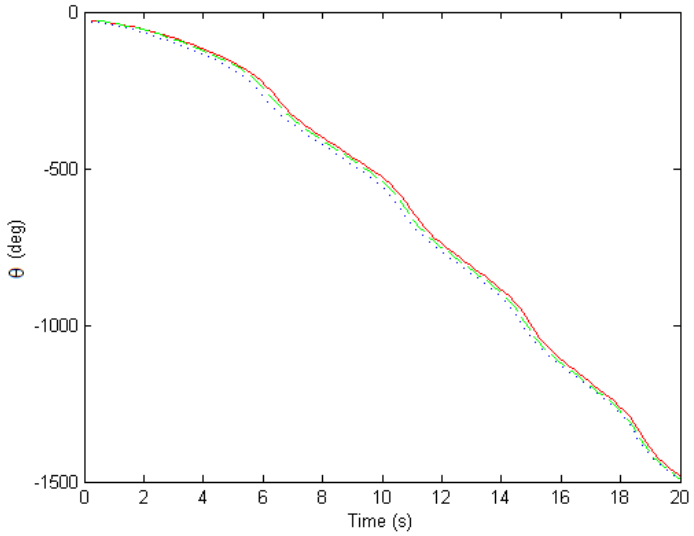

Figure B.57: Angle of the Hovercraft with the Inertial Frame for Setup 15

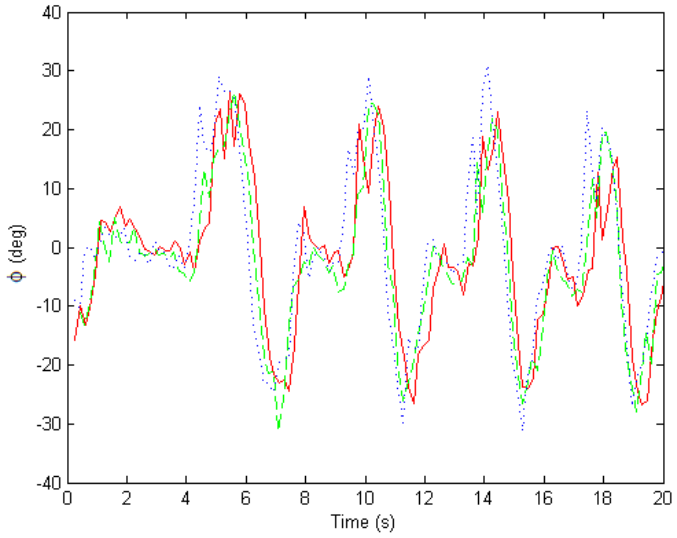

Figure B.58: Attitude of the Hovercraft for Setup 15

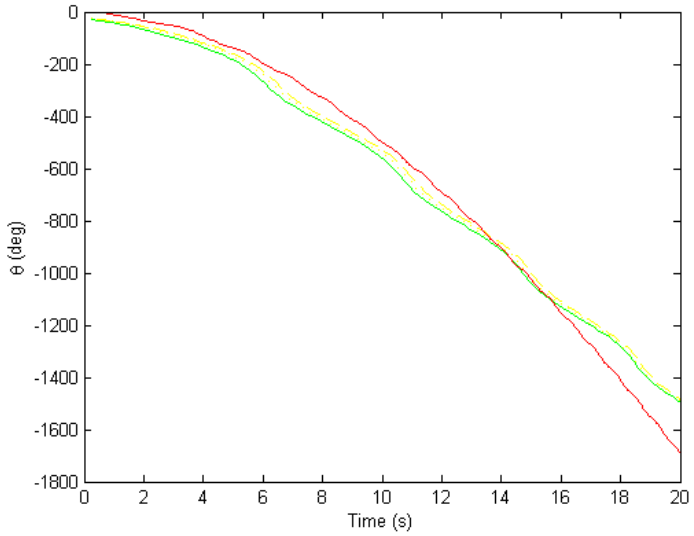

Figure B.59: Comparison of the Analytical and Experimental Results of Tether Angle for Setup 15

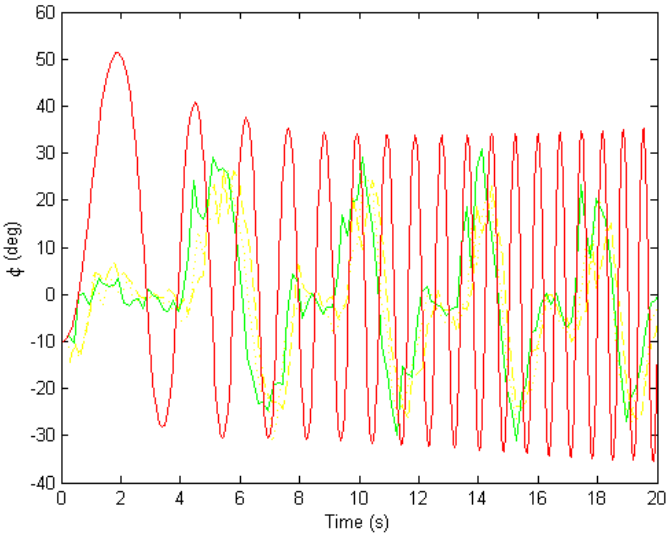

Figure B.60: Comparison of the Analytical and Experimental Results of Hovercraft Attitude for Setup 15

B.16 Setup 16

Table B.16: Configuration of Setup 16

Length of Tether	1.270m
Length of $r_{P/Q}$	0.16m
Angle of Tether Attachment	45° (on same side as the thrust fan)
Offset of Center of Mass	0.02m
Offset Angle of Center of Mass	$-90°$
Mass of Hovercraft	1.0223kg
Inertia of Hovercraft	$.016kgm^2$
Angle of Thrust Fan	90°
Thrust Force	0.421N
Friction Expression	$.124\sqrt{\dot{\theta}} + 0.007\dot{\theta}$
Rotational Friction Expression	$-0.025\sqrt{\dot{\theta}}$

The next three setups examine the effect of repositioning the tether attachment. Setup 16 has to be the best example of damped oscillations. It appears that only every third oscillation is actually not damped out. The analytic result would again match well if all the oscillations were of equal magnitude. The average value of the attitude of the analytic result does noticeably differ from the experimental. This may be a result of an improper measurement; probably the angle of the center of mass.

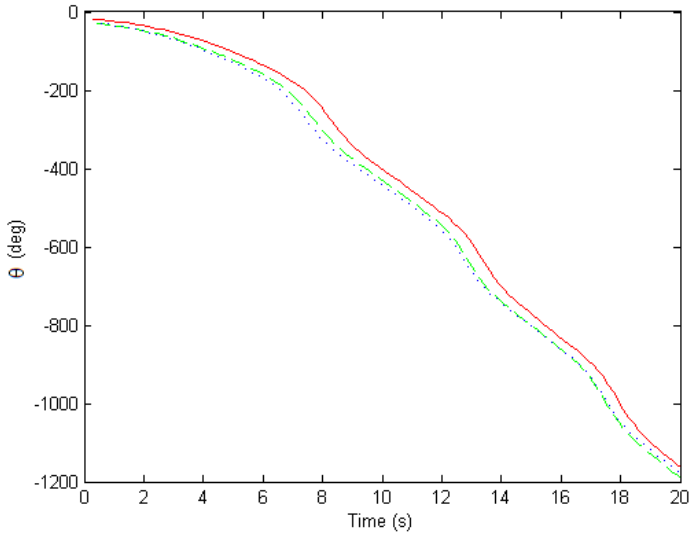

Figure B.61: Angle of the Hovercraft with the Inertial Frame for Setup 16

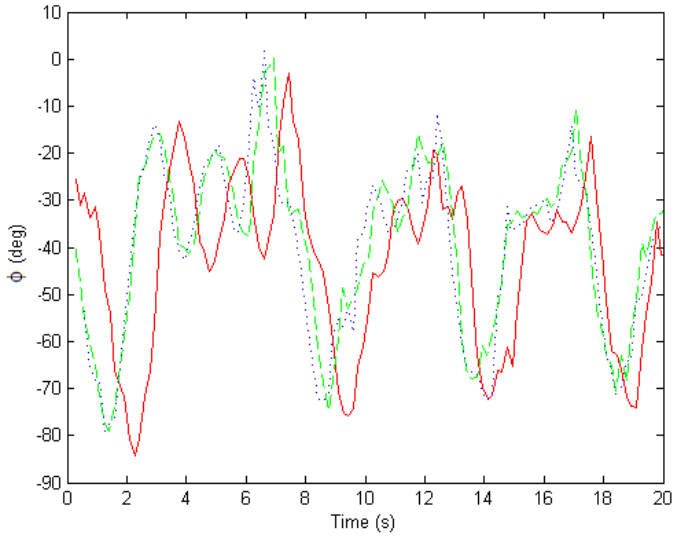

Figure B.62: Attitude of the Hovercraft for Setup 16

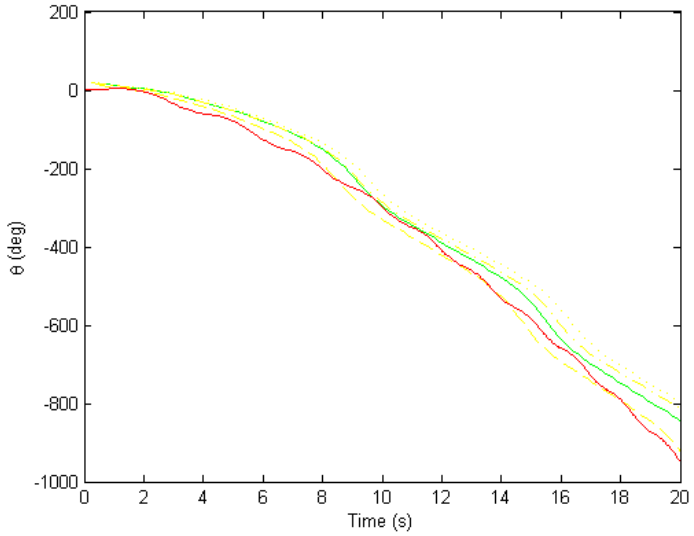

Figure B.63: Comparison of the Analytical and Experimental Results of Tether Angle for Setup 16

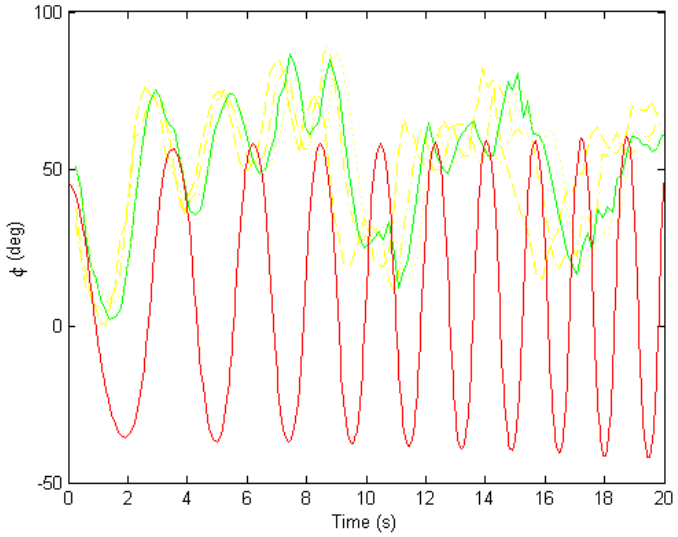

Figure B.64: Comparison of the Analytical and Experimental Results of Hovercraft Attitude for Setup 16

B.17 Setup 17

Table B.17: Configuration of Setup 17

Length of Tether	1.270m
Length of $r_{P/Q}$	0.16m
Angle of Tether Attachment	45° (on same side as the thrust fan)
Offset of Center of Mass	0.02m
Offset Angle of Center of Mass	$-90°$
Mass of Hovercraft	1.0223kg
Inertia of Hovercraft	$.016kgm^2$
Angle of Thrust Fan	105°
Thrust Force	0.421N
Friction Expression	$.124\sqrt{\dot{\theta}} + 0.007\dot{\theta}$
Rotational Friction Expression	$-0.025\sqrt{\dot{\theta}}$

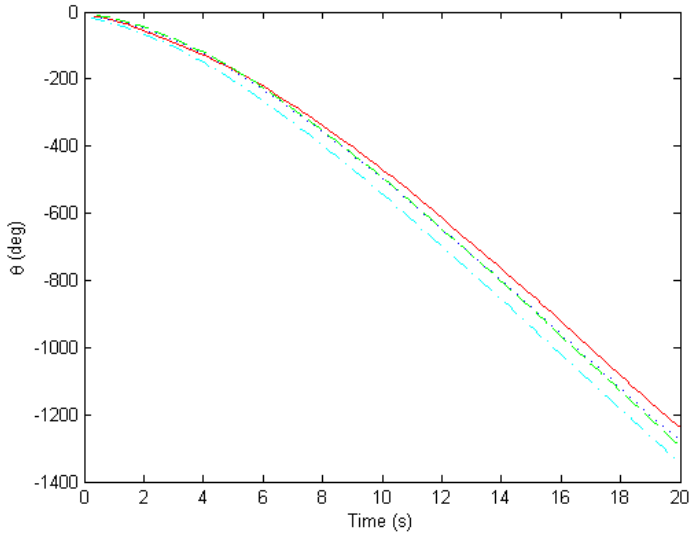

Figure B.65: Angle of the Hovercraft with the Inertial Frame for Setup 17

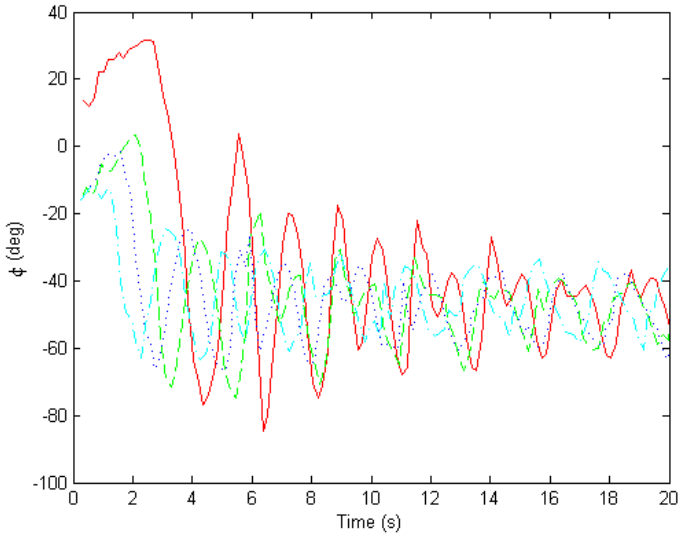

Figure B.66: Attitude of the Hovercraft for Setup 17

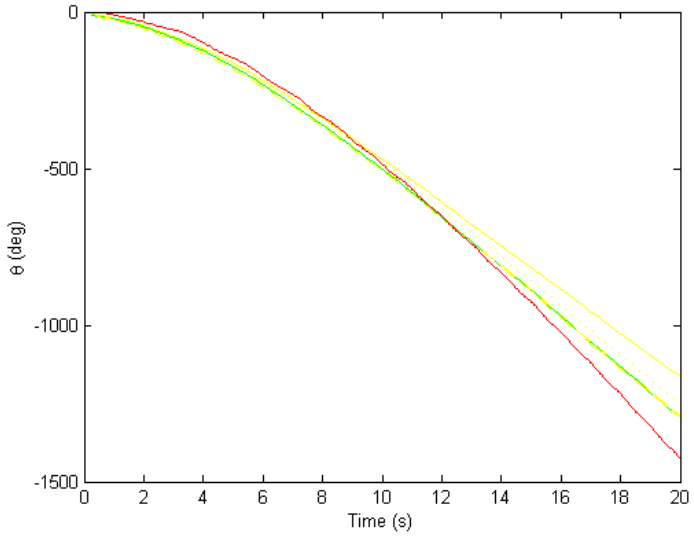

Figure B.67: Comparison of the Analytical and Experimental Results of Tether Angle for Setup 17

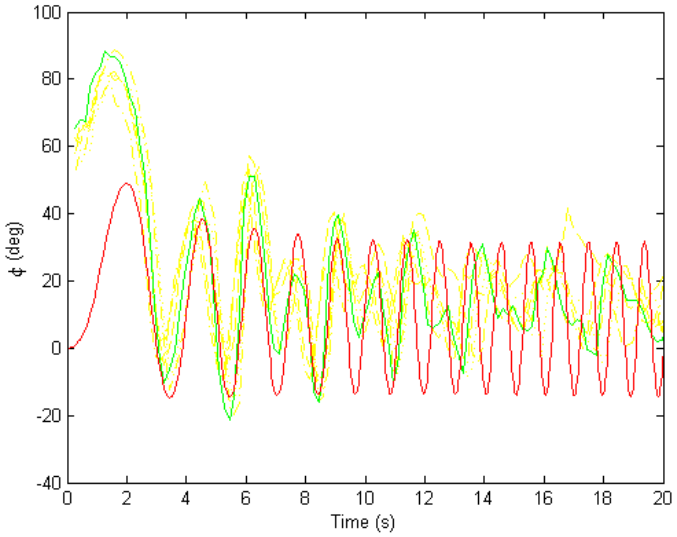

Figure B.68: Comparison of the Analytical and Experimental Results of Hovercraft Attitude for Setup 17

B.18 Setup 18

Table B.18: Configuration of Setup 18

Length of Tether	1.270m
Length of $r_{P/Q}$	0.16m
Angle of Tether Attachment	45° (on same side as the thrust fan)
Offset of Center of Mass	0.02m
Offset Angle of Center of Mass	$-60°$
Mass of Hovercraft	1.0223kg
Inertia of Hovercraft	$.016kgm^2$
Angle of Thrust Fan	120°
Thrust Force	0.421N
Friction Expression	$.073\sqrt{\dot{\theta}} + 0.220\dot{\theta}$
Rotational Friction Expression	$-0.015\sqrt{\dot{\theta}}$

The damping is once again evident. Almost every major crest has a dip which happens to correspond to an oscillation in the analytic result.

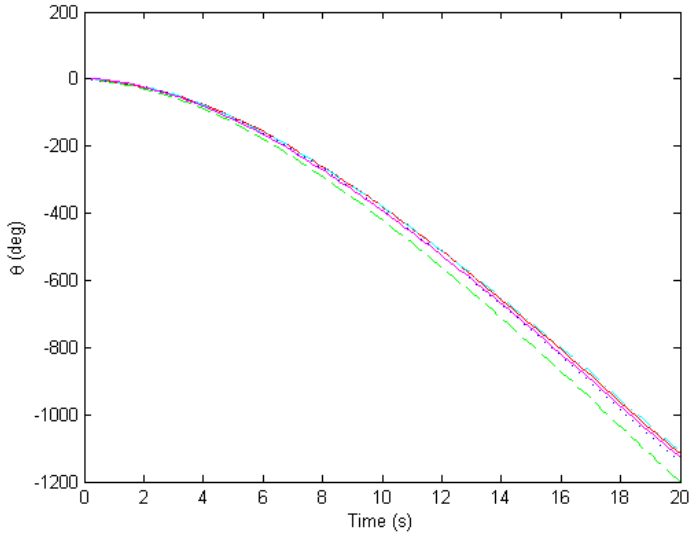

Figure B.69: Angle of the Hovercraft with the Inertial Frame for Setup 18

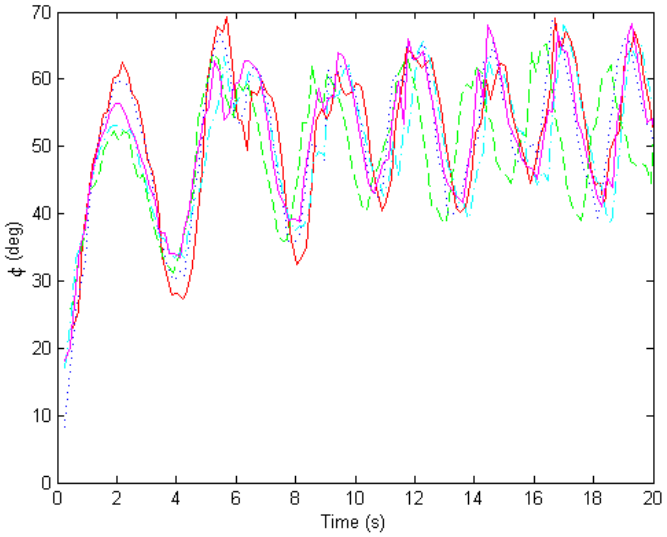

Figure B.70: Attitude of the Hovercraft for Setup 18

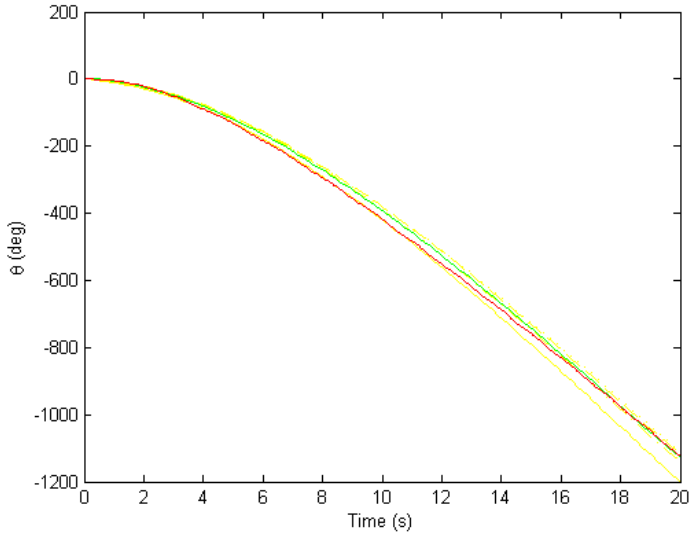

Figure B.71: Comparison of the Analytical and Experimental Results of Tether Angle for Setup 18

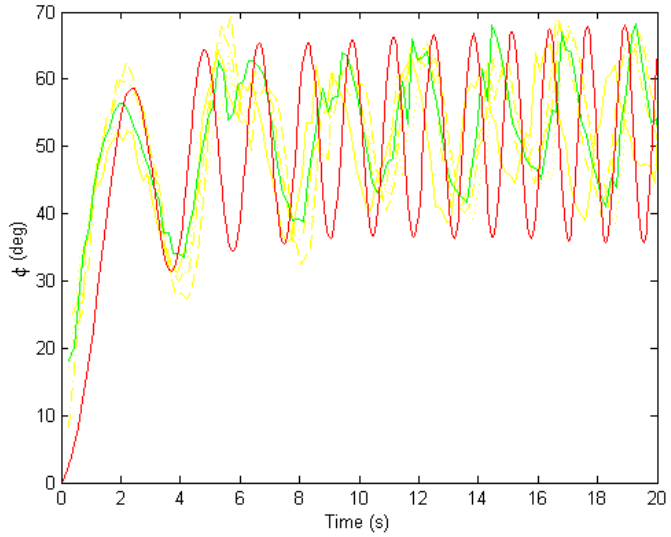

Figure B.72: Comparison of the Analytical and Experimental Results of Hovercraft Attitude for Setup 18

B.19 Setup 19

Table B.19: Configuration of Setup 19 For the First 10 Seconds

Length of Tether	2.14m
Rate of Length Change	0m/s
Length of $r_{P/Q}$	0.2m
Angle of Tether Attachment	0°
Offset of Center of Mass	0.01m
Offset Angle of Center of Mass	−180°
Mass of Hovercraft	1.1233kg
Inertia of Hovercraft	$.0175kgm^2$
Angle of Thrust Fan	60°
Thrust Force	0.421N
Friction Expression	$.015\sqrt{\dot{\theta}} + 0.029\dot{\theta}$
Rotational Friction Expression	$-0.003\sqrt{\dot{\theta}}$

Table B.20: Configuration of Setup 19 After 10 Seconds

Length of Tether	$(2.14 - 0.0195time)$m
Rate of Length Change	-0.0195m/s
Length of $r_{P/Q}$	0.2m
Angle of Tether Attachment	0°
Offset of Center of Mass	0.01m
Offset Angle of Center of Mass	−180°
Mass of Hovercraft	1.1233kg
Inertia of Hovercraft	$.0175kgm^2$
Angle of Thrust Fan	60°
Thrust Force	0N
Friction Expression	$.035\sqrt{\dot{\theta}(-0.000112time^2 - 0.005602time + 1.10805)}$ $+0.029\sqrt{\dot{\theta}(-0.000112time^2 - 0.005802time + 1.10805)}$
Rotational Friction Expression	$-0.007\sqrt{\dot{\theta}(-0.000112time^2 - 0.005602time + 1.10805)}$

This setup fully demonstrates the experiment's ability to show the trends of the analytic results. First, consider the angle of the tether about the inertial reference, θ. In the first 10 seconds it accelerates because the thrust fan is turned on. After it is turned off, for the majority of the time the hovercraft maintains a nearly constant velocity as it is reeling in. It actually slows down slightly due to friction, and this can be seen by the slight curvature in both the analytic and experimental results. In the final 15 seconds the tether accelerates as the effects of reduced inertia overcome the drag from the friction.

Next, consider the attitude of the hovercraft, ϕ. There is an initial large oscillation which drops and then gradually increases. In the final seconds the amplitude of the oscillations increase sharply. Each of these effects occurred in both the experimental and analytic results. However, again the main difference is that the frequency of the analytic result is significantly greater than in the experimental result.

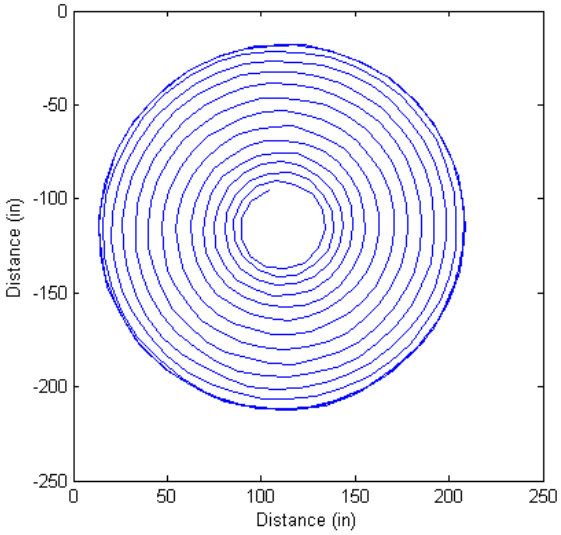

Figure B.73: Position of the Hovercraft on the Squash Court for Setup 19

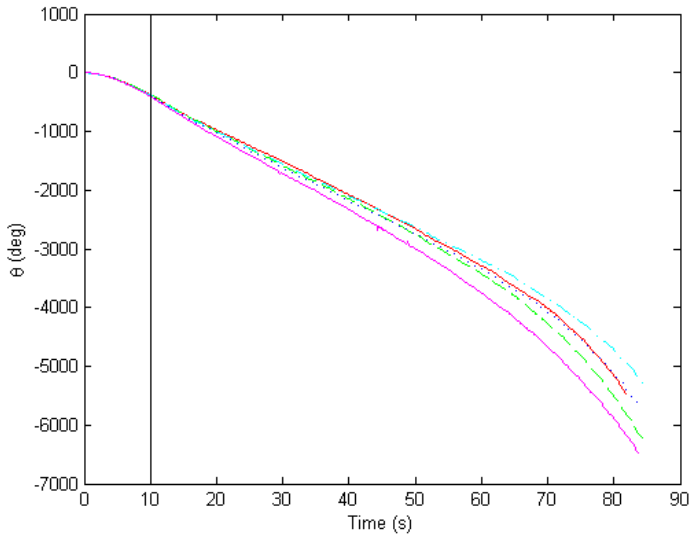

Figure B.74: Angle of the Hovercraft with the Inertial Frame for Setup 19

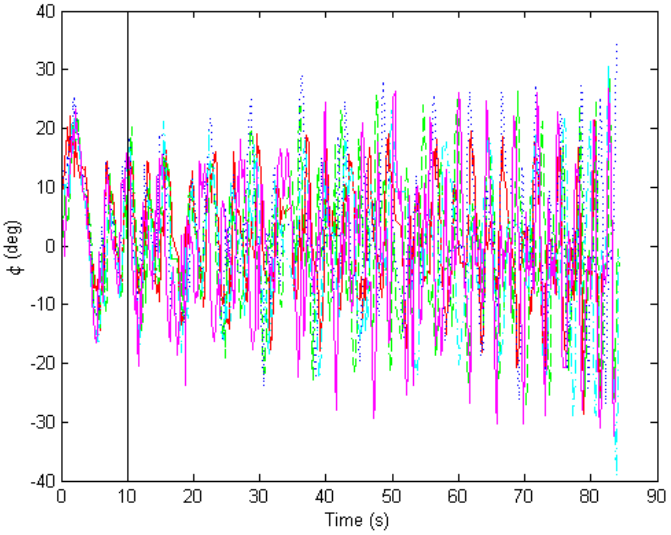

Figure B.75: Attitude of the Hovercraft for Setup 19

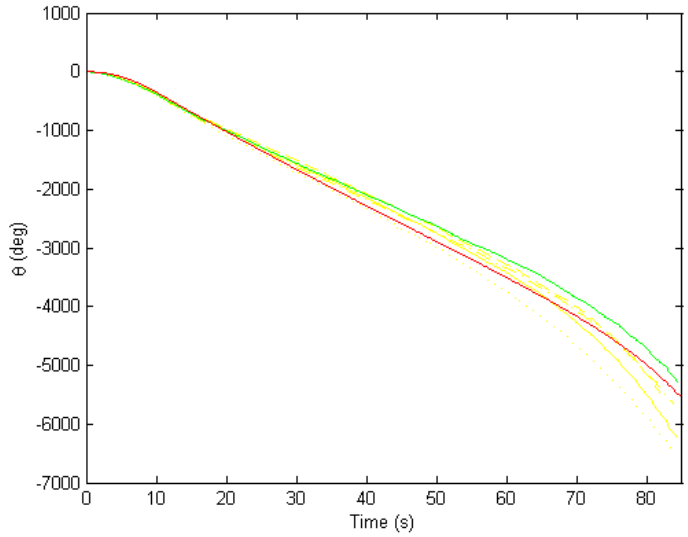

Figure B.76: Comparison of the Analytical and Experimental Results of Tether Angle for Setup 19

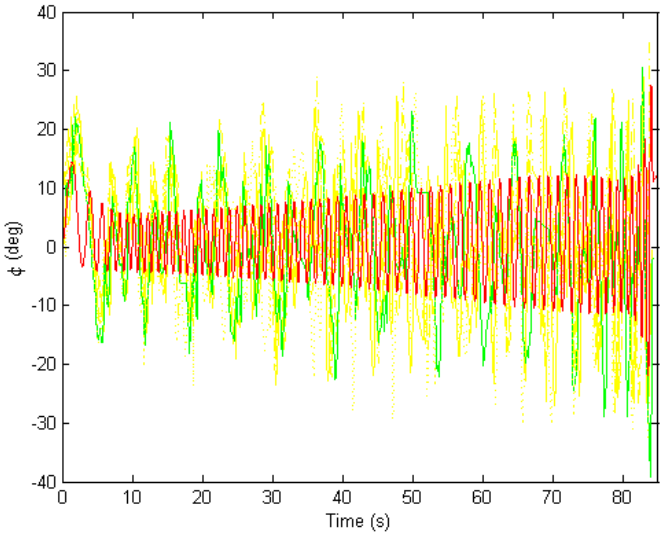

Figure B.77: Comparison of the Analytical and Experimental Results of Hovercraft Attitude for Setup 19

B.20 Setup 20

Table B.21: Configuration of Setup 20 For the First 10 Seconds

Length of Tether	25.5cm
Length of $r_{P/Q}$	22.5cm
Angle of Tether Attachment	0°
Offset of Center of Mass	2cm
Offset Angle of Center of Mass	−135°
Mass of Hovercraft	1.1233kg
Inertia of Hovercraft	$.0175kgm^2$
Angle of Thrust Fan	60°
Thrust Force	0.421N
Friction Expression	$.04\sqrt{\dot{\theta}}$
Rotational Friction Expression	$-0.04\sqrt{\dot{\theta}}$

Table B.22: Configuration of Setup 20 After 10 Seconds

Length of Tether	$(2.14 + .031time)$m
Rate of Length Change	0.031m/s
Length of $r_{P/Q}$	0.2m
Angle of Tether Attachment	0°
Offset of Center of Mass	0.02m
Offset Angle of Center of Mass	−135°
Mass of Hovercraft	1.1233kg
Inertia of Hovercraft	$.0175kgm^2$
Angle of Thrust Fan	60°
Thrust Force	0N
Friction Expression	$.035\sqrt{\dot{\theta}(-0.00007time^2 + 0.03637time + 0.0655)}$ $+0.02\sqrt{\dot{\theta}(-0.00007time^2 + 0.03637time + 0.0655)}$
Rotational Friction Expression	$-0.007\sqrt{\dot{\theta}(-0.00007time^2 + 0.03637time + 0.0655)}$

In the reel out trial θ still does well identifying the reduction in velocity due to the increase inertia. However, while the relations between the experimental and analytic results of ϕ are

still in tact, they are less obvious. The experimental result shows that the amplitude of the oscillations dies down and at some point eventual begins to increase. The frequency increases as the amplitude decreases, and then greatly decreases as the amplitude slightly increases. The analytic result shows this, however the effects are greatly amplified. The unusual profile seen in previous experimental setups can be observed. This may once again imply that the setup was unbalanced altering the results.

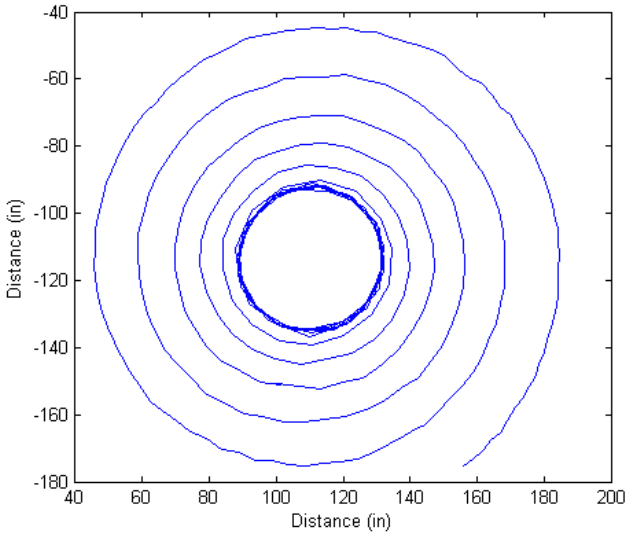

Figure B.78: Position of the Hovercraft on the Squash Court for Setup 20

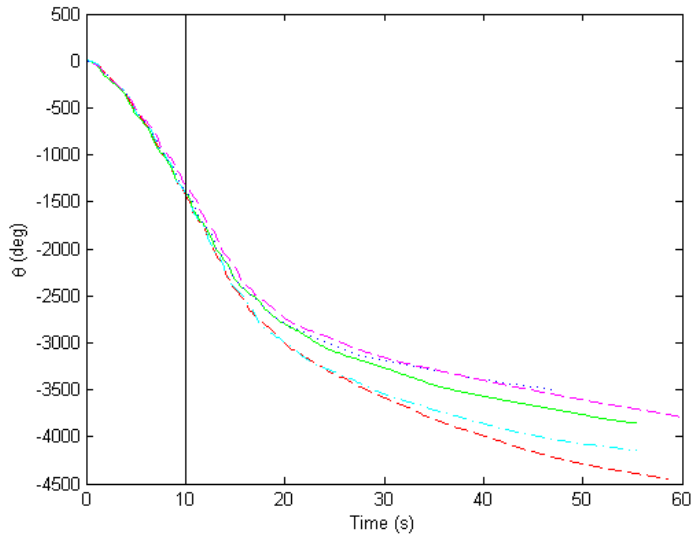

Figure B.79: Angle of the Hovercraft with the Inertial Frame for Setup 20

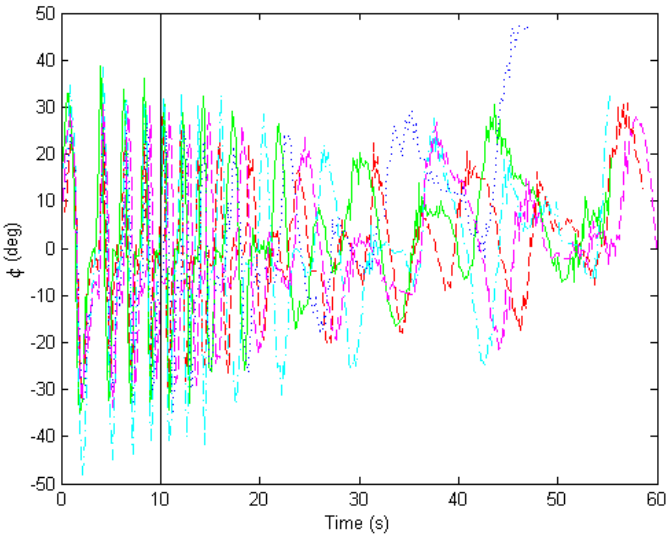

Figure B.80: Attitude of the Hovercraft for Setup 20

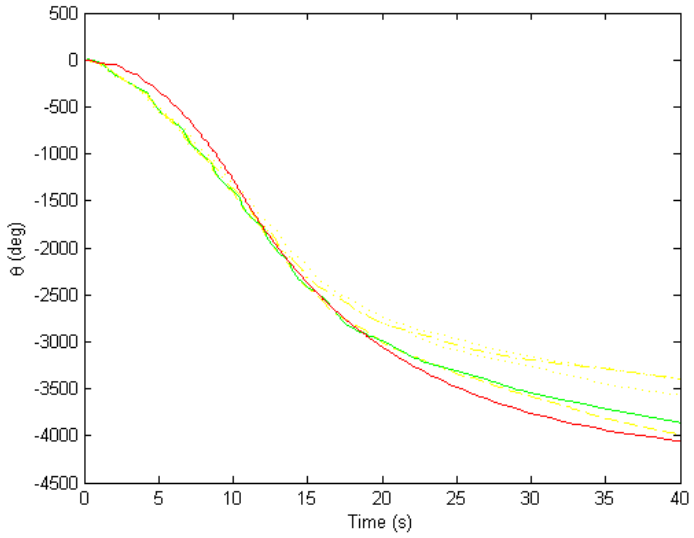

Figure B.81: Comparison of the Analytical and Experimental Results of Tether Angle for Setup 20

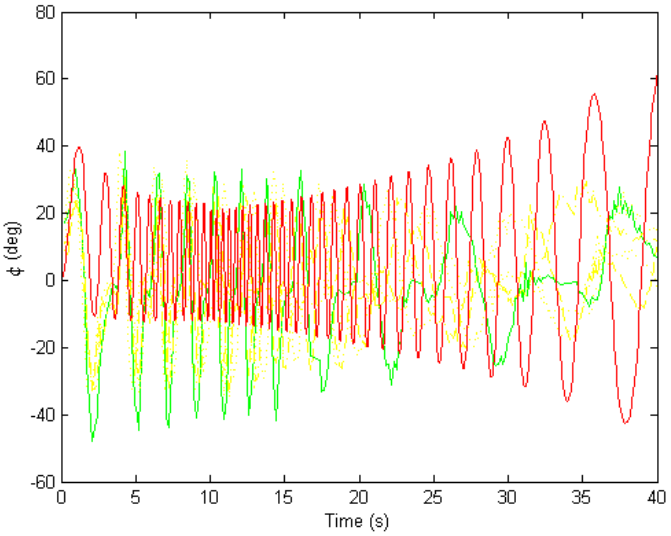

Figure B.82: Comparison of the Analytical and Experimental Results of Hovercraft Attitude for Setup 20